

# A Toolbox for Lithium–Sulfur Battery Research: Methods and Protocols

Ge Zhang, Ze-Wen Zhang, Hong-Jie Peng, Jia-Qi Huang, and Qiang Zhang\*

Favorable characteristics, such as high energy density, cost efficiency, and environmental benignity, render lithium–sulfur (Li–S) batteries a promising candidate to meet the increasing demand for efficient and economic energy-storage systems. Many efforts have been devoted to and much progress has been achieved in Li–S-battery research from both the scientific and technological viewpoints. Various tools, methods, and protocols have been developed for Li–S-battery research. Here, these advancements are summarized, from spectroscopic to electrochemical techniques, and the landscape of Li–S chemistry is painted from reactions to transport phenomena. The aim is to provide a comprehensive toolbox for Li–S-battery research and spur future development in multi-electron chemistry, multiphase conversion, and related energy-storage systems and fields.

## 1. Introduction

The recent decades have witnessed an ever-increasing research enthusiasm for advanced energy-storage systems to harvest renewable but intermittent energy and integrate it into smart grids. Sustainable and cost-effective technologies are among the top priorities in the research community. In particular, electrochemical energy-storage technologies, especially secondary batteries, are attracting growing interest.<sup>[1–3]</sup> After years of rapid development, lithium-ion batteries (LIBs) are now widely employed in commercial electronics, and also furthered into surging markets such as electrical vehicles. Nowadays, increasingly attractive post-LIB technologies, such as lithium–sulfur (Li–S), lithium–air, sodium-ion, and magnesium batteries, have grasped much attention globally due to either their high energy density or their low cost.<sup>[4–7]</sup>

G. Zhang, Z.-W. Zhang, H.-J. Peng, Prof. Q. Zhang  
Beijing Key Laboratory of Green Chemical Reaction Engineering and Technology  
Department of Chemical Engineering  
Tsinghua University  
Beijing 100084, China  
E-mail: zhang-qiang@mails.tsinghua.edu.cn

Prof. J.-Q. Huang  
Advanced Research Institute for Multidisciplinary Science  
Beijing Institute of Technology  
Beijing 100081, China

 The ORCID identification number(s) for the author(s) of this article can be found under <https://doi.org/10.1002/smt.201700134>.

DOI: 10.1002/smt.201700134

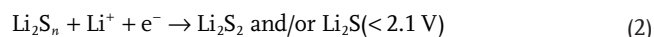
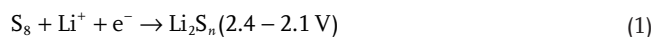
Of these, the Li–S battery is widely recognized as a promising alternative to its counterparts based on intercalation chemistry, and is expected to meet the practical demands of growing markets.<sup>[8–14]</sup> Their multi-electron redox reactions endow Li–S batteries with a theoretical gravimetric energy density of 2600 W h kg<sup>-1</sup>. In addition to the high theoretical capacity of 1672 mA h g<sup>-1</sup>, the valuable characteristics of the natural abundance of sulfur, the cost efficiency, and the environmental benignity have lent competitive edges to Li–S batteries. Further advancements of this technology require novel target-oriented design of functional materials and in-depth perspectives of the underlying science and engineering.

Questions have been asked about the thermodynamics and kinetics of the redox reactions, as well as the evolution of the active materials. Characterization techniques are in great demand to paint the landscape of Li–S chemistry, including, but not limited to, the electronic structure, chemical composition, crystallinity, phase transformation, and spatial distribution of the electrode materials, as well as the temporal dependence of these characteristics upon electrochemical reactions. Therefore, advanced characterization tools, analytical methods, and protocols together are of great importance for the development of Li–S batteries.

Here, we will focus on questions around the redox reactions and transport phenomena, which are mostly concerning the research community, and we will discuss each of them accordingly, from macroscopic to microscopic perspectives. To start with, we make a brief introduction of standard methods for studying Li–S batteries. As Li–S systems involve extremely complicated chemical and physical processes, the next three sections are all devoted to summarizing the progress in elucidating the mechanism behind these phenomena, with the assistance of, in particular *in situ* and *in operando*, advanced characterization tools and electrochemical techniques (**Figure 1**). Varieties of species, their electrochemical reactions and transport phenomena, as well as their profound influence on Li–S batteries, are explicitly discussed. To close, current understanding and future directions for Li–S-battery development are proposed. Note that we emphasize the uniqueness of the Li–S battery, which mainly originates from the great complexity of sulfur chemistry and differs from other lithium-metal batteries. Therefore, the highly concerning problems with lithium-metal anodes, which are beyond the scope of this contribution, will not be included in this review, and have been discussed elsewhere.<sup>[15–17]</sup>

## 2. Standard Methods

Basically, a Li–S battery is composed of a cathode containing sulfur, an anode of lithium metal, and an organic electrolyte with dissolved lithium salt (Figure 2A-i). The electrochemical reactions of a Li–S battery involve multistep lithium-ion ( $\text{Li}^+$ )-coupled electroreduction/oxidation.<sup>[18,19]</sup> Between elemental  $\text{S}_8$  and lithium sulfide ( $\text{Li}_2\text{S}$ ), many intermediate products exist, which are generally referred to as polysulfides. Typically, polysulfides are chain-like dianions,  $\text{S}_n^{2-}$  ( $n = 3-8$ ), with two negatively charged terminal sulfur ( $\text{S}_\text{T}$ ) atoms and ( $n - 2$ ) nearly neutral bridge sulfur ( $\text{S}_\text{B}$ ) atoms in the middle. There is also evidence of the presence of radicals ( $\text{S}_n^{\bullet}$ ) in Li–S batteries, but dianions are still considered to be the dominant species. With  $\text{Li}^+$  counter ions readily coordinated by organic solvents, these polysulfides are believed to have considerable solubility in the electrolyte, unlike the insoluble  $\text{S}_8$  and  $\text{Li}_2\text{S}$ . Owing to the existence of these soluble intermediates, Li–S batteries using elemental sulfur as the starting cathode materials exhibit unique two-plateau electrochemical discharge reactions:



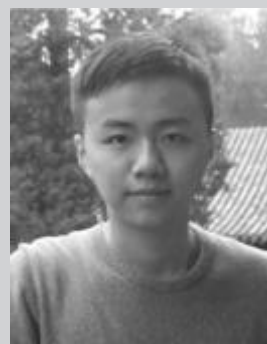
where the existence of lithium disulfide ( $\text{Li}_2\text{S}_2$ ) is still controversial; that will be discussed in Section 3.1. The soluble polysulfides can easily diffuse through the separator, react with the lithium anode, and diffuse back. Such an internal redox, i.e., so-called “shuttle” phenomenon, induces loss in capacity and Coulombic efficiency and is thereby regarded as one of the major bottlenecks impeding the development of Li–S batteries.<sup>[20,21]</sup>

Aside from elemental sulfur and lithium metal, a  $\text{Li}_2\text{S}$  cathode and a nonmetallic anode have also been proposed for Li–S batteries in an unconventional configuration (Figure 2A-ii). The electrochemistry is essentially the same as that of conventional Li–S batteries except for the first cycle.<sup>[22]</sup> Unlike such a liquid–solid–liquid and polysulfide-involved chemistry, there is also a quasi-solid-state electrochemical mechanism for some unique sulfur allotropes that are either under strong geometric constraint or covalently bonded (Figure 2A-iii).<sup>[23,24]</sup> In general, their differences in electrochemistry should be considered first for standard electrochemical evaluation.

Electrochemical cycling is one of the most common methods in evaluating battery performance, and one cycle comprises alternate charge and discharge steps. Typically, galvanostatic (under a constant current density) tests are routinely carried out, while under some circumstances, other methods like potentiostatic tests are favored for certain purposes. In most cases, the termination of the charge or discharge of a Li–S battery is indicated by an abrupt rise or drop in cell voltage, although some discrepancies in the working voltage window exist. Normally, the cut-off voltage for discharge and charge is within the range of 1.0–1.9 and 2.6–3.0 V (vs  $\text{Li}^+/\text{Li}$ ). A low cut-off voltage for discharge, e.g., 1.0–1.5 V, favors a remarkable discharge overpotential and thus discharge capacity by prolonging the kinetically sluggish solid–solid conversion from  $\text{Li}_2\text{S}_2$  to  $\text{Li}_2\text{S}$  (Figure 2B-i).<sup>[25]</sup> However, it is difficult to recover the electrically insulating and kinetically inert  $\text{Li}_2\text{S}$  phase during subsequent electrochemical oxidation,



**Ge Zhang** will receive his bachelor's degree in chemical engineering (2017) at Tsinghua University in China. He is now working with Prof. Qiang Zhang on high-energy-density electrochemical systems, with a focus on cathode and electrolyte design for lithium–sulfur batteries.



**Ze-Wen Zhang** will receive his Bachelor's Degree of materials science and engineering (2017) at Tsinghua University in China. He is currently carrying out his undergraduate research with Prof. Qiang Zhang in nanomaterials-based energy storage, especially lithium–sulfur batteries.



**Qiang Zhang** received his bachelors and Ph.D. degrees from Tsinghua University in 2004 and 2009, respectively. After a stay in Case Western Reserve University, USA, and the Fritz Haber Institute of the Max Planck Society, Germany, he was appointed an associate professor in Tsinghua University at 2011. His interests focus on energy materials, includes lithium–sulfur batteries, lithium-metal anodes, 3D graphene, and electrocatalysts.

contributing to significant capacity loss. On the contrary, a higher discharge cut-off voltage, e.g., 1.7–1.9 V, enables better cycling stability but lower initial discharge capacity (Figure 2B-ii). Another variant in determining the cut-off discharge voltage is the addition of lithium nitrate ( $\text{LiNO}_3$ ) into the electrolyte, which is commonly employed to protect a lithium-metal anode from polysulfide corrosion.  $\text{LiNO}_3$  decomposition has been reported to occur at the sulfur-cathode side when the cell voltage drops below 1.6 V (Figure 2B-iii).<sup>[26]</sup> Such a voltage threshold for cathodic  $\text{LiNO}_3$  decomposition may depend on the materials and  $\text{LiNO}_3$  concentration. As a result, a discharge cut-off voltage of 1.8 V was also reported.<sup>[27]</sup> Unlike elemental sulfur cathodes, sulfur that is encapsulated in ultra-micropores or bound to an organic backbone undergoes a quasi-solid-state electrochemical reaction with an average discharge voltage lower than 1.7 V, demanding



**Figure 1.** A toolbox for Li-S battery research.

a low discharge cut-off voltage of 1.0–1.2 V (Figure 2B-iv).<sup>[28]</sup> With regard to the cut-off charge voltage, only one exception to the routine range of 2.6–3.0 V is a cut-off voltage of 3.5–4.0 V for the first charge of Li<sub>2</sub>S cathodes, for which the first-cycle oxidation barrier is usually insurmountable below 3.0 V (Figure 2B-v).<sup>[29]</sup> In general, a test window of 1.7–1.9 V (discharge) to 2.6–3.0 V (charge) is suggested for Li-S cells with LiNO<sub>3</sub> additives. In some cases, nonmetallic anode materials such as graphite and silicon are used to replace lithium metal. Correspondingly, it is better to adjust the voltage window by ca. –0.1 to –0.6 V to offset the voltage loss induced by lithiation/delithiation of these nonmetallic anode materials (Figure 2B-vi).<sup>[30]</sup> As always, the charge and discharge profiles are plotted out as voltage vs specific capacity (mostly based on the weight of sulfur).

Rate tests are also a good touchstone for cell performance. The “C-rate” is a commonly used term referring to a specific

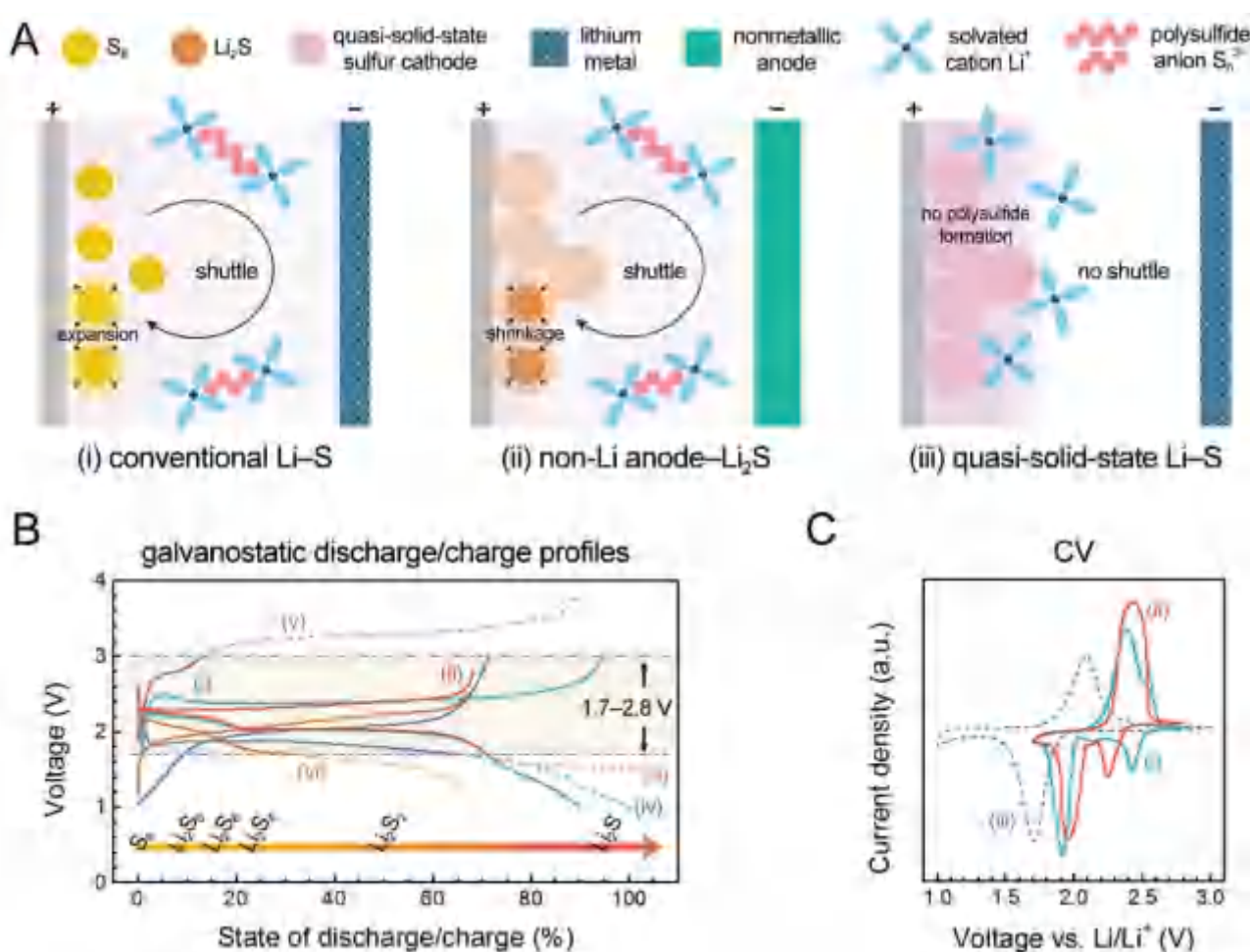


**Figure 2.** Li-S cell configurations and standard evaluation methods. A) Schematics of three types of Li-S batteries: i) conventional Li-S, ii) non-lithium-anode–Li<sub>2</sub>S, and iii) quasi-solid-state Li-S batteries. B) Typical galvanostatic discharge/charge profiles of Li-S batteries at the 1st cycle: i) w/o LiNO<sub>3</sub> (1.0–3.0 V), ii) with LiNO<sub>3</sub> (1.7–2.8 V), iii) with LiNO<sub>3</sub> but it decomposes at a voltage of <1.6 V ((i)–(iii) data from ref. [25]); iv) quasi-solid-state sulfur cathode with single-plateau feature and lower redox potential (1.0–3.0 V) (data from ref. [28]); v) the 1st charge profile of pristine Li<sub>2</sub>S cathode with a high charge barrier at the initial (data from ref. [29]); and vi) silicon–Li<sub>2</sub>S cell with lower working voltage (1.2–2.5 V) (data from ref. [30]). C) Typical CV curves of Li-S batteries: i, ii) conventional Li-S with different ether electrolytes, and iii) quasi-solid-state sulfur cathode. i) Data from ref. [31]; ii) Data from ref. [25]; iii) Data from ref. [28].

current density applied. A rate of 1C indicates that the half cycle, either charge or discharge, is expected to be complete in exactly one hour assuming full charge or discharge to the theoretical capacity without any self-discharge or overcharge. Different C-rates are proportional to applied current densities. The theoretical capacity of the sulfur cathode, derived from electrochemical Faraday's law, is 1672 mA h g<sup>-1</sup> and therefore "1C" corresponds to 1672 mA g<sup>-1</sup>. In the majority of Li-S battery research, C-rates range from 0.01C to 10C and typical rate tests include an ascending rate sequence starting from 0.05C or 0.1C, up to a higher rate ranging from 2 to 10C. The polarization normally becomes more severe as the C-rate increases. The cut-off voltage for discharge can be selectively lowered by 0.1 to 0.2 V to ensure the complete reaction.

Apart from the cycle performance, cyclic voltammetry (CV) is also a convenient but crucial tool for Li-S-battery investigation. CV profiles provide important information about electrode reactions, such as kinetics parameters and beyond. The voltage window of CV tests for Li-S batteries is always set to be the same as cycle tests. CV curves are drawn as a plot of current vs voltage. In commonly used ether-based electrolytes (e.g., 1,3-dioxolane (DOL), 1,2-dimethoxyethane (DME or glyme), tetra(ethylene glycol) dimethyl ether (TEGDME or tetraglyme), etc.), two cathodic peaks normally appear at around 2.2–2.4 and 1.9–2.1 V for elemental sulfur cathodes, corresponding to conversion of sulfur to polysulfides and eventually to Li<sub>2</sub>S, respectively. There are also two anodic peaks, referring to a consecutive oxidation of Li<sub>2</sub>S (Figure 2C-i).<sup>[31]</sup> However, the two anodic peaks are often overlapping, making it difficult to differentiate and decouple them (Figure 2C-ii).<sup>[25]</sup> Moreover, the position of each peak may be influenced by several factors, such as the composition of electrolytes, the loading amount of sulfur, and the scan rate of the CV tests. Similar to galvanostatic discharge/charge profiles, CV curves of sulfur cathodes based on a quasi-solid-state mechanism usually exhibit a couple of reverse cathodic/anodic peaks (Figure 2C-iii).<sup>[28]</sup>

The abovementioned tools are standard but indispensable in battery research, and they may help to evaluate the overall cell performance, providing basic understandings of working electrodes.

### 3. Speciation

#### 3.1. Solid Phases

Investigation of the solid composition and structure can provide important insights into the Li-S mechanism. Regarding the solid phases, several questions as to the crystallinity and composition have been widely considered:

- Are they crystalline or amorphous?
- Is the discharge product Li<sub>2</sub>S or Li<sub>2</sub>S<sub>2</sub>?
- Does S<sub>8</sub>/Li<sub>2</sub>S remain after full discharge/charge?

##### 3.1.1. In Operando X-ray Diffraction (XRD)

Since battery operation is a dynamic process, real-time information of the working cathode is necessary to unambiguously answer the questions above. Therefore, in situ or in operando

characterization is preferred, rather than ex situ techniques. Furthermore, short circuit of the disassembled electrochemical cell and its exposure to moisture may significantly alter the state of electrode materials, leading to misinterpretation in ex situ characterization.

To probe the crystallinity and composition, this section will mainly focus on in situ XRD study of Li-S batteries. In situ or in operando XRD is a powerful tool for detecting the structural evolution of battery materials upon cycling. Mostly, synchrotron X-ray sources and transmission mode are adopted for in situ XRD.<sup>[32–37]</sup> A conventional diffractometer and the reflection mode are also used by a few studies.<sup>[38]</sup> Synchrotron radiation sources usually offers higher light intensity, which is beneficial for obtaining high-quality diffraction patterns within a short time. The transmission mode allows the detection of a signal from all depths of both electrodes. With appropriate cell design, it is also possible to collect data from the sulfur cathode only.<sup>[34]</sup>

Aiming at the identification of the discharge products, in 2012, Nelson et al. carried out an in operando XRD study on a Li-S pouch cell for the first time (Figure 3A).<sup>[32]</sup> During the first cycle at C/8 in a commonly used lithium bis(trifluoromethane sulfonyl)imide (LiTFSI)-DOL/DME electrolyte, no crystalline Li<sub>2</sub>S was detected in the working cell, while ex situ XRD showed the characteristic peaks of Li<sub>2</sub>S. They suggested that Li<sub>2</sub>S appeared in amorphous form at the end of discharge, and crystalline Li<sub>2</sub>S formed only when the discharged cell was allowed to rest. In contrast, other studies all suggested the appearance of nanocrystalline Li<sub>2</sub>S during the second discharge plateau, although at different stages: Waluś et al. observed Li<sub>2</sub>S throughout the entire lower plateau (Figure 3B),<sup>[34]</sup> Cañas et al.<sup>[38]</sup> and Schneider et al.<sup>[37]</sup> identified a Li<sub>2</sub>S signal midway through the lower plateau, and Lowe et al.<sup>[33]</sup> did not find Li<sub>2</sub>S until the end of lower plateau (>80% depth of discharge (DOD) (Figure 3C)). All the detected Li<sub>2</sub>S signals corresponded well with its standard cubic structure, exhibiting a particle size of less than 10 nm,<sup>[35]</sup> and vanished before 80% state of charge (SOC) upon charge.

For charge products, orthorhombic  $\alpha$ -S<sub>8</sub>, as the starting cathode material of common Li-S batteries, disappeared completely during the first discharge plateau in all these reports.<sup>[32–38]</sup> It is worth noting that recrystallized S<sub>8</sub> was found to be another allotrope, monoclinic  $\beta$ -S<sub>8</sub>, which has been verified by at least five in operando XRD studies.<sup>[33–37]</sup> Since  $\alpha$ -S<sub>8</sub> is thermodynamically favored at room temperature, the formation of  $\beta$ -S<sub>8</sub> may indicate that the nucleation of the  $\alpha$ -phase is kinetically unfavorable compared with the  $\beta$ -phase. After resting the working cell for several hours, Waluś et al. reported the phase transformation from  $\beta$ -S<sub>8</sub> to  $\alpha$ -S<sub>8</sub>,<sup>[34]</sup> while Lowe et al.<sup>[33]</sup> and Schneider et al.<sup>[37]</sup> both found the transformation to amorphous sulfur instead. Such transformation phenomena probably result from the metastable nature of  $\beta$ -S<sub>8</sub>, although the phase in equilibrium might be different due to the detailed chemical environment.

According to the above in situ XRD results, it is generally agreed that phase evolution of sulfur cathode occurs in the following way:

- At the first discharge,  $\alpha$ -S<sub>8</sub> is reduced to soluble polysulfides on the upper discharge plateau, and Li<sub>2</sub>S nanocrystals form at some point of the lower discharge plateau.

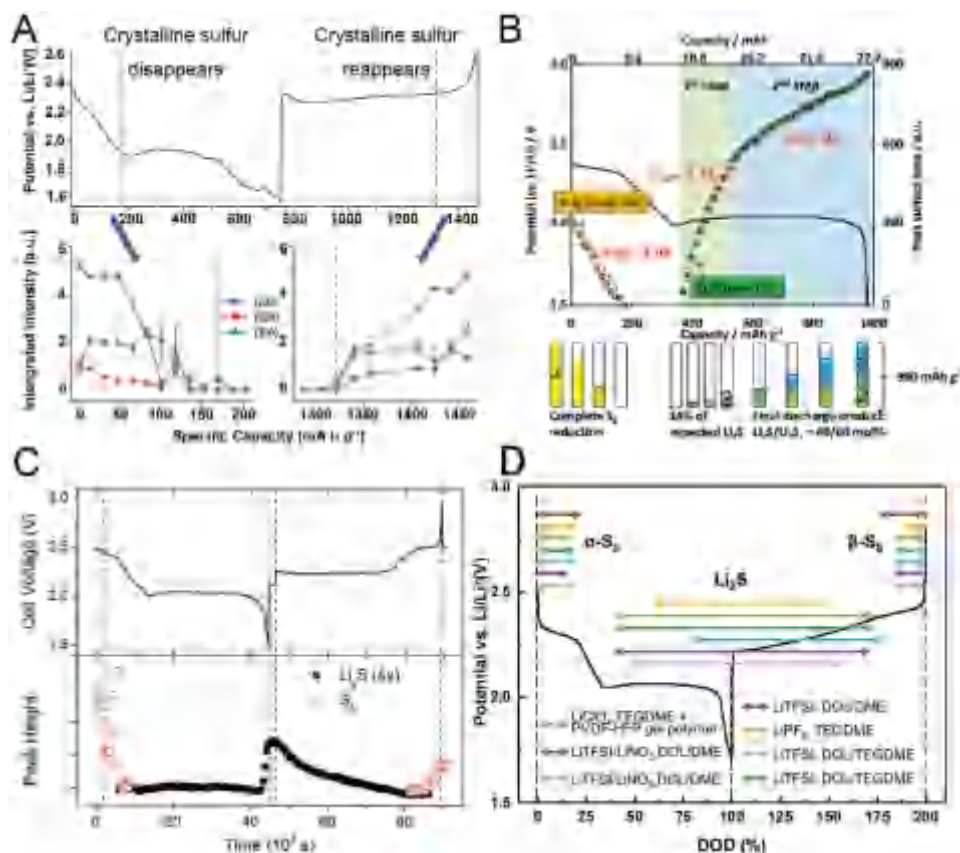


**Figure 3.** Identification of solid species: in operando XRD. A) Integrated diffraction-peak intensities of elemental sulfur for a Li–S cell cycled at C/8, and the corresponding voltage profile. Adapted with permission.<sup>[32]</sup> Copyright 2012, American Chemical Society. B) Integrated surface area of the most intense peaks during the first discharge with the galvanostatic voltage profile. The change in slope of  $\text{Li}_2\text{S}$  formation was accounted by the reaction of  $\text{Li}_2\text{S}$  and long-chain polysulfides to form  $\text{Li}_2\text{S}_2$ . Reproduced with permission.<sup>[35]</sup> Copyright 2015, Wiley-VCH. C) Evolution of integrated peak area for  $\text{S}_8$  and  $\text{Li}_2\text{S}$  upon the first cycle. Reproduced with permission.<sup>[33]</sup> Copyright 2014, Royal Society of Chemistry. D) Detection of  $\text{S}_8$  and  $\text{Li}_2\text{S}$  from different in situ XRD studies, from top to bottom (red to gray): ref. [32], ref. [38], ref. [34], ref. [35], ref. [33], ref. [36], and ref. [37].

- Upon the first charge,  $\text{Li}_2\text{S}$  is consumed and sulfur is recovered as  $\beta\text{-S}_8$ , which continues to exist in the following cycles.

The onset DOD for  $\text{Li}_2\text{S}$  crystallization, however, is still controversial. A similar contradiction also exists among results from other characterization techniques. For example, Grey and co-workers observed the formation of a  $\text{Li}^+$ -containing solid at the very beginning of discharge using  $^7\text{Li}$  NMR,<sup>[39]</sup> whereas Huff et al. demonstrated that  $\text{Li}_2\text{S}$  is produced near the end of discharge using  $^6\text{Li}$  and  $^{33}\text{S}$  magic-angle-spinning (MAS) NMR.<sup>[40]</sup> This discrepancy may arise from: i) different recipes for preparing the electrodes and electrolytes, ii) various operational and instrumental parameters, and iii) the intrinsic complexity of Li–S reactions. The periods during which crystalline phases were detected in related references are summarized in Figure 3D.

Considering the questions mentioned at the beginning of this section, for the first one, XRD alone may not be sufficient as it is not capable of detecting amorphous solid. Regarding the second question,  $\text{Li}_2\text{S}_2$  has sometimes been suggested as another solid product of discharge,<sup>[41,42]</sup> yet little experimental evidence of its existence has been reported.<sup>[43]</sup> The presence of

solid-state  $\text{Li}_2\text{S}_2$  has seldom been confirmed by in situ XRD, although it was proposed by Waluś et al. to account for a two-step formation of  $\text{Li}_2\text{S}$  (Figure 3B).<sup>[35]</sup> XRD patterns of chemically synthesized lithium polysulfides have proved that  $\alpha\text{-S}_8$  and  $\text{Li}_2\text{S}$  are the only stable crystalline phases among all  $\text{Li}_2\text{S}_n$ .<sup>[44]</sup>  $^7\text{Li}$  NMR and density functional theory (DFT) calculation further disproved the formation of solid  $\text{Li}_2\text{S}_2$ .<sup>[39]</sup> Therefore,  $\text{Li}_2\text{S}_2$  possibly exists as a transient species rather than a stable end product.<sup>[43,45]</sup> For the last question, crystalline  $\text{S}_8$  and  $\text{Li}_2\text{S}$  have been verified to undergo complete consumption during cycling, although the possible existence of amorphous  $\text{S}_8/\text{Li}_2\text{S}$  after full discharge/charge cannot be ruled out. Indeed, armed with in situ X-ray absorption near-edge structure (XANES) spectra and a full series of reference spectra ( $\alpha\text{-S}_8$ ,  $\text{S}_6^{2-}$ ,  $\text{S}_4^{2-}$ ,  $\text{S}_2^{2-}$ ,  $\text{Li}_2\text{S}$ ), Cuisinier et al. found that 20% of the original  $\text{S}_8$  remained, even at 100% DOD, but  $\text{Li}_2\text{S}$  was not detected after full charge.<sup>[44]</sup>

### 3.2. Liquid Intermediates

As intermediate products of sulfur reduction, polysulfides play a vital role in Li–S electrochemistry. Hence, identification

and quantification of polysulfide species are critical for understanding of the reaction routes and enhancing the battery performance. Considerable efforts have been devoted to the characterization of various lithium polysulfides in solution or the solid state. However, isolation and identification of any individual lithium polysulfide are very difficult, because multiple species in complex equilibrium coexist in chemically prepared stoichiometric polysulfide solutions, and dry powders derived from these solutions usually consist of  $S_8$ ,  $Li_2S$ , and some unknown amorphous phases.<sup>[39,44]</sup>

Solid-state lithium polysulfides have been considered to be amorphous, as Cuisinier et al. demonstrated in the XRD patterns of polysulfides prepared by reducing sulfur with lithium triethylborohydride in tetrahydrofuran (THF).<sup>[44]</sup> However, later work by Xu et al. suggested a new crystalline phase in  $Li_2S_n$  powders obtained from reacting  $Li_2S$  and sulfur in DME.<sup>[46]</sup>  $^7Li$  MAS NMR was also employed in the characterization of polysulfide powders, which revealed two chemical environments for lithium nuclei in all lithium polysulfides except two end members:  $Li_2S$  and  $Li_2S_8$ .<sup>[47]</sup> The peak at low field (chemical shift  $\approx 2.5$  ppm) corresponds to lithium in  $Li_2S$  crystals; whereas the other peak (chemical shift  $\approx 1.0$  ppm) can be roughly attributed to polymeric  $Li_2S_n$  domains.<sup>[44,47]</sup> Slightly different from these results, Cuisinier et al. found only one single peak at  $\approx 1.0$  ppm for  $Li_2S_6$  but two peaks for  $Li_2S_8$ , as shown in Figure 4A.<sup>[44]</sup> MAS NMR is preferred as it provides higher resolution and narrower peaks, especially for solid samples, which suffer from severe peak broadening because of strong dipolar

coupling (Figure 4B).<sup>[48]</sup> These studies have made us aware that solid lithium polysulfides are a mixture of two or more phases. Nevertheless, further study is still necessary to analyze their composition and structure in detail.

Dissolved polysulfides, instead of dry powders, are considered more frequently since they are actual redox intermediates in working Li-S cells. Many studies on the speciation of polysulfide anions and radicals in an organic electrolyte have been realized, utilizing various characterization techniques such as NMR,<sup>[39,40,44,47,48]</sup> X-ray absorption spectroscopy (XAS),<sup>[33,44,47,49–55]</sup> UV-vis spectroscopy,<sup>[56–61]</sup> Raman spectroscopy,<sup>[62–66]</sup> liquid chromatography–mass spectrometry (LC-MS),<sup>[56,61,67,68]</sup> and electron paramagnetic resonance/electron spin resonance (EPR/ESR).<sup>[69–71]</sup> Some enlightening results revealed by these techniques will be briefly introduced in this section, together with their features, applications, and limitations.

### 3.2.1. NMR

Both  $^7Li$  and  $^6Li$  NMR are capable of distinguishing lithium nuclei in soluble polysulfides from those in solid  $Li_2S$ . Contrary to solid samples, solution NMR always shows a single peak in the range of  $-1$  to  $0.2$  ppm, and the position of this peak depends on the concentration, the chain lengths, and the composition of electrolytes (Figure 4C,D).<sup>[39,47]</sup> Fast exchange between solvated  $Li^+$  and  $Li^+$  bonded with  $S_n^{2-}$  may account for the merging of NMR signals from lithium salts and different lithium polysulfides.<sup>[71]</sup>

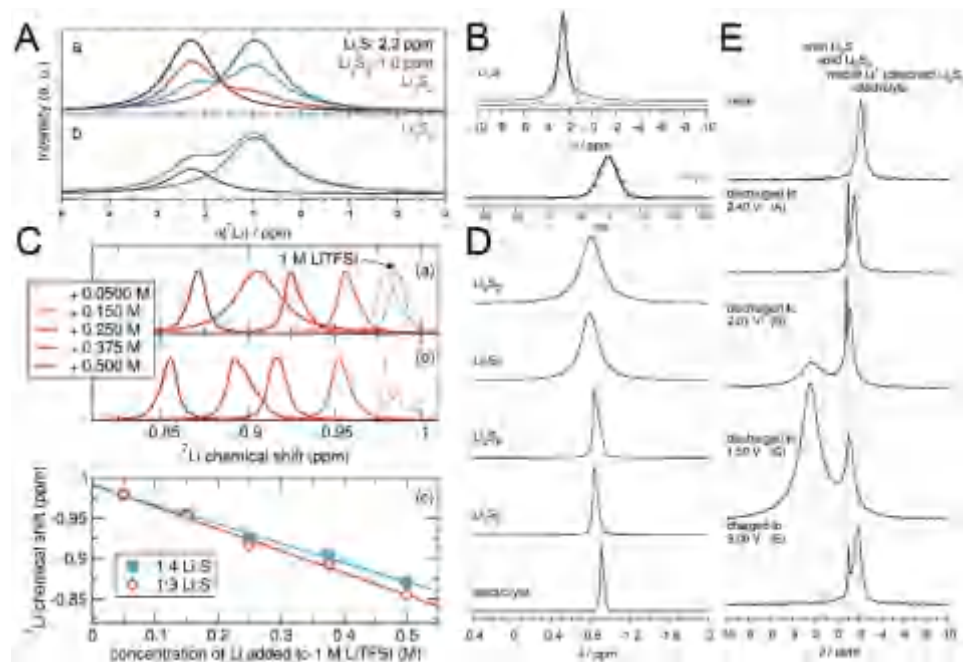


**Figure 4.** Identification of liquid species: NMR. A)  $^7Li$  MAS NMR of the synthesized solid lithium (poly)sulfides and two-component ( $Li_2S$  and  $Li_2S_6$ ) fitting for  $Li_2S_8$ . Reproduced with permission.<sup>[44]</sup> Copyright 2013, American Chemical Society. B) Comparison of MAS NMR (upper) and regular NMR (lower) spectra of solid  $Li_2S$ . Upper: Reproduced with permission.<sup>[47]</sup> Copyright 2014, Wiley-VCH; Lower: Reproduced with permission.<sup>[48]</sup> Copyright 2015, American Chemical Society (reproduced from the Supporting Information). C) Solution  $^7Li$  NMR spectra of varying concentrations of  $Li_2S_n$  in an electrolyte with 1.0 M LiTFSI in DOL/DME, (a) and (b) correspond to  $Li_2S_8$  and  $Li_2S_6$ , respectively. Reproduced with permission.<sup>[39]</sup> Copyright 2014, American Chemical Society. D) Solution  $^7Li$  NMR spectra of lithium polysulfides in sulfolane electrolyte with 1.0 M LiTFSI. E) Ex situ  $^7Li$  MAS NMR of cathodes at different cell potential. D,E) Reproduced with permission.<sup>[47]</sup> Copyright 2014, Wiley-VCH.

See et al.<sup>[39]</sup> and Patel et al.<sup>[47]</sup> found that the lithium nuclei resonance shifted to a higher frequency as the sulfur chain length decreased and the concentration increased. However, due to the large influence of the concentration and the vicinity of the chemical shifts of different polysulfide species, it is not yet possible to differentiate them from each other. Therefore, in situ and ex situ NMR studies have mainly used NMR to detect all soluble polysulfides together.<sup>[39,40,47]</sup> Polysulfides were detected during the whole process of charge and discharge, indicating that low capacity partly resulted from the incomplete conversion of  $\text{Li}_2\text{S}_n$  (Figure 4E).<sup>[39,47]</sup>  $^{33}\text{S}$  NMR has seldom been used in probing lithium polysulfides because of the low natural abundance (0.76%), large quadrupole moment, and low receptivity of  $^{33}\text{S}$ .<sup>[40]</sup>

### 3.2.2. XAS

XAS is a promising method for Li–S-battery investigation. It is performed with synchrotron radiation sources possessing appropriate energy. The spectrum of XAS can generally be divided into three parts: the pre-edge, XANES, and the extended X-ray absorption fine structure (EXAFS). XANES is also known as near-edge X-ray absorption fine structure (NEXAFS). XANES is often used in the study of Li–S batteries, since it corresponds to the excitation of inner-core electrons from lower-energy occupied orbitals to higher-energy

free orbitals, and reflects the electronic state of the atoms. Unlike XRD, XANES reveals atomic information and therefore does not require the sample to be crystalline. XANES helps to decide the chemical states of each component, in which the sulfur K-edge spectrum is the mostly widely employed to identify different sulfur-containing species.<sup>[33,44,47,49–55]</sup> Polysulfide dianions exhibit a pre-peak at around 2470.5 eV in addition to the characteristic “white line” of elemental sulfur at 2472.5 eV, which differs clearly from those of crystalline  $\text{Li}_2\text{S}$  (doublets at 2474 and 2476 eV).<sup>[33,47,49–53,55]</sup> The peak position might be slightly displaced from the above values as different standard materials were used for energy calibration.<sup>[44,54]</sup> Both experimental and theoretical investigations have shown that the spectra of  $\text{S}_n^{2-}$  are dependent on the sulfur chain length: the area ratio between two peaks (main peak/pre-peak) grows almost linearly with the increasing chain length.<sup>[47,51]</sup> Using first-principles calculations, Pascal et al. determined that the pre-peak is mainly contributed by  $\text{S}_T$  atoms, while the main peak is due to other  $(n - 2)$  bridge sulfur atoms in the chain (Figure 5A).<sup>[51]</sup> Divergence exists upon the spectrum of  $\text{S}_2^{2-}$ : a single peak at 2471 eV was expected according to simulation; yet two peaks were observed for chemically synthesized  $\text{Li}_2\text{S}_2$  solid,<sup>[47]</sup> suggesting its tendency towards disproportionation. Besides, sodium polysulfides have frequently been utilized as alternative reference materials due to the instability of lithium polysulfides. XAS spectra of  $\text{Na}_2\text{S}_n$  follow the same trend

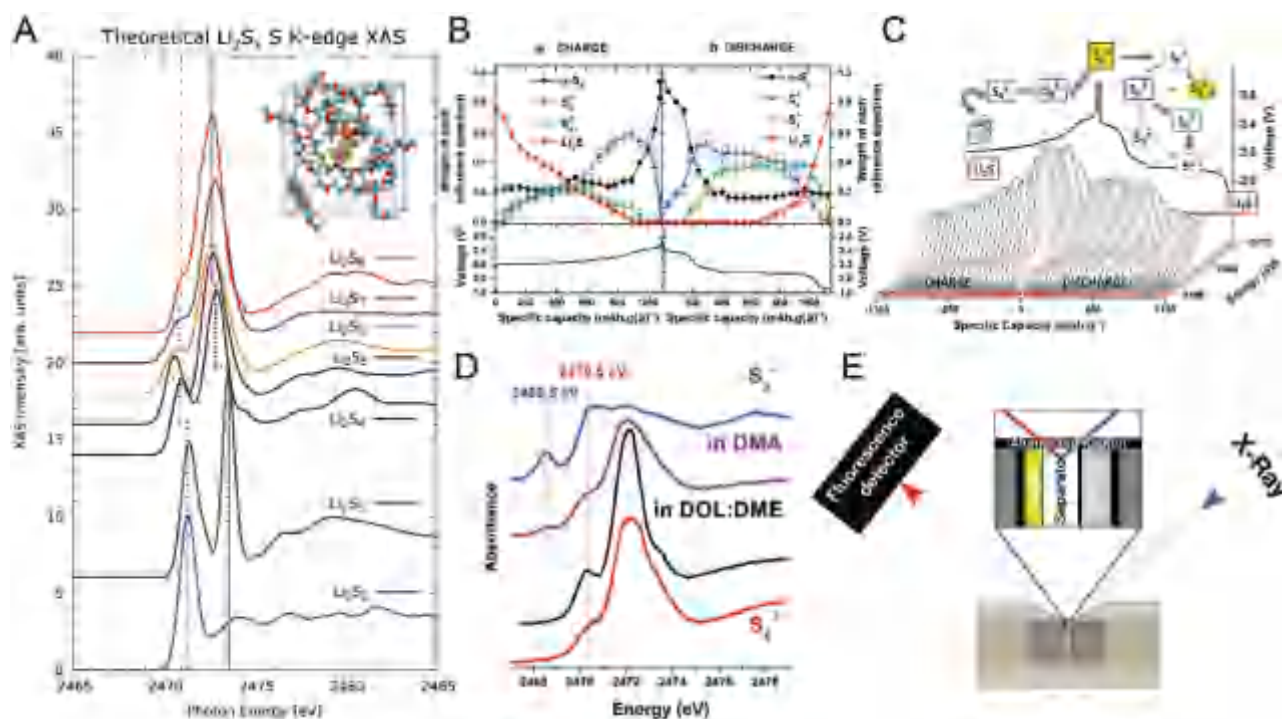


**Figure 5.** Identification of liquid species: XANES. A) First-principles simulation of the sulfur K-edge XAS spectra of  $\text{Li}_2\text{S}_n$  dissolved in TEGDME. Reproduced with permission.<sup>[51]</sup> Copyright 2014, American Chemical Society. B) Linear combination fitting of sulfur K-edge XANES upon galvanostatic cycling, using four reference materials ( $\text{S}_8$ ,  $\text{S}_6^{2-}$ ,  $\text{S}_4^{2-}$ , and  $\text{Li}_2\text{S}$ ). C) In operando XANES during one galvanostatic cycle and the proposed reaction mechanism for Li–S batteries. B,C) Reproduced with permission.<sup>[44]</sup> Copyright 2013, American Chemical Society. D) Experimental XANES around  $340 \text{ mA h g}^{-1}$  for Li–S cells using DMA vs DOL/DME electrolytes, with  $\text{S}_3^{2-}$  and  $\text{S}_6^{2-}$  as references. Reproduced with permission.<sup>[53]</sup> Copyright 2015, Wiley-VCH. E) A novel setup for in situ XANES that allows detection of X-ray fluorescence from all layers in the cell. Reproduced with permission.<sup>[55]</sup> Copyright 2015, The Electrochemical Society.

as  $\text{Li}_2\text{S}_n$ , although the peaks are broader than  $\text{Li}_2\text{S}_n$ .<sup>[47]</sup> The experimentally acquired spectrum of  $\text{Na}_2\text{S}_2$  perfectly resembled the single-peak feature of the calculated  $\text{Li}_2\text{S}_2$  spectrum, which reflects the higher stability of sodium polysulfides.<sup>[44,47]</sup>  $\text{S}_n^{\bullet-}$  radicals have significantly different properties from polysulfide dianions. Although highly reactive and short-lived, the  $\text{S}_3^{\bullet-}$  radical has been proposed in many mechanisms as a result of  $\text{S}_6^{2-}$  cleavage.<sup>[53,71]</sup> The stabilized  $\text{S}_3^{\bullet-}$  radical in ultramarine pigment exhibited in a characteristic pre-peak at 2468.5 eV,<sup>[72]</sup> which has been used to identify  $\text{S}_3^{\bullet-}$  in Li–S batteries.

Equipped with the tools mentioned above, researchers have been able to interpret the in operando XANES spectra of Li–S batteries. The appearance of large amounts of  $\text{S}_3^{\bullet-}$  (>20% of the total sulfur) in dimethyl acetamide (DMA) solvent was confirmed unambiguously,<sup>[53,55]</sup> whereas its concentration was not measurable by XANES (<<5%) in glyme or gel polymer electrolyte (Figure 5B–D).<sup>[52,55]</sup> It should be noted that polysulfide dissociation may occur during cell storage, since  $\text{S}_3^{\bullet-}$  radical formation could be observed in a cell that was rested for three days using a polystyrene–poly(ethylene oxide) copolymer electrolyte.<sup>[49]</sup> DFT calculation has also suggested that the dissociation reaction of  $\text{S}_6^{2-}$  is thermodynamically favorable.<sup>[71]</sup> Solvents with high donor number (DN) and dielectric constant ( $\epsilon$ ), like DMA, dimethyl sulfoxide (DMSO), and dimethyl formamide (DMF), not only stabilize  $\text{S}_3^{\bullet-}$  free radicals, but also significantly alter the reaction routes of Li–S batteries. Compared with cells using conventional ether-based electrolyte (DOL/DME or TEGDME), cells using DMA can be characterized by a three-plateau feature.<sup>[53]</sup> Reduction of short-chain polysulfides ( $\text{S}_{3-4}^{2-}$ ) is decoupled from the precipitation of  $\text{Li}_2\text{S}$ , probably due to the higher stability of  $\text{S}_{3-4}^{2-}$ , which postpones the deposition. However, side reactions between DMA and metallic lithium render a poor capacity, large overpotential, and low Coulombic efficiency.<sup>[55]</sup> Nazar and co-workers overcame this disadvantage by using a TEGDME electrolyte at the anode side, and achieved a high discharge capacity of 1580 mA h g<sup>-1</sup>, indicating a more thorough utilization of sulfur in the DMA electrolyte.<sup>[53]</sup>

When performing in situ XANES analysis, several aspects should be considered: i) the structure of the operando cell, ii) the influence of lithium salt on the spectra, and iii) the methods for analyzing the data. The relatively weak interaction between the high-energy photons and matter makes XANES a bulk-sensitive technique.<sup>[52]</sup> However, the penetration depth of incident X-rays ranges from several to tens of micrometers,<sup>[32,47]</sup> which may not be enough to go through the entire cathode and separator layers. A smart cell design with the X-ray window on the side of cell was presented by Gorlin et al. to ensure that the data could be collected from the entire depth of the cathode and separator (Figure 5E).<sup>[55]</sup> Commonly used LiTFSI has a strong peak at 2478 eV,<sup>[47,54]</sup> which adds to the difficulty of interpreting XANES spectra. Thus, lithium perchlorate ( $\text{LiClO}_4$ ), instead of LiTFSI, has been mostly employed for in situ XANES, and this substitution was proved to have only a minor effect on the electrochemical behavior.<sup>[33,49,50,53,55,72]</sup> Although a complete set of polysulfide spectra has been available for several years, quantitative analysis of data from working cells still involves no more than two kinds of polysulfide dianions (Figure 5B).<sup>[44,47,53,54]</sup> Such a limitation arises from the overlapping of their peaks. In contrast, sulfur,  $\text{Li}_2\text{S}$ , and  $\text{S}_3^{\bullet-}$  can be well separated and

quantified using linear curve fitting and/or principle-component analysis.<sup>[52]</sup> It is also worth mentioning that energy calibration should be unified to avoid confusion in peak attribution.

### 3.2.3. UV–Vis Spectroscopy

The excitation of electrons from the highest occupied molecular orbital (HOMO) to the lowest unoccupied molecular orbital (LUMO) of  $\text{Li}_2\text{S}_n$  clusters induces a series of absorption bands in the UV–vis region. Therefore UV–vis spectroscopy is also widely used for polysulfide speciation. Traditionally, UV–vis spectroscopy is coupled with electrochemical tools to analyze solution-based electrochemical reactions. Numerous spectro-electrochemical studies have been conducted using inert electrodes and transmission-mode spectroscopy to monitor the reaction of  $\text{S}_8$  dissolved in many kinds of solvent.<sup>[73–77]</sup> Combining these studies with DFT calculation, consensus has been achieved about the origin of some absorption bands of the polysulfide solution. Elemental sulfur exhibits strong absorption below 300 nm;<sup>[56,59]</sup> other absorption bands in the range of 350 to 500 nm result from polysulfide dianions; the  $\text{S}_3^{\bullet-}$  radical has a characteristic band around 620 nm (Figure 6A–C).<sup>[56,59–61]</sup> Generally, longer-chain polysulfides tend to have stronger absorption at larger wavelength. For example, the absorption band with the largest wavelength is around 500 nm in the spectrum of  $\text{Li}_2\text{S}_8$ , whereas it is 400 nm for  $\text{Li}_2\text{S}_4$ . These studies are important for establishing the reaction routes of the  $\text{S}_8$  reduction. Nevertheless, in situ measurement of the transmitted light poses a limit on the total concentration of sulfur, because the solubility of  $\text{S}_8$  in common electrolyte (glyme-based, DMSO, DMF, etc.) is usually below 20 mmol L<sup>-1</sup>.<sup>[68]</sup>  $\text{S}_8$  must be dissolved in the electrolyte since a suspension is not suitable for transmission-mode UV–vis spectroscopy. As a result, the setup of these spectro-electrochemical cells may differ from the practical Li–S cells. To analyze the normal Li–S batteries, ex situ UV–vis experiments have also been conducted.<sup>[56,59,61]</sup> However, the post-mortem processing of a charged/discharged cathode may influence the equilibrium of polysulfides: i.e., cathodes have to be washed with pure solvent to dilute the resulting solution to a concentration suitable for measurement. To obtain the in situ UV–vis spectra of a practical Li–S cell, reflection-mode was adopted by Dominko and co-workers.<sup>[57,58]</sup> Quantitative analysis was realized by calibrating the spectra of chemically synthesized lithium polysulfide solutions. Meanwhile, the designation of absorption peaks (in the first-order derivative spectra) is quite hard due to the lack of knowledge about the reflection spectra of polysulfides.

### 3.2.4. Raman Spectroscopy

Different from XANES and UV–vis spectroscopy, Raman spectroscopy detects the changes in vibrational energy levels. The Raman response of polysulfide ions can be theoretically predicted by DFT calculation.<sup>[63,64]</sup> Typically, Raman shifts (fundamental frequency) of polysulfide dianions and radicals are all below 550 cm<sup>-1</sup>.<sup>[63]</sup> The number of peaks increases with increasing chain length, as there are more vibrational

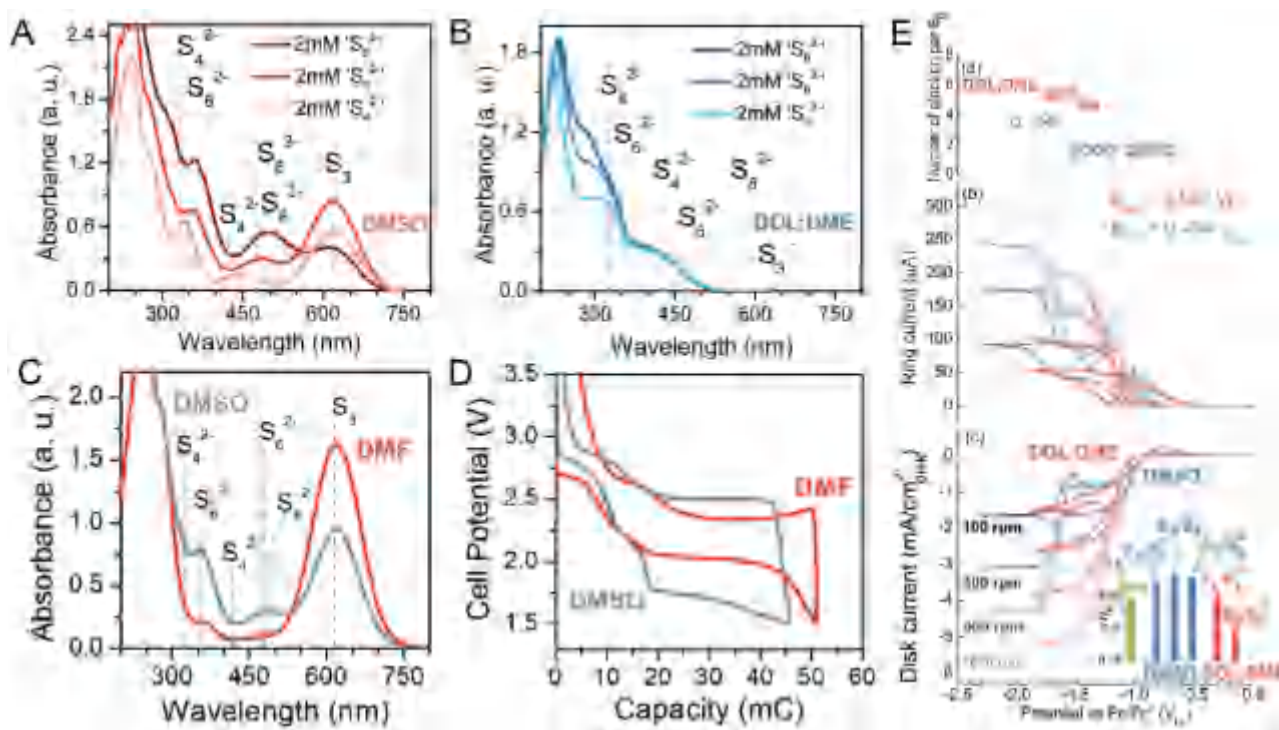


**Figure 6.** Identification of liquid species: A,B) UV-vis spectroscopy. UV-vis spectra of  $2.0 \times 10^{-3}$  M chemically synthesized nominal  $S_n^{2-}$  in DMSO (A) and DOL/DME (B) solvents. C) Comparison of UV-vis absorption spectra of  $2.0 \times 10^{-3}$  M nominal  $S_6^{2-}$  in DMSO vs DMF. D) Voltage profiles of Li-S cell consisting of  $10 \mu\text{L}$  of  $4.0 \times 10^{-3}$  M  $S_8$  in DMSO or DMF electrolytes at 1 C ( $17 \mu\text{A}$ ). A–D) Reproduced with permission.<sup>[60]</sup> Copyright 2016, American Chemical Society. E) RRDE experiments of  $4.0 \times 10^{-3}$  M  $S_8$  dissolved in DMSO and DOL/DME solvents. From top to bottom: a) Number of electrons transferred during the reduction of  $S_8$ ; b,c) ring (b) and disk (c) current recorded at  $50 \text{ mV s}^{-1}$  in  $4 \times 10^{-3}$  M  $S_8$  solution in 0.2 M  $\text{LiClO}_4$ -DMSO (blue) and 1.0 M  $\text{LiTFSI}$ -DOL/DME (red) at different rotation rates while holding the gold ring electrode at constant potential. Inset: geometric and the average collection efficiency of different reactions in two electrolytes. Reproduced with permission.<sup>[127]</sup> Copyright 2014, American Chemical Society.

modes for longer chains; but there is no obvious trend in the wavelength of these peaks. In many cases, in situ and ex situ Raman spectra were able to capture the peaks of  $S_8$  ( $150$ ,  $220$ , and  $470 \text{ cm}^{-1}$ ) and long-chain polysulfide dianions like  $S_8^{2-}$  and  $S_6^{2-}$  ( $\approx 400 \text{ cm}^{-1}$ ), but failed to detect shorter ones like  $S_3^{2-}$  and  $S_2^{2-}$ .<sup>[62–66,78]</sup> Inconsistency around the identification and attribution of some peaks could happen between studies from different groups, because many peaks from the different polysulfides are overlapped with each other. Therefore, quantification of different polysulfides has not been available for in situ Raman spectroscopy until now. Contrarily, the peak position of the  $S_3^{\cdot-}$  radical ( $525$ – $535 \text{ cm}^{-1}$ ) is highly consistent in most theoretical and experimental studies.<sup>[62,63,66]</sup>

### 3.2.5. LC-MS

The combination of LC and MS is probably the most effective way to distinguish polysulfide ions with different chain lengths. Retention time on reverse-phase high-performance LC increases monotonically with the chain length of polysulfide dianions.<sup>[56,61,67]</sup> From MS analysis, the exact species corresponding to each peak in LC can be specified.<sup>[61]</sup>  $S_8$  cannot be separated from  $\text{Li}_2S_8$  in this method and  $\text{Li}_2S$  may not be detected since it is insoluble,<sup>[56]</sup> however, all other polysulfides can be quantitatively analyzed without uncertainty.<sup>[61]</sup>

To prevent the composition from being affected by spontaneous disproportionation reactions,<sup>[67]</sup> lithium polysulfides were chemically converted to much more stable methylated/benzylated polysulfides.<sup>[56,61]</sup> In this manner, Kawase et al. successfully determined the amount of every individual polysulfide species (including  $\text{Li}_2S$ ) and proposed a detailed mechanism for charge/discharge of Li-S batteries: the higher plateau is related to a reduction of  $S_8$  and other long-chain polysulfides, whereas the lower plateau is dominated by the reduction of  $S_3^{2-}$  to  $S_2^{2-}$  and  $S^{2-}$  and discharge ceases when  $\text{Li}_2S_2$  is further reduced to  $\text{Li}_2S$  (Figure 7).<sup>[61]</sup> Despite of the great advantages in speciation of polysulfides, LC and MS are intrinsically ex situ techniques and are not capable of detecting unstable radicals.

As discussed above, the real-time identification and quantification of all polysulfide species in a working Li-S cell are so challenging, that no such work is available yet. Commonly, only several representative species are selected to be identified and quantified. Based on these studies, a general discharge reaction process of Li-S batteries can be constructed:

- The higher plateau is related to  $S_8$  reduction to long-chain polysulfides ( $S_8^{2-}$  and  $S_6^{2-}$ ).
- The slope between the two plateaus is mainly associated with the formation of  $S_4^{2-}$ .
- The lower plateau is dominated by the reduction to  $S_2^{2-}$  and  $\text{Li}_2S$ .

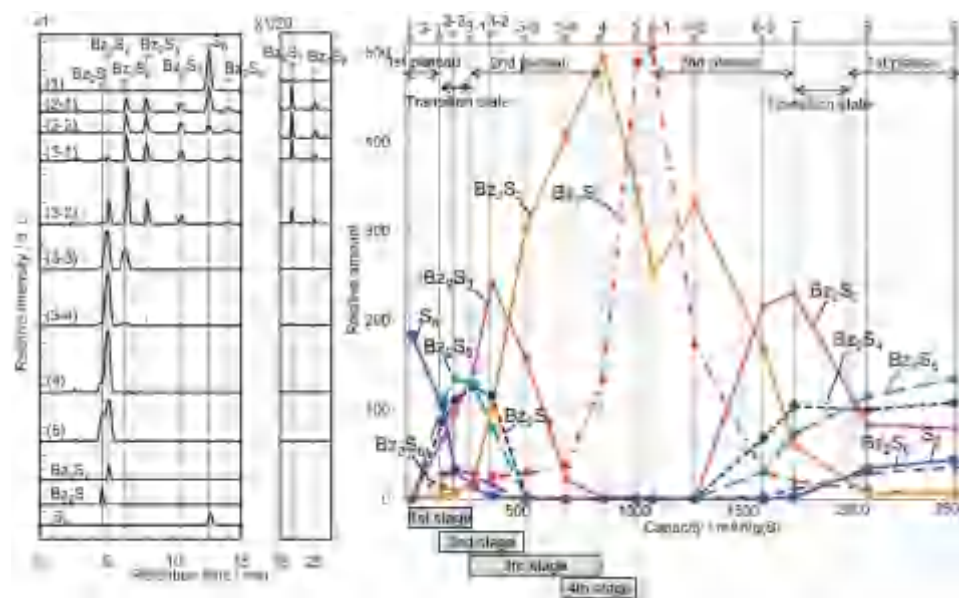


**Figure 7.** Identification of liquid species: LC-MS. LC-MS results at different stages of cell discharge/charge. Left: LC data; Right: relative quantity of benzylated polysulfides ( $Bz_2S_n$ ) as estimated from LC data. Reproduced with permission.<sup>[61]</sup> Copyright 2014, Royal Society of Chemistry.

In principle, multiple electrochemical and chemical reactions always occur concurrently in the discharge of a Li-S battery. Many studies have suggested that the higher plateau mainly involves electrochemical reduction of  $S_8$  and long-chain polysulfides, while the lower plateau proceeds through chemical dissociation of polysulfides to deposit  $Li_2S$ .<sup>[33,44,56,60]</sup> Consequently, the higher plateau exhibits fast kinetics and low polarization and the lower plateau is limited by chemical steps, with partially reduced polysulfides at the end of discharge.

Besides the intensively considered polysulfide dianions, the  $S_3^{\bullet-}$  radical has gained special attention because of its relatively high stability among polysulfide radicals and its ubiquitous presence in the environment.<sup>[79,80]</sup> Interestingly,  $S_3^{\bullet-}$  radicals usually give out a characteristic signal (2468.5 eV in XANES, 620 nm in UV-vis,  $525\text{ cm}^{-1}$  in Raman spectra) due to its unique structure, which makes it much easier to identify than any polysulfide dianions. Moreover, EPR/ESR provides undoubted evidence of the existence of  $S_3^{\bullet-}$  radicals in both high-DN (DMSO) and low-DN solvents (DOL/DME and TEGDME).<sup>[56,69-71]</sup> The amount of  $S_3^{\bullet-}$ , however, cannot be inferred from EPR results.  $S_3^{\bullet-}$  has been suggested to act as an internal redox mediator,<sup>[53,81]</sup> much like superoxide radicals ( $O_2^{\bullet-}$ ) in Li- $O_2$  batteries.<sup>[82-84]</sup> Nevertheless, the detailed reaction and role of  $S_3^{\bullet-}$  in Li-S chemistry are not clear yet, and need to be further explored.

Comparison of the characterization capabilities and limitations has been systematically summarized by Wild et al. in their review.<sup>[81]</sup> In addition to their summary, we would like to make the following comments:

- In situ techniques are preferable, but care must be taken to ensure a similar electrochemical behavior between the characterized and common cells.

- Most spectroscopic tools (except LC and MS) can be carried out at in situ mode, but ex situ characterization may also play an important role such as reference or standard.
- Special attention should be paid to the configuration of in situ cells, so that the penetration length of incident light can be long enough to reach the desired zone for characterization.
- Charge may proceed in a different path from that of discharge in Li-S batteries (the charge mechanism will be discussed in Section 4.4).
- The results of any characterization techniques are probably sensitive to many factors, like electrolyte/cathode composition, sulfur loading, electrolyte/sulfur (E/S) ratio, etc.
- Considering the limitations of every single technique, combinatorial characterization methods and appropriate cell design are needed to offer further insight into the entire reaction mechanism of the Li-S system.

To summarize, we list the characteristic peaks in UV-Vis and Raman spectra of various sulfur-containing species from different studies in **Table 1** and **2**), as a reference for future studies in this field.

#### 4. Electrochemical Reactions

Numerous novel anode structures, cathode materials, and electrolyte recipes have been proposed for improving the overall performance of Li-S batteries. The capacity, cycling stability, and rate capability can be solely evaluated by standard galvanostatic discharge/charge. However, more studies should be devoted to elucidating the detailed mechanism behind the improvement of the cell performance. Hence, the effect of the electrolyte and the cathode host materials on the electrochemical reactions in Li-S batteries are elaborated in this section.

**Table 1.** Summary of absorption peak positions in UV–Vis spectra of  $S_8$ , polysulfide dianions and radicals.

Detection mode	Ref No.	Solvent	Peak wavelength [nm]								
			$S_8$	$S_8^{2-}$	$S_7^{2-}$	$S_6^{2-}$	$S_5^{2-}$	$S_4^{2-}$	$S_3^{2-}$	$S_2^{2-}$	$S_3^{\cdot-}$
Transmission	[56]	TEGDME/DOL	280	560		470	450	420	340	265	617
	[59]	TEGDME	265					425			615
	[61]	DME		430				400			610
	[60]	DOL/DME		560		470, 350		420, 320			617
		DMSO		492		475, 350		420, 325	270		617
	[76]	DMSO		492		475		420			
	[74]	DMSO		490		450					610
	[73]	DMSO				505		435			
	[77]	DMF		490	470	450, 340	435	420	334	280	600
Reflection (1st derivative)	[57]	Sulfolane		572	567	555	536	513	494	479	
	[57]	Sulfolane		580	570	550	530	510	490	470	
	[57]	TEGDME/DOL		620	620	600	580	560	530	450, 520	

#### 4.1. Electrolyte Effect on Li–S Discharge Reactions

With a general concept of sulfur species and their properties, it is easy to understand the effect of the electrolyte composition on the behavior of sulfur cathode. This section gives an introduction to the methods for investigating the stability, and the interfacial and kinetic behaviors of various electrolytes. Several electrochemical techniques for measuring the kinetic properties of an electrolyte are highlighted. Regular electrochemical tests, such as galvanostatic discharge/charge, CV, and electrochemical impedance spectra (EIS) have been discussed in many studies,<sup>[81,85]</sup> and therefore will not be specially introduced here. Common types of solvents, salts, and additives for Li–S batteries, as well as some special electrolyte recipes are also briefly discussed.

##### 4.1.1. Stability and Interfacial Behaviors

*Spectroscopic Tools for Investigating Electrolyte Stability:* So far, the stability of different solvents can be analyzed by both theoretical calculation and experimental characterization of their decomposition products. An acceptable electrolyte should be at least stable to both electrodes during repeated cycling, and have sufficient  $Li^+$  ionic conductivity. From this point of view, carbonate solvents (e.g., ethylene carbonate, propylene carbonate, diethyl

carbonate, etc.), which are prevalent in commercial LIBs, are not suitable for Li–S systems. Through XANES, NMR, Fourier transform infrared (FTIR) spectroscopy, gas-chromatography (GC) analysis, and DFT computation, it has been found that nucleophilic polysulfide anions attack either the carbonyl-C atom or the ethereal-C, and cause the decomposition of carbonate.<sup>[50,86–88]</sup> Recently, the stability of ethylene carbonate toward lithium metal was also theoretically proved to be lower than ether solvents, because of its lower LUMO energy level than ether.<sup>[89]</sup> However, it is safe to use carbonate electrolyte when sulfur is strictly restrained in the quasi-solid-state so that the formation of polysulfides and their contact to carbonate are completely inhibited. To meet this demand, sulfur can either be confined in sub-nanometer micropores of carbon,<sup>[28,90–92]</sup> or covalently bound to conductive polymer (like polyacrylonitrile),<sup>[93–95]</sup> functionalized graphene,<sup>[96]</sup> etc.

Ether solvents are conventionally used for Li–S batteries due to their compatibility with sulfur cathodes and, in particular, polysulfides. Linear ethers, such as glyme (G1, i.e., DME), diglyme (G2), triglyme (G3), tetraglyme (G4, i.e., TEGDME), and poly(ethylene glycol) dimethyl ether, as well as cyclic ethers, usually DOL, are applied as either a single solvent or a part of mixed solvents.<sup>[19,97,98]</sup> DME and TEGDME are used much more frequently than G2 and G3, probably because DME has the lowest viscosity and TEGDME has the strongest solvating ability. DOL is preferred owing to its unique role at

**Table 2.** Summary of peak positions in Raman spectra of  $S_8$ ,  $Li_2S$ , polysulfide dianions and radicals.

	Ref No.	Solvent	Raman shift [ $cm^{-1}$ ]									
			$S_8$	$S_8^{2-}$	$S_7^{2-}$	$S_6^{2-}$	$S_5^{2-}$	$S_4^{2-}$	$S_3^{2-}$	$S_2^{2-}$	$Li_2S$	$S_3^{\cdot-}$
Ex situ	[65]	TEGDME/DOL	156, 221, 473		280, 410, 450, 746 ( $S_4^{2-}$ to $S_8^{2-}$ )						378	535
	[78]	DOL/DME	152, 218, 470		400 ( $S_6^{2-}$ to $S_8^{2-}$ )							
In situ	[64]	DOL/DME	154, 220, 474		340–420 ( $S_6^{2-}$ to $S_8^{2-}$ )		420–480 ( $S_3^{2-}$ to $S_5^{2-}$ )		200, 148			535
	[63]	TEGDME/DOL			429, 369 ( $S_6^{2-}$ to $S_8^{2-}$ )							525
	[62]	TEGDME/DOL	217	217	766 ( $S_4^{2-}$ to $S_8^{2-}$ )		234					534
	[66]	DOL/DME	150, 219, 474			398, 509		202, 445		452		535

the lithium anode: it can produce a robust yet flexible solid electrolyte interphase (SEI) through ring-opening polymerization according to FTIR spectra.<sup>[99–102]</sup> However, DOL is actually more reactive toward lithium metal according to DFT calculation and GC analysis of gas produced in a pouch cell.<sup>[89]</sup> DOL gives rise to severe gas evolution (mainly composed of ethane), which is dangerous for practical pouch cells. Moreover, low polysulfide solubility in DOL impedes the reaction kinetics and the utilization of sulfur, especially at high sulfur loading and high rate.<sup>[103]</sup> As a result, DOL/DME or DOL/TEGDME binary solvents could be a better and more conventional choice. Normally, the volume ratio of DOL and DME/TEGDME is 1:1 for coin-cell evaluation. For Li–S pouch cells, such a ratio ought to be further engineered to reduce undesirable gas evolution mainly resulting from the decomposition of DOL.<sup>[89]</sup>

**Analysis of the SEI:** A surface film will form at the interface between the electrolyte and the electrode, commonly lithium metal, which is referred to as the SEI.<sup>[104]</sup> Composed of organic and inorganic species, the SEI is closely related to the electrochemical performance of the lithium anode. A thorough discussion on the formation mechanism, composition, and function of the anode SEI can be found in a recent review.<sup>[105]</sup> Here, to make this section concise, we will only mention several studies using X-ray photoelectron spectroscopy (XPS) to analyze the role of salts and additives in modifying the properties of the anode SEI, and a few studies on the cathode SEI.

In general, salts mainly serve as the source of Li<sup>+</sup> in an electrolyte. However, many recent studies have suggested that decomposition products of salts represent an important origin of inorganic components in the SEI. For example, lithium fluoride (LiF) is frequently detected by XPS in the SEI when fluorine-containing salts (e.g., LiTFSI) are used.<sup>[27,106–108]</sup> LiTFSI is the mainstream choice for most cases, owing to its outstanding dissociation ability, thermal stability, compatibility with ether solvents, and film-forming properties at the lithium side. It is noticeable that some other salts may offer comparable conductivity and additional benefits. Yushin and co-workers took advantage of the more reactive lithium bis(fluorosulfonyl)imide (LiFSI) to initiate local polymerization at the cathode surface and a LiF coating at the anode surface.<sup>[106]</sup> As a result, both electrodes were well protected by Li<sup>+</sup>-permeable passivating layers, solving the problems of lithium dendrites and polysulfide shuttling simultaneously. However, the concentration of LiFSI (5.0 mol L<sup>-1</sup>, i.e., 5 M) is much higher than that of common electrolytes (1.0 M LiTFSI) in order to provide sufficient protection on both electrodes. In comparison, lithium trifluoromethyl-4,5-dicyanoimidazole (LiTDI) might be a better choice, as it has been proved to passivate the anode and minimize polysulfide shuttling at a moderate concentration (1.0 M).<sup>[107]</sup>

As discussed above and in some reviews, many of the successful lithium salts have a fluorine-containing anion, which is largely due to the unique effect of LiF in the SEI. Recently, LiF has been verified to significantly promote Li<sup>+</sup> diffusion in the SEI, which renders uniform lithium plating and stripping in organic electrolyte.<sup>[109]</sup> A similar function can be accomplished by electrolyte additives like fluoroethylene carbonate (FEC) and lithium difluoro(oxalato) borate.<sup>[110–113]</sup> Another important additive, LiNO<sub>3</sub>, is so pervasively used that it almost becomes a regular ingredient in glyme electrolyte. Only 1–2% (by weight) of

LiNO<sub>3</sub> can prominently improve the Coulombic efficiency from below 90% to over 98%. Reduced Li<sub>x</sub>NO<sub>y</sub> and oxidized Li<sub>x</sub>SO<sub>y</sub> species were both observed on the surface of the lithium, protecting the anode from polysulfide corrosion and dendrite formation.<sup>[26,113–115]</sup>

The interface between the electrolyte and cathode is rarely studied, and the existence of an SEI layer is not often reported. Besides the polymerized film on the cathode induced by LiFSI,<sup>[106]</sup> FEC is also capable of protecting the cathode. By one deep discharge cycle to 0.1 V (vs Li<sup>+</sup>/Li), FEC induced the formation of LiF-containing SEI on the cathode, which mitigates polysulfide migration.<sup>[116]</sup>

#### 4.1.2. Kinetics of the Liquid Electrolyte

**Exchange Current Density:** When the electrode is at the equilibrium potential of a redox reaction, electron-transfer processes continue at the electrode/solution interface in both directions. The cathodic current, however, is balanced by the anodic current and the net current is zero. Normalized by the electrode surface area, this current density is called the exchange-current density, which reflects the intrinsic electron-transfer rate between the electrode and the solution.

Chiang and co-workers systematically compared the exchange-current density of Li<sub>2</sub>S<sub>6</sub> redox with different glyme solvents.<sup>[117]</sup> The exchange-current density (*i*<sub>0</sub>) could be obtained by either EIS or galvanostatic polarization. Charge-transfer resistance (*R*<sub>ct</sub>) was measured from two-electrode EIS, and converted to *i*<sub>0</sub> through Equation (3) as follows:

$$i_0 = \frac{RT}{zFAR_{ct}} \quad (3)$$

where *z* is the number of electrons transferred in a single step and *A* is the active area of the electrode. Voltage polarization under several current densities was monitored using a three-electrode configuration to avoid polarization on the lithium anode. Extrapolating data in the linear regimes on the semi-logarithmic Tafel plot also gave out *i*<sub>0</sub>. Two methods gave consistent results: *i*<sub>0</sub>, together with the ionic conductivity, decreases from G2 to G4 as the molecular size increases (Figure 8A,B). It should be mentioned that as multiple polysulfide species exist in solution simultaneously, the measured current density was a superficial activity of many different reactions, rather than the inherent property of any single reaction. Moreover, the exchange-current density is not the only factor that influences the performance of Li–S batteries. DOL/DME with a lower *i*<sub>0</sub> but a higher ionic conductivity has better rate performance than G2, which suggests ionic conductivity, instead of exchange-current density, is responsible for the incomplete exploitation of capacity at a high rate (Figure 8C).

**Symmetric Cells:** As the measurement of the exchange-current density requires a large amount of polysulfide electrolyte and inert electrodes such as glassy carbon, this method has not been widely used in Li–S-battery research. An alternative way of probing the kinetics of the electrolyte is CV analysis of symmetric cells.<sup>[118]</sup> This method uses two identical electrodes such as carbon-paper or interdigitated-array electrodes, which

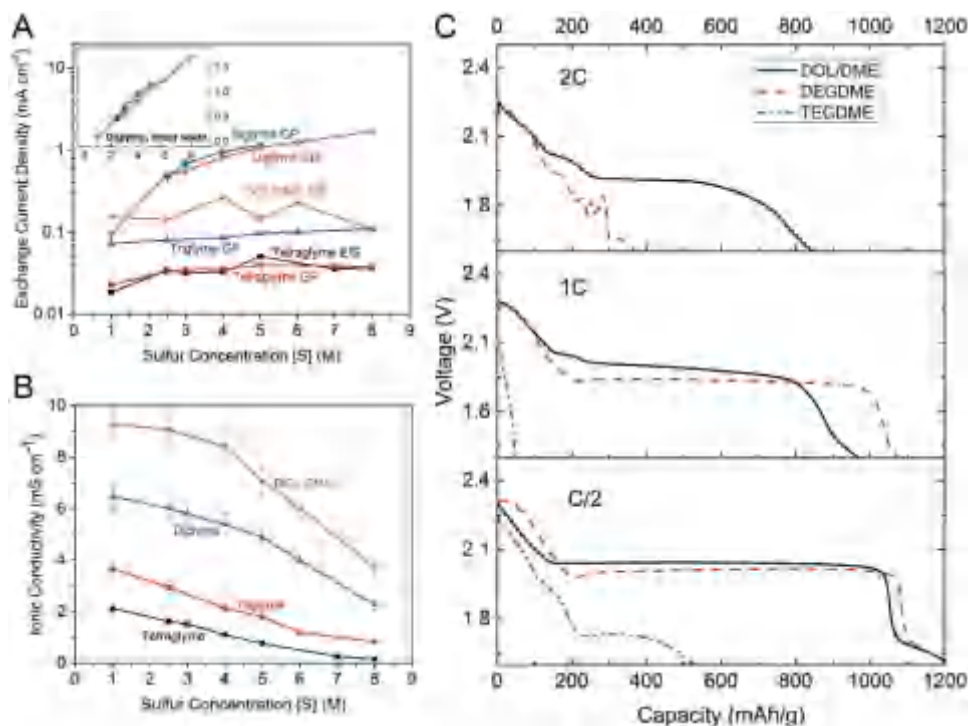


**Figure 8.** Electrolyte effects on discharge reactions: polysulfide redox kinetics. A,B) Exchange current density (A) and ionic conductivity (B) of  $\text{Li}_2\text{S}_6$  in different ether-based electrolytes with various concentrations. C) Voltage profiles of  $\text{Li}$ -polysulfide cells at several rates using three representative solvents. Reproduced with permission.<sup>[117]</sup> Copyright 2016, The Electrochemical Society.

are separated by a polymer separator. Polysulfide electrolytes with high sulfur content (usually around 3.0 M) are sandwiched between two electrodes.  $I$ - $V$  curves from symmetrically sweeping the voltage from the open-circuit potential, along with  $R_{ct}$  from the EIS of the symmetric cell, can reflect the relative activity of liquid-phase polysulfide redox. High polysulfide concentration and fast sweeping speed are often employed so that the transport limitation will not be a significant issue. The most remarkable advantage of the symmetric cell is the prevention of any influence at the lithium side.

**Potentiostatic  $\text{Li}_2\text{S}$  Precipitation:** Aside from the redox kinetics in solution, the mechanism of  $\text{Li}_2\text{S}$  precipitation is also of great importance, since this phase-transformation step is closely related with the length of the second plateau, which accounts for up to 75% of the theoretical capacity. Chiang and co-workers conducted pioneering work on this aspect.<sup>[119]</sup> Potentiostatic discharge and scanning electron microscopy (SEM) were used to study the behavior of  $\text{Li}_2\text{S}$  nucleation and growth in glyme electrolytes. A critical overpotential was found to be necessary for overcoming the  $\text{Li}_2\text{S}$  nucleation barrier, which corresponded well with the “dip” between two discharge plateaus usually seen in the galvanostatic voltage profile. The Avrami equation was employed to explain the nucleation and growth behavior.  $\text{Li}_2\text{S}$  follows a two-dimensional (2D) growth mechanism on a triple phase boundary; therefore, the potentiostatic current profile has a maximum point when insulating  $\text{Li}_2\text{S}$  domains are in contact with each other (Figure 9A). The combined rate constant for both nucleation and growth can be derived by fitting the current curve with Equation (4), which decreases by the same order of magnitude as the exchange-current density from G2

to G4 (Figure 9B). As demonstrated by ab initio molecular-dynamics simulation, the slower kinetics arise from a stronger binding between solvent molecules with  $\text{Li}_2\text{S}_n$  clusters, which is a good example of the chelating effect.

$$Y = 1 - \exp(-Bt^n) \quad (4)$$

In Equation (4),  $Y$  is the fraction of  $\text{Li}_2\text{S}$  that has been transformed,  $B$  is the combined kinetic constant of nucleation and growth rate, and  $n$  is the Avrami exponent indicating the dimension of growth. During the discharge process,  $\text{Li}_2\text{S}$  nuclei are continuously generated, which is similar to the homogeneous nucleation process in a supersaturated solution. Correspondingly, the dimension of growth is  $(n - 1)$ .

**Applications in Electrolytes with Redox Mediators:** The above-mentioned kinetic properties can be tuned by changing the composition of the electrolyte. Here, we choose a redox mediator (RM) as an example to show the application of these novel methods. Catalogued by their different redox potentials ( $E_{RM}$ ) vs  $\text{Li}^+/\text{Li}$ , RMs can be divided into three types:

- Type I,  $E_{RM} \leq 2.0$  V;
- Type II,  $2.0 < E_{RM} \leq 2.5$  V;
- Type III,  $E_{RM} > 2.5$  V.

For the purpose of oxidizing the pristine  $\text{Li}_2\text{S}$  cathode at the first cycle, molecules belonging to Type III are recommended by Aurbach and co-workers.<sup>[120]</sup> However, this prerequisite is not necessary for RMs playing other roles in  $\text{Li}$ -S chemistry, especially except the first cycle of pristine  $\text{Li}_2\text{S}$  cathodes.

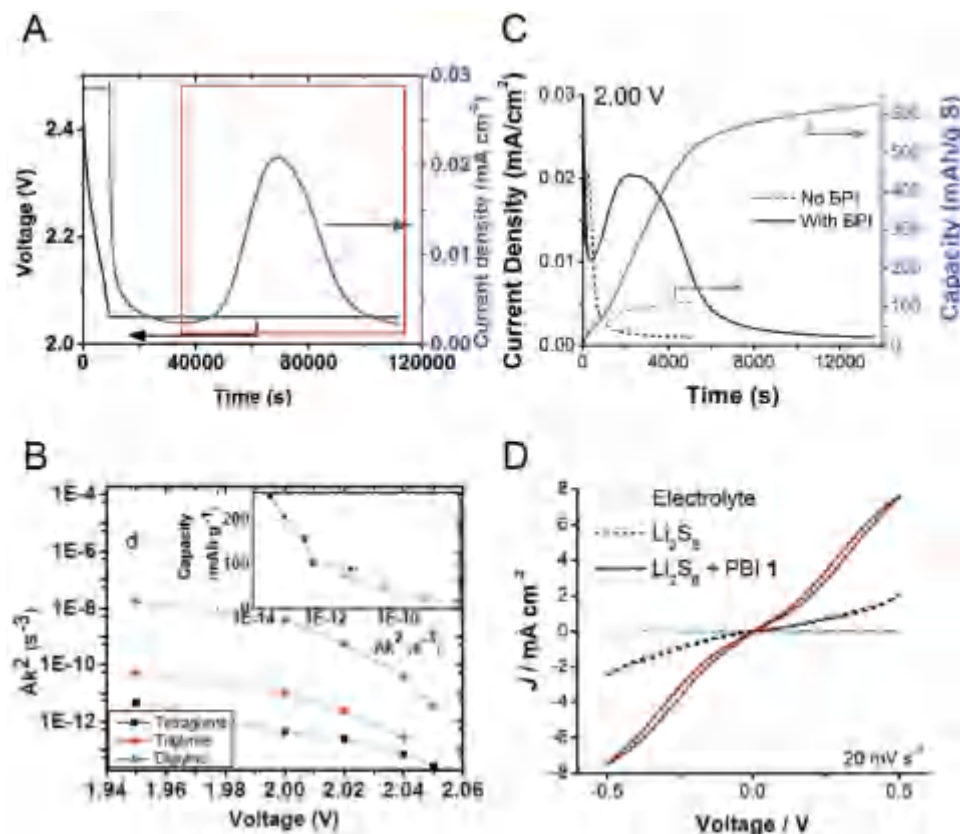


**Figure 9.** Electrolyte effects on discharge reactions:  $\text{Li}_2\text{S}$  deposition kinetics. A) Voltage and current profiles in a nucleation experiment of  $\text{Li}-\text{Li}_2\text{S}_8$  cell. B) Combined nucleation and growth rate constants obtained by fitting the potentiostatic discharge profiles. Inset: Deposition capacity vs rate constant for diglyme and tetraglyme. A,B) Reproduced with permission.<sup>[117]</sup> Copyright 2015, Wiley-VCH. C) Potentiostatic discharge current and capacity showing the promoted  $\text{Li}_2\text{S}$  precipitation when BPI redox mediator is added. Reproduced with permission.<sup>[122]</sup> Copyright 2015, American Chemical Society. D) CV of  $\text{Li}_2\text{S}_8$  symmetric cells exhibiting the enhanced electron transfer with PBI additives. Reproduced with permission.<sup>[118]</sup> Copyright 2015, American Chemical Society.

Decamethylchromocene ( $\text{Cr}(\text{Cp}^*)_2$ ) with  $E_{\text{RM}}$  of 2.0 V was paired with decamethylnickelocene ( $\text{Ni}(\text{Cp}^*)_2$ ,  $E_{\text{RM}}$  of 2.5 V) for a  $\text{Li}-\text{S}$  redox flow battery.<sup>[121]</sup> Working separately at discharge and charge,  $\text{Cr}(\text{Cp}^*)_2$  and  $\text{Ni}(\text{Cp}^*)_2$  transfer electrons from the current collector to the sulfur and  $\text{Li}_2\text{S}$ , respectively.

Further studies on the detailed role of different types of RMs have been conducted by Helms and co-workers.<sup>[118,122]</sup> Searching through over 80 polycyclic aromatic hydrocarbons, benzo[ghi]peryleneimide (BPI) and perylene bisimide (PBI) were screened out by Helms and co-workers as representative RMs.<sup>[122]</sup> The strong intermolecular  $\pi-\pi$  interaction causes the stacking of these additives and forms electrically conductive nanofibers in the electrolyte. Although electrolyte gelation occurred after RM addition, the diffusion of ions and electrons was not impeded but rather improved. BPI (Type I) promotes the liquid–solid transformation upon  $\text{Li}_2\text{S}$  deposition/dissolution,<sup>[122]</sup> while PBI additive (Type II) has a significant role in accelerating liquid-phase polysulfide redox that occurs around 2.4 V.<sup>[118]</sup> Besides regular tests of  $\text{Li}-\text{S}$  asymmetric cells, such as CV and galvanostatic cycling, experiments targeted at the specific reactions were also conducted. Potentiostatic discharge experiments, as described before, were conducted to determine the role of BPI. The time for the current peak to appear was

much later with BPI than without it, enabling a 5.5-fold higher capacity at the same potential (Figure 9C). SEM characterization revealed a three-dimensional (3D) growth of  $\text{Li}_2\text{S}$  in BPI-containing electrolyte, which not only favors a higher discharge capacity, but also reduces the overpotential at charge, compared with the fully covered 2D passivating layer in a regular electrolyte. In CV tests of symmetric cells with dissolved  $\text{Li}_2\text{S}_8$ , PBI induced a 3-fold increase in current response, validating the enhanced charge transfer to liquid phase (Figure 9D).

The use of soluble RMs, however, causes a shuttling effect analogous to polysulfides. This accounts for a lower Coulombic efficiency despite the higher capacity when RMs are present.<sup>[118]</sup> Alternatively, polysulfides (not limited to  $\text{S}_3^{\bullet-}$ ) are intrinsic RMs in the  $\text{Li}-\text{S}$  system, although they have relatively slower kinetics than artificially added ones. Rationally understanding and designing highly effective and efficient RMs could be very promising for  $\text{Li}-\text{S}$ -battery development.

1.0 M LiTFSI–DOL/DME (v/v = 1:1) is currently the most popular recipe for  $\text{Li}-\text{S}$ -battery electrolytes.<sup>[123–125]</sup> However, no evidence has indicated this recipe to be the optimal choice. Most studies on other electrolytes were done before the recent renaissance in cathode materials. To follow up with their development in  $\text{Li}-\text{S}$  batteries, it is necessary to revisit

and reoptimize the solvent composition. Recently, some new approaches of designing alternative electrolytes have been proposed. High-DN solvents with higher polysulfide solubility than ethers render a more thorough utilization of active materials (Figure 6D).<sup>[73,74,77,126–130]</sup> On the contrary, sparingly solvating electrolytes, i.e., electrolyte with low solvating ability, especially room-temperature ionic liquids and their analogs, enhance the Coulombic efficiency and capacity retention by restricting the dissolution of polysulfides.<sup>[112,131–143]</sup> However, neither of these approaches is mature enough:

- Electrolytes based on high-DN solvents are troubled by their high reactivity with lithium metal;
- Sparingly solvating electrolytes suffer from high viscosity and low ionic conductivity.

Advanced electrochemical measurements, such as symmetric cells, potentiostatic nucleation, and rotating ring-disk electrode (RRDE) voltammetry,<sup>[127]</sup> help reveal the intrinsic properties of Li–S reactions in various liquid electrolytes (Figure 6E). For example, Lu and co-workers combined RRDE with UV–vis spectroscopy to study the different reaction routes in high-DN vs low-DN solvents. These studies suggested that the rate capability seems to be sacrificed when the saturation concentration of polysulfides increases. Significant polarization at the low plateau could be observed in a DMSO-based electrolyte even at a low current density. This might be due to the better stability of short-chain polysulfides in DMSO, which suppresses the rate-limiting chemical reactions.

Overall, the development of liquid electrolytes has been somehow sluggish in recent years, compared with the flourish in advanced electrode materials. The demand for a safer battery with high sulfur loading and low E/S ratio calls for a more rational design of the electrolyte, therefore high-throughput screening of solvents, salts, and additives should be conducted both experimentally and theoretically. The latest progress in gel, polymer, and ceramic electrolytes shows an emerging new approach for high-safety batteries.<sup>[144–151]</sup> However, liquid electrolytes still outperform their solid counterparts for their lower resistance, especially at the electrolyte/electrode interfaces.<sup>[149,152]</sup> Hence, a continuous modification in liquid electrolyte is desired to render a stable SEI and fast interfacial transport. The combination of liquid and quasi-solid electrolytes might be preferred from engineering perspective.

## 4.2. Host Effect on Li–S Discharge Reactions

The variety of cathode host materials has seen explosive growth since Nazar and co-workers first demonstrated a high-capacity sulfur cathode based on mesoporous carbon in 2009.<sup>[153]</sup> Here, instead of comprehensively introducing the large amount of work employing carbon, polymer, inorganic, and hybrid materials,<sup>[10,154–163]</sup> we aim at providing a mechanistic insight into the influence of the host materials on several important processes in Li–S batteries, namely i) polysulfide–host interactions, ii) polysulfide redox, and iii) Li<sub>2</sub>S deposition.

### 4.2.1. Polysulfide–Host Interactions

As cathode additives, commercial carbon black constructs a conductive matrix that works well for traditional cathodes of LIBs. However, control over the diffusion of polysulfides is lost with such a simple cathode design in Li–S batteries. Hence, physical confinement through carbon materials with finely tuned pore structures<sup>[164–169]</sup> and chemical adsorption through polar hosts<sup>[170–172]</sup> have been widely adopted to trap polysulfides. Chemical entrapment is being proposed more and more often due to the stronger interactions between polysulfides and the polar host materials than for nonpolar carbon.<sup>[31,173]</sup> The nature of this stronger interaction can be studied microscopically or macroscopically. To directly demonstrate the effectiveness of trapping polysulfides, visualized experiments are sometimes carried out, most of which use static adsorption. A few reports have observed chemical adsorption during dynamic discharge, including materials like porous carbon, metal oxides, covalent organic frameworks, etc.<sup>[154–156]</sup> The little change in the color of the bulk electrolyte provides solid evidence for a successful trapping of polysulfides. Detailed information about the bond formation, variation in electron density, and orbital overlapping upon adsorption will be briefly summarized in the following subsection. Various methods have been applied to elucidate the informatics of the polysulfide–host interactions.

**IR and Raman Spectroscopy:** IR and Raman spectroscopy are useful in detecting chemical bonds and functional groups regarding to p-block elements. IR and Raman spectroscopy are convenient in the sense that they can both be handled under ambient pressure and samples for the latter do not need any preprocessing. By absorbing or scattering radiation, IR and Raman spectroscopy respond to different vibration modes in molecules, and they serve to mutually support each other. Normally IR spectroscopy is used for analyzing vibrations from polar species while Raman spectroscopy is for nonpolar ones. Seh et al. confirmed the interaction between Li<sub>2</sub>S and graphene oxide (GO) through the redshift of the Li<sub>2</sub>S peak in the Raman spectrum (Figure 10A).<sup>[174]</sup> Nazar and co-workers firstly employed IR and Raman spectroscopy to investigate the adsorption behavior of polysulfides on titanium dioxide (TiO<sub>2</sub>). In the IR spectra, they found a new band which they denoted as S–Ti–O referring to sulfur–TiO<sub>2</sub> interactions, and in the Raman spectra they noticed a slight shift of the peaks for TiO<sub>2</sub> in accordance with the alternation of the local environment for TiO<sub>2</sub> (Figure 10B,C).<sup>[175]</sup> Liang and co-workers also employed Raman spectroscopy to probe a novel redox mechanism of S–S chain scission/recombination in a lithium polysulfidophosphates (Li<sub>3</sub>PS<sub>4+n</sub>) cathode, in which elemental sulfur was tethered on the terminal thiol groups of thiophosphate anions (PS<sub>4</sub><sup>3-</sup>), for Li–S batteries.<sup>[176]</sup> IR and Raman spectroscopy evidence shed light on sulfur–host interactions and even open up new ways of exploring Li–S batteries. Unfortunately, they are unable to clarify how the electron transitions take place and whether or not and which chemical bonds are formed.

**XPS:** XPS is one of the most powerful techniques to analyze the chemical composition of materials, as well as the oxidation states of atoms near the surface. In Li–S batteries, XPS or high-energy XPS is suitable to picture the surface chemistry of the host material and its interaction with sulfur species since the

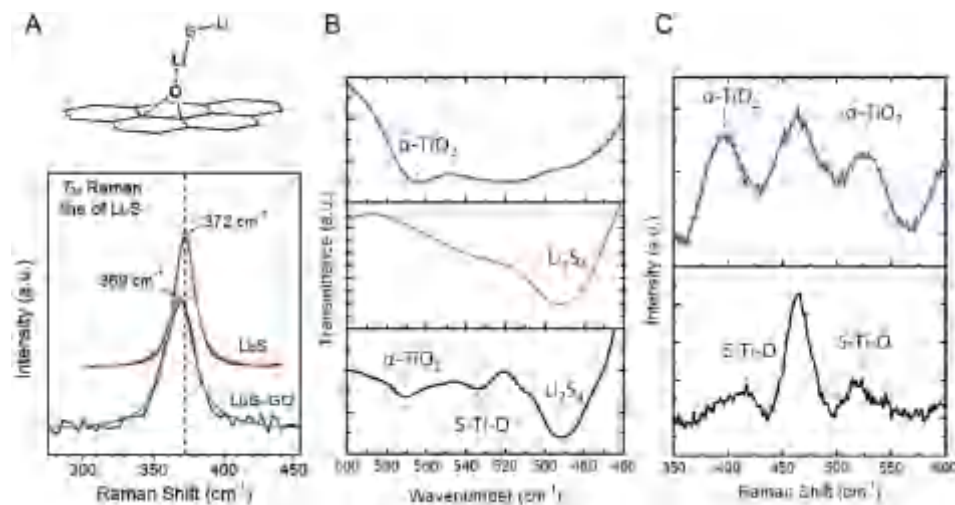


**Figure 10.** Host effects on discharge reactions: IR and Raman spectroscopy of polar host/lithium polysulfides. A) Raman spectra of the  $T_{2g}$  phonon mode of  $\text{Li}_2\text{S}$  in pristine  $\text{Li}_2\text{S}$  and  $\text{Li}_2\text{S-GO}$  composites, together with their respective fitted peaks. Reproduced with permission.<sup>[174]</sup> Copyright 2014, The Royal Society of Chemistry. B) FTIR spectra of neat  $\alpha\text{-TiO}_2$  (blue), neat  $\text{Li}_2\text{S}_4$  (orange), and neat  $\text{Li}_2\text{S}_4/\text{TiO}_2$  (black). C) Raman spectra of neat  $\alpha\text{-TiO}_2$  (blue) and neat  $\text{Li}_2\text{S}_4/\text{TiO}_2$  (black). B.C) Reproduced with permission.<sup>[175]</sup> Copyright 2012, American Chemical Society.

conversion of polysulfides mainly occurs at the electrode/electrolyte interface. The partial charge transfer and intermediate coordination can be plainly identified by XPS.

Generally, there are three types of polar surface host materials: i) heteroatom-doped carbonaceous framework with dopants, ii) conductive polymers with functional groups, and iii) metal compounds with ionic sites, for all of which the chemisorption is realized via different kinds of chemical bonds.<sup>[158,177–180]</sup> Lithium polysulfides in the electrolyte are mostly in clusters; therefore, the binding of which can be realized by bonds with  $\text{Li}^+$ ,  $\text{S}_n^{2-}$ , or both. To figure out and differentiate between these interactions, XPS of cycled or working electrodes is very useful. Pang and Nazar confirmed the electron transition from the nitrogen atom in graphitic carbon nitride ( $g\text{-C}_3\text{N}_4$ ) to  $\text{Li}^+$ , corresponding to the Li–N bond through analysis of Li 1s spectra.<sup>[181]</sup> Unlike electron-rich dopants like nitrogen and oxygen, for which chemisorption occurs mainly through lithium bonds, electron-deficient dopants such as boron work through a different way. Guo and co-workers studied boron-doped graphene and found slight charge transfer from the sulfur to the carbon framework through S 2p spectra, indicating chemisorption directly through the sulfur in redox intermediates.<sup>[182]</sup> Furthermore, Nazar and co-workers identified N, S-co-doped carbon materials with synergistic chemisorption, in which nitrogen was negatively charged and sulfur was positively charged. By probing the Li 1s spectra and S 2p spectra, they found not only Li–N bonds but also  $\text{S}_T\text{-S}\delta^+$  (referring to sulfur dopants on carbon) in this configuration.<sup>[183]</sup> Manthiram and co-workers also demonstrated such a synergistic binding effect to polysulfides by N, S-co-doped graphene aerogels.<sup>[184]</sup>

Similar to carbon with electron-rich dopants, heteroatom-conjugated polymers commonly bind polysulfides through Li–heteroatom bonds. One of the major differences between doped carbon and polymers lies in the stronger clarity of probing the binding sites. For example, polysulfides were demonstrated to

be fastened on polypyrrole via Li–pyrrolic N bonds as shown in **Figure 11A**,<sup>[185]</sup> whereas it is not usually easy to verify to which nitrogen dopants in carbon it is that the polysulfide binds. Goodenough and co-workers investigated polymers with different functional groups, ranging from fluorine and ether to ester and sulfone. The XPS spectra unambiguously validated the existence of Li–X ( $X = \text{F}, \text{O},$  and  $\text{COOR}$ ) bonds, through which polysulfides bound to polymers according to lithium-bond theory.<sup>[186]</sup>

Aside from these p-block covalent cathode frameworks, metal compounds are emerging rapidly as they are intrinsically ionic for interaction with polysulfides. Metal compounds investigated in Li–S batteries, ranging from binary compounds such as oxides, nitrides, carbides, sulfides, and halogenides to ternary compounds such as perovskites, can generally be divided into two categories: with unsaturated coordination metal sites or without.<sup>[187–210]</sup>

- Compounds without unsaturated coordination metal sites, i.e., alkali or alkali-earth compounds and transitional compounds in which metal ions are of their highest valence, interact with polysulfides mainly through lithium bonds, which has been evidenced by the shift in the XPS of Li and lattice anions. Meanwhile, XPS of metal cations merely changes, indicating they are not bonding with polysulfides.
- Compounds with unsaturated coordination metal sites interact with polysulfides via a different but more interesting way.  $\text{S}_T$  atoms in polysulfides are partially negatively charged and have lone-pair electrons, which serve as ligands to bind with unsaturated metal sites.

Xiao and co-workers firstly demonstrated this kind of interaction in metal–organic frameworks (MOFs) with nickel and cobalt centers (Ni-MOF and Co-MOF), respectively.<sup>[211]</sup> They observed the lowering of the binding energy of the metal ions in their 2p spectra, which indicates the decrease in metal

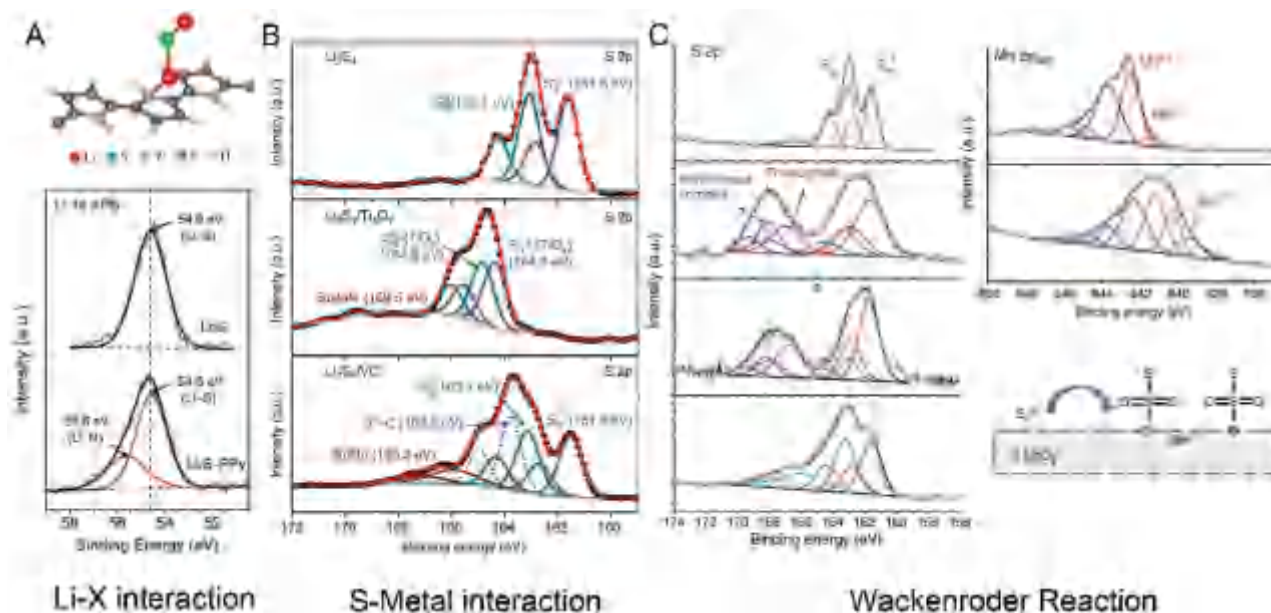


**Figure 11.** Host effects on discharge reactions: XPS of polar host/lithium polysulfides. A) Li 1s spectra and fittings of pristine  $\text{Li}_2\text{S}$  (top) and  $\text{Li}_2\text{S}$ -PPy composites (bottom). Reproduced with permission.<sup>[185]</sup> Copyright 2014, The Royal Society of Chemistry. B) S 2p spectra of  $\text{Li}_2\text{S}_4$  (top),  $\text{Li}_2\text{S}_4/\text{Ti}_4\text{O}_7$  (middle) and  $\text{Li}_2\text{S}_4/\text{Vulcan carbon (VC)}$  (bottom). Reproduced with permission.<sup>[213]</sup> Copyright 2015, Nature Publishing Group. C) S 2p spectra of  $\text{Li}_2\text{S}_4$  (left first),  $\text{Li}_2\text{S}_4/\text{MnO}_2$  (left second),  $\text{Li}_2\text{S}_4/\text{GO}$  (left third), and  $\text{Li}_2\text{S}_4/\text{graphene}$  (left fourth); Mn 2p<sub>3/2</sub> spectra of  $\text{MnO}_2$  (right first) and  $\text{Li}_2\text{S}_4/\text{MnO}_2$  (right second); and schematic illustration of redox mechanism on  $\delta\text{-MnO}_2$ . Reproduced with permission.<sup>[216]</sup> Copyright 2015, Nature Publishing Group.

valence and thereby the formation of S-metal bonds. A Lewis-acid-base interaction mechanism was proposed, shedding fresh light on the coordination effect of unsaturated metal sites. Cui and co-workers theoretically predicted and experimentally demonstrated that unsaturated coordination titanium (Ti) sites in Magnéli-phase  $\text{Ti}_n\text{O}_{2n-1}$  could bind with  $\text{S}_\text{T}$  atoms.<sup>[212]</sup> Nazar and co-workers have also shown Ti-S bonds in Magnéli-phase  $\text{Ti}_4\text{O}_7$ <sup>[213]</sup> and MXene-phase  $\text{Ti}_2\text{C}$ .<sup>[213,214]</sup> As the S 2p spectra in Figure 11B show, the binding energies of all the sulfur species shifted to a higher position for  $\text{Ti}_4\text{O}_7$ , indicating the electron transfer from sulfur, probably to defect sites in the  $\text{Ti}_4\text{O}_7$ .<sup>[213]</sup> Different from  $\text{Ti}_4\text{O}_7$ , in MXene the formation of Ti-S bonds was realized through the replacement of surface -OH functional groups by sulfur, invoking new thoughts on metal-S bond formation.<sup>[214]</sup> Peng, Zhang, et al. moved further to other transitional elements such as iron and nickel. In layered double hydroxide (LDH) and nitrogen-doped graphene (NG) hybrids, they found Ni-S bonds inside the strained LDH lattice as well as N/O-Li bonds on the NG via a series of S 2p, N 2p, and Ni 2p spectra. The formation of two kinds of bonds cooperatively offer strong binding toward the redox intermediates.<sup>[215]</sup> Furthermore, Liang et al. also reported a unique surface redox mechanism in oxidative transitional compounds like birnessite manganese oxide ( $\delta\text{-MnO}_2$ ) in Li-S batteries. With  $\text{LiClO}_4$ , rather than sulfur-containing LiTFSI, as the lithium salt, they still found the peak due to thiosulfates in the S 2p spectra of the discharged cathode, and also peaks due to polythionate and sulfite, indicating a surface oxidation process of polysulfide species by  $\text{Mn}^{4+}$ . This was also supported by the appearance of  $\text{Mn}^{3+}$  and  $\text{Mn}^{2+}$  peaks in the Mn 2p<sub>3/2</sub> spectra. Thiosulfates could serve as surface-bound RMs to offer a surface-dominated redox pathway (Figure 11C).<sup>[216]</sup> They then delved deeper into

the as-proposed internal redox mechanism based on thiosulfate/polythionate and screened throughout various transition-metal oxides with different redox potentials. With detailed analysis of XPS spectra, they found the universal existence of thiosulfate-polythionate conversion (Wackerroder's reaction) on metal oxides with higher redox potentials than in-solution polysulfide redox.<sup>[217]</sup>

To provide a convenient source of the XPS data appearing in Li-S-battery research, some useful peak positions are collected in Table 3. Of note, although XPS is a powerful tool in chemical

**Table 3.** Summary of S 2p peak and Li 1s peak positions in XPS.<sup>[177-179,185,200,203,213-217]</sup>

Sulfur	Peak	Lithium	Peak
$\text{Li}_2\text{S}$	160.2–160.5 eV	$\text{Li}_2\text{S}$	54.6–54.8 eV
$\text{Li}_2\text{S}_2$	161.7–162.1 eV	$\text{Li}_2\text{S}_4$	55.4 eV
$\text{S}_\text{T}(\text{Li}_2\text{S}_4/\text{Li}_2\text{S}_6)$	161.4–161.9 eV/161.7 eV	$\text{Li}_2\text{S}_6$	56.3 eV
$\text{S}_\text{B}(\text{Li}_2\text{S}_4/\text{Li}_2\text{S}_6)$	163.0–163.8 eV/162.9 eV	Li-N( $\text{Li}_2\text{S}/\text{Li}_2\text{S}_4$ )	55.4–55.6 eV
$\text{S}_8$	163.2–164.2 eV	Li-O	55.4 eV( $\text{Li}_2\text{S}$ )
thiosulfate ( $\text{S}_2\text{O}_3^{2-}$ )	167.2–167.9 eV (central sulfur) 161.5 eV (peripheral sulfur)		
polythionate	167.3–168.2 eV		
sulfite	166.3 eV		
sulfate	168.6–170.2 eV		
S-C	163.1–163.7 eV		
S-O	167 eV		
S-Metal	162.1–162.5 eV		

analysis, it can only make use of the electrons that have escaped from the top 10 nm near surface. Besides, it typically operates under high vacuum, making in situ characterization of liquid systems very difficult. However, ex situ analysis has its own drawbacks in correctly interpreting the data. The information obtained should be carefully read to prevent over-interpretation or being misled.

**XAS:** In addition to XPS, XAS is another option to probe the chemical states and interactions, and is often coupled with XPS to mutually support each other. More importantly, it could be an operando method and also provides information on a bulk rather than a surface scale. Zhang and co-workers investigated Li–S batteries with XAS firstly in 2011 and proposed GO as a sulfur immobilizer.<sup>[159]</sup> In their work, from the C K-edge they discovered that sulfur would partially reduce GO and possibly form C–S bonds. Moreover, they also found C–S bonds in NG cathodes via S 1s spectra and, interestingly, Li<sub>2</sub>S<sub>n</sub>–N bonds at fully discharged state, which corresponds well with other reports of XPS.<sup>[218]</sup> Wang and co-workers compared the O K-edge spectra of the carbon matrix both with and without nitrogen dopants, and found that in the presence of polysulfides, nitrogen dopants enhance the interactions between sulfur atoms and oxygen from –COOH or >C=O functional groups on graphene.<sup>[170]</sup> In other words, S–O bonds formed rather than S–N bonds. This kind of interpretation of the role of nitrogen dopants differs from the abovementioned view that electron-rich dopants mainly interact with Li<sup>+</sup> by forming lithium bonds, and is worthy of further investigation. Sun and co-workers also detected the formation of S–O chemical bonds between a molecular-layer-deposited alucone coating and elemental sulfur using high-energy XPS and NEXAFS.<sup>[206]</sup> An understanding of how the S–O, C–S, and S–S bonds evolved upon charge and discharge was obtained.

**NMR:** Besides speciation, NMR spectra can also provide interesting perspectives in understanding the redox mechanisms in Li–S batteries. Li and co-workers claimed to find C–S chemical bonds in sulfur copolymer cathodes, as evidenced by solution <sup>13</sup>C NMR spectra of cathode materials.<sup>[219]</sup> Beyond <sup>13</sup>C NMR, the above-discussed <sup>7</sup>Li NMR could also be expected to generate more interesting results regarding the redox routes since NMR can be used in both ex situ and in situ modes.

In brief summary on polysulfide–host interactions, many characterization techniques have been employed and developed for Li–S-battery research. Among them, spectroscopy using X-ray radiation, in particular XPS, is the most widely adopted characterization tool. XPS and XAS are powerful in providing more information about how charges are transferred, chemical states are changed, and bonds are formed. These details are crucial in determining the possible redox mechanism for electrochemical reactions. XPS is much more common but only capable of static or ex situ investigation, while XAS can provide dynamic or in situ information but synchrotron radiation sources are needed, which are quite expensive and currently rare. IR and Raman spectroscopy, as well as NMR, are routine but only capable of qualitative characterization. On the contrary, XPS and XAS are more effective, yet expensive. They require more careful handling with the sample in a specific operation environment such as high vacuum.

#### 4.2.2. Liquid-Phase Polysulfide Redox

Previous studies have probed a fast kinetics for liquid-phase polysulfide redox reactions using RRDE in dilute solution of S<sub>8</sub> (4.0 × 10<sup>−3</sup> M).<sup>[127]</sup> However, this may not be the case for practical Li–S batteries, as the sulfur concentration should be much higher than 1.0 M (E/S ratio << 10:1), otherwise the energy density would be even lower than that of commercial LIBs.<sup>[220]</sup> EIS measurement of Li–S coin cells has also suggested the highest impedance may appear at the high plateau rather than the low plateau.<sup>[221,222]</sup> Therefore, the kinetics of a concentrated Li<sub>2</sub>S<sub>n</sub> solution might be quite slow in a real cell. Introducing an insulating polysulfide adsorbent such as silica into a sulfur cathode could lead to an even higher impedance, although polysulfides are effectively trapped.<sup>[223]</sup> Furthermore, polysulfides immobilized by insulating metal oxides require an additional surface diffusion step to reach conductive matrix, as Tao et al. indicated.<sup>[188]</sup>

Peng, Zhang, et al. emphasized the importance of adsorbent conductivity in the electrochemical kinetics of Li–S batteries.<sup>[224]</sup> A model system was designed to probe the polysulfide redox reactions on the surfaces of congeneric Ti-based inorganics with significantly different conductivities. Similar to the approach for probing the kinetic properties of electrolytes, symmetric cells were assembled by sandwiching Li<sub>2</sub>S<sub>6</sub> electrolyte (3.0 M) between two identical carbon-paper (CP)-based electrodes loaded with titanium carbide (TiC) or TiO<sub>2</sub>. Both CV and EIS indicated apparently enhanced electrochemical kinetics on the TiC surface, while CP loaded with TiO<sub>2</sub> did not show any difference from the behavior of bare CP (**Figure 12**). Semi-metallic pyrite-type cobalt disulfide (CoS<sub>2</sub>) (with an electrical

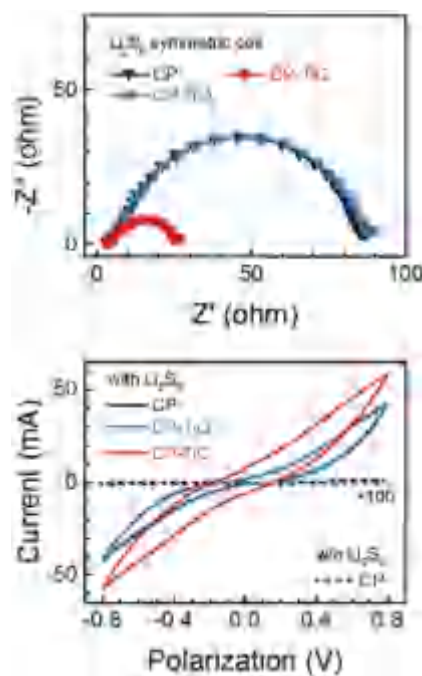


**Figure 12.** Host effects on discharge reactions: polysulfide redox in symmetric cells. EIS spectra (top) and CV curves (bottom) of Li<sub>2</sub>S<sub>6</sub> symmetric cells showing the accelerated polysulfide redox on conductive polar surface of TiC. Reproduced with permission.<sup>[224]</sup> Copyright 2016, Wiley-VCH.

conductivity of  $6.7 \times 10^3 \text{ S cm}^{-1}$ ) also has a positive effect on the redox current of  $\text{Li}_2\text{S}_6$  electrolyte.<sup>[225]</sup> This methodology reveals the similarity between conductive polar host materials, regarded as immobile solid electrocatalysts or RMs, and dissolved mobile RMs in catalyzing polysulfide redox kinetics. However, these immobile solid electrocatalysts have additional advantages over dissolved ones:

- Their polar surfaces help enrich  $\text{Li}_2\text{S}_n$  within the cathode scaffold, preventing the loss of active materials;
- They suppress rather than contribute to shuttling phenomena because of their immobility, ensuring high Coulombic efficiency and suppressing self-discharge.

Careful analysis of the CV profiles of regular cells (composed of lithium-metal anode and cathode current collectors wetted by  $\text{Li}_2\text{S}_n$  catholyte) also gave some evidence for the catalytic effect of tungsten disulfides (Figure 13A) and  $\text{g-C}_3\text{N}_4$ ,<sup>[226,227]</sup> but a symmetric cell would give a much more straightforward and explicit proof.

The mostly used poly(vinylidene fluoride) (PVDF) binder for sulfur cathodes, which is insulating and nonpolar, has no function other than adhesion. Frischmann et al. replaced PVDF with a redox-active PBI supramolecular binder, as it offers extra

conductivity and reaction sites for polysulfide redox.<sup>[228]</sup> Chen and co-workers reported a multifunctional sulfur-trapping and catalytic binder based on radical poly(2,2,6,6-tetramethyl-1-piperidinyloxy-4-yl methacrylate) (PTMA).<sup>[229]</sup> Once charged to 4.0 V, the PTMA would be oxidized to  $\text{PTMA}^+$ , which was capable of adsorbing polysulfides. Linear sweep voltammetry of polymer films in polysulfide solution suggested a remarkable catalytic capability of the  $\text{PTMA}^+$  (Figure 13B), which was mainly attributed to the lower LUMO of the  $[\text{PTMA}^+-\text{S}_n^{2-}]$  complex than that of  $\text{S}_n^{2-}$ , making the complex more readily reduced. These advancements in redox-active polymer additives or binders may open up a new avenue toward high-performance Li–S batteries, but their thermodynamic and kinetic stability should be further explored.

#### 4.2.3. $\text{Li}_2\text{S}$ Deposition

The properties of the host materials not only dictate the activity of liquid–liquid transformations, but also play a crucial role at the liquid–solid boundary. Variation in the interfacial energy between  $\text{Li}_2\text{S}$  and the host materials may lead to deviation from the 2D growth mechanism on carbon fiber.<sup>[224]</sup> Identical CP electrodes loaded with TiC and  $\text{TiO}_2$ , as used for symmetric cells, were assembled into Li–polysulfide cells for a potentiostatic nucleation experiment. Under the same procedure and comparable conditions, quite different growth mechanisms for the two materials were observed. According to the integrated capacity, TiC strongly favored  $\text{Li}_2\text{S}$  precipitation with an 80% increase in capacity, whereas  $\text{TiO}_2$  poisoned the conductive carbon surface, as reflected by its lower capacity ( $45 \text{ mA h g}^{-1}$ ) than pristine CP ( $54 \text{ mA h g}^{-1}$ ). Note that bulk particles of TiC and  $\text{TiO}_2$  provided a much smaller surface area than the CP substrate. The difference in precipitation capacity must be explained by the change in growth mechanism. Fan et al. attributed the termination of  $\text{Li}_2\text{S}$  growth to the impingement of isolated and insulating  $\text{Li}_2\text{S}$  islands until full coverage of active surfaces was attained.<sup>[119]</sup> Thus the increased capacity may be caused by a radial growth, and the two peaks in the current profile of CP-TiC may be the result of two-step impingement. This result again points to the vital role of conductive polar mediators in Li–S electrochemistry. Consistently, the composite of LDH and NG (as mentioned in Section 4.2.1) promoted  $\text{Li}_2\text{S}$  precipitation more significantly than LDH alone (Figure 14A).<sup>[215]</sup>

SEM and transmission electron microscopy (TEM) are both powerful tools for characterizing the morphology of cathode materials. As can be seen in Figure 14B, after potentiostatic discharge, CP decorated by conductive polar particles exhibited a thick layer of  $\text{Li}_2\text{S}$  fully covering the entire surface, in contrast to the thin and incomplete deposition on pristine CP. Alternatively, the morphologies of cathode materials after galvanostatic discharge can also reflect the nucleation and growth mechanism on different kinds of surfaces. Yao et al. found that under the same C-rate,  $\text{Li}_2\text{S}$  particles deposited on carbon fibers embedded in indium-doped tin oxide (ITO) was much smaller and denser than those on pristine carbon fibers.<sup>[230]</sup> This is accounted by the ability of the polar conductive ITO to control the spatial distribution of the  $\text{Li}_2\text{S}$  nuclei.

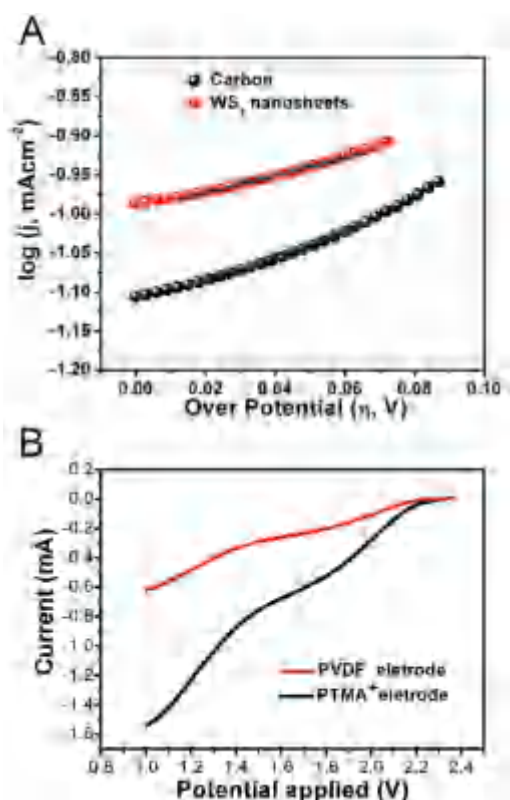


**Figure 13.** Host effects on discharge reactions: polysulfide redox in Li–S cells. A) Tafel plots for carbon and tungsten disulfide nanosheet electrodes in  $\text{Li}_2\text{S}_4$  catholyte. Reproduced with permission.<sup>[227]</sup> Copyright 2017, American Chemical Society. B) Linear sweep voltammetry results of polysulfide reduction on  $\text{PTMA}^+$  and PVDF-coated rotating-disk electrodes. Reproduced with permission.<sup>[229]</sup> Copyright 2016, Elsevier.

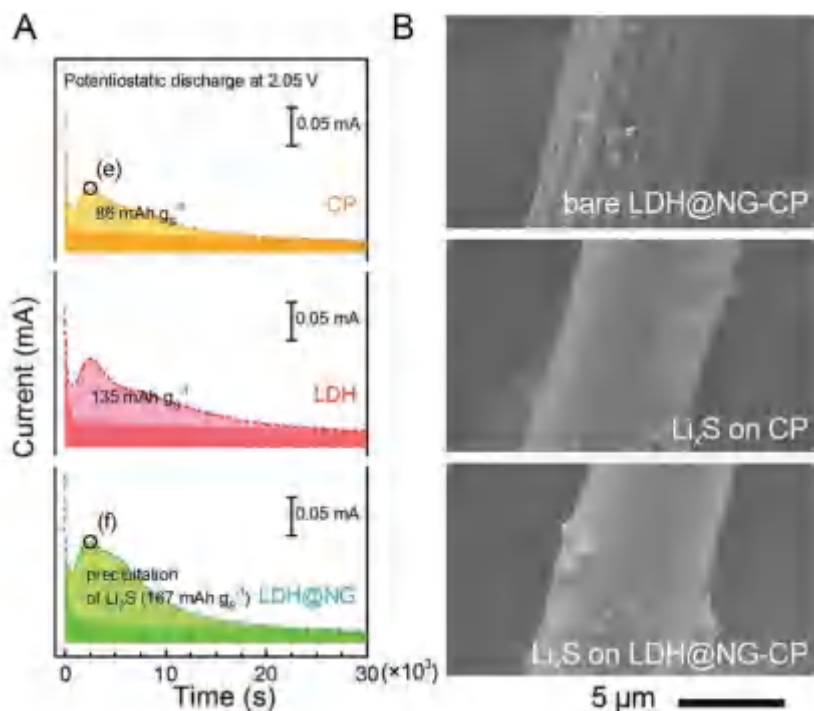


**Figure 14.** Host effects on discharge reactions: Li<sub>2</sub>S deposition. A,B) Potentiostatic discharge current (A) and SEM characterization showing the promoted Li<sub>2</sub>S precipitation on carbon fibers with LDH@NG composites (B). Reproduced with permission.<sup>[215]</sup> Copyright 2016, Wiley-VCH.

In the absence of conductive polar sites, a weak interaction between the polysulfides and the substrate leads to a high barrier for Li<sub>2</sub>S nucleation, and therefore few nuclei can form, which causes the appearance of sparse and large particles. It is difficult for these bulk Li<sub>2</sub>S aggregates to be fully reoxidized during subsequent charge, because of their high resistance and insufficient contact with conductive networks. In contrast, polar particles or atoms doped on a carbon surface serve as heterogeneous nucleation points for Li<sub>2</sub>S: then, the distribution of Li<sub>2</sub>S is even and huge aggregates are avoided. At the same time, moderate conductivity should ensure fast electron transfer to Li<sub>2</sub>S nanoparticles and a highly reversible charge can be realized.

### 4.3. Sulfur Distribution

Upon cycling, sulfur experiences multiple phase transformation, from soluble polysulfides to insoluble Li<sub>2</sub>S/Li<sub>2</sub>S<sub>2</sub>. Consequently, the continuous dissolution and deposition will alter the spatial distribution of sulfur within the cathode framework.<sup>[231,232]</sup> Uneven sulfur redistribution will substantially affect the cathode performance, since sulfur might aggregate and a small portion of the carbon framework could then not contact the sulfur species; namely, the available conductive surface area shrinks. On the other hand, soluble polysulfides might get trapped in the separator, which induces capacity fading as well.<sup>[78,233]</sup> Therefore, it is of great importance to observe and map out sulfur redistribution during cycling.

#### 4.3.1. 2D Mapping

Scanning photoelectron microscopy (SPEM) is a powerful analytical tool for mapping a specific element at an identical chemical state with higher-energy resolution and surface sensitivity than conventional energy-dispersive X-ray spectroscopy implemented in SEM and TEM. Sung and co-workers have found more homogeneous sulfur distribution during low-rate activation cycles, which mitigated the initial sulfur aggregation and therefore alleviated internal stress in the cathode framework upon full discharge.<sup>[234]</sup>

Transmission X-ray microscopy (TXM) is another option for 2D mapping of element distribution, especially for in operando study on microstructural evolution in working cells. Cui and co-workers pioneered the work of TXM adopted in Li-S battery study.<sup>[32]</sup> With TXM, they were able to track the evolution of a single sulfur particle upon cycling, and found no significant polysulfide dissolution that might promote crystallization of sulfur at the end of the charge cycle (Figure 15A). Lin et al. have coupled quantitative modeling with TXM and derived a complex dependence of the polysulfide dissolution rate on the lithium stoichiometry, indicating that polysulfide redistribution is nucleation-limited.<sup>[235]</sup>

Yu et al.<sup>[231]</sup> and Risse et al.<sup>[232]</sup> also showed the availability of using in situ X-ray radiography to map out the sulfur distribution throughout the entire electrode, instead of tracing several particles. Measuring the intensity of fluorescence or the transmittance, they managed to provide a macroscopic picture of sulfur concentration within the cathode. Sulfur dissolution, re-distribution, and deposition were all observed in both cases.

#### 4.3.2. 3D Tomography

Apart from 2D mapping, a bigger and steric picture of how sulfur distribution evolves within the whole cell is critical in providing deeper insights into Li-S batteries. X-ray microtomography (XRM) is thereby applied as it provides more information from a 3D perspective. By reconstructing a 3D model of as-observed objects, XRM can help determine the sulfur content spatially. Cheng and co-workers firstly employed XRM in Li-S battery investigation.<sup>[236–239]</sup> They examined the sulfur distribution in their sandwich cathode configuration after cycling, and, for the first time, quantitatively analyzed the sulfur proportions in each part of the cathode and the separator. Zielke et al. observed a gradual loss of active materials in the cathode and contact via phase-contrast XRM with higher resolution during cycling (Figure 15B).<sup>[240]</sup> Moreover, Zhou et al. further extended this method to study poly(dimethylsiloxane) (PDMS)-coated graphene-foam (Figure 15C,D).<sup>[238]</sup> The 3D tomography is able to reconstruct the detailed electrode structure, especially when

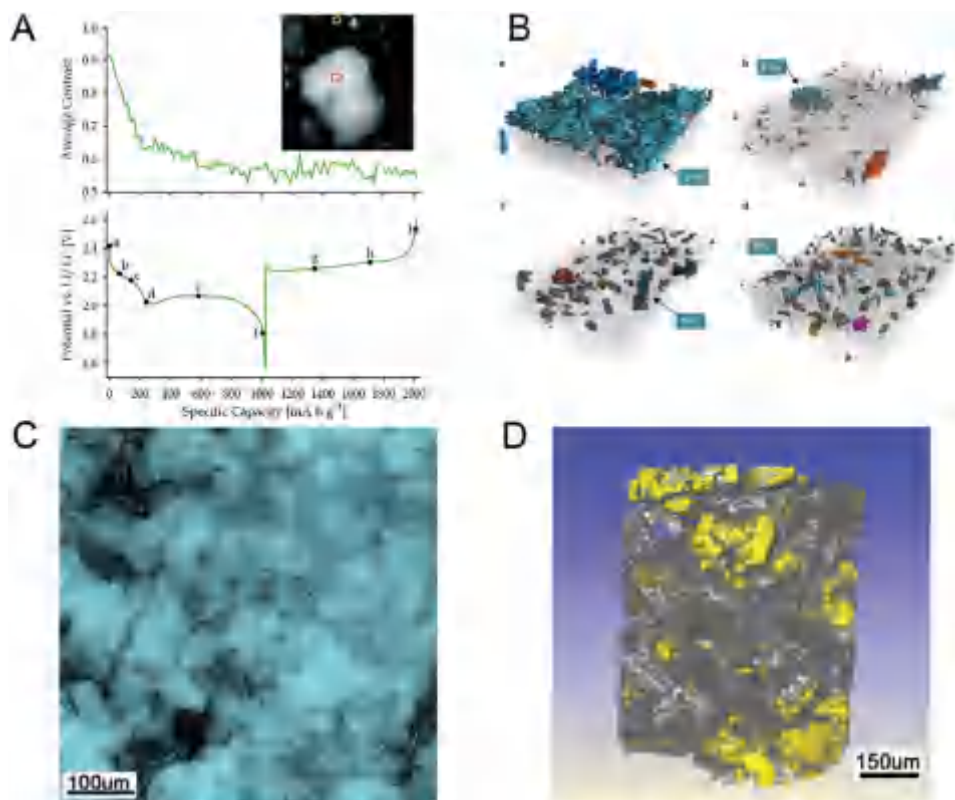


**Figure 15.** Sulfur distribution: A) Change in average contrast vs specific capacity in TXM images of a Li–S battery cycled at C/8 and the cell potential. Reproduced with permission.<sup>[32]</sup> Copyright 2012, American Chemical Society. B) 3D distribution of sulfur particles in samples after a given number of cycles: uncycled (a), 1 cycle (b), 2 cycles (c), 10 cycles (d). Only the sulfur phase is emphasized, all other phases are set to semi-transparent, or transparent. The colored particles are the largest ten clusters. Reproduced with permission.<sup>[240]</sup> Copyright 2015, Nature Publishing Group. C) XRM 2D projections of sulfur–PDMS/GF electrodes with  $10.1 \text{ mg cm}^{-2}$  sulfur loading. D) 3D images of the reconstructed sulfur–PDMS/GF electrodes with  $10.1 \text{ mg cm}^{-2}$  sulfur loading (graphene and carbon black marked in grey, sulfur particles marked in yellow and PDMS marked in white). C,D) Reproduced with permission.<sup>[238]</sup> Copyright 2015, Elsevier.

multiphase components are presented and interpenetrated. More steric information can be gained than from routine 2D mapping.

As well as direct imaging, other analytical tools such as  $\text{N}_2$  isothermal physisorption can also be adopted to study the distribution of the active phase. As Kaskel and co-workers demonstrated very recently, phase migration, which resulted from repeated dissolution/deposition of sulfur species, had profound influence on the maintenance of the porous cathode structure, and such influence depended on SOC, C-rates, and electrolyte composition.<sup>[241]</sup> More insights into sulfur distribution upon cycling are expected to be acquired by combining imaging and physicochemical characterizations.

#### 4.4. Charge Reactions

When we look at the galvanostatic voltage profiles and CV curves of normal Li–S batteries, it is quite easy to notice the different electrochemical behavior during charge and discharge. The voltage gap between the two discharge plateaus is much more obvious than that between the two charge plateaus. The charge plateaus sometimes even merge and only one sloping plateau can be seen. The voltage dip before the second discharge

plateau has been never observed in charging; while a barrier is often present at the initiation of charging. The former is attributed to the overpotential for  $\text{Li}_2\text{S}$  nuclei formation and the latter is accounted by the barrier of extracting  $\text{Li}^+$  from highly insulating  $\text{Li}_2\text{S}$ .<sup>[242–244]</sup> All these features correspond well with CV curves, where the two reduction peaks are always separated and the two oxidation peaks cannot be clearly distinguished. Hence it is reasonable to suggest that charging proceeds in a different pathway, rather than simply reverses the reaction sequence of discharging.

Nevertheless, the charging process receives much less attention than discharging, hindering a further understanding of the fading mechanism of Li–S batteries upon prolonged cycling. Some of the in situ studies mentioned in Section 3 have monitored the Li–S batteries during the first one or two cycles and discovered several characteristics of charging:

- $\text{Li}_2\text{S}$  almost always persists for a longer period during charging than discharging;
- Sulfur recrystallization is quite late compared with the time of its disappearance, and its amount and structure both differ from those of the original sulfur;
- The species and their amounts in the cell are different at the same depth of charge vs discharge.

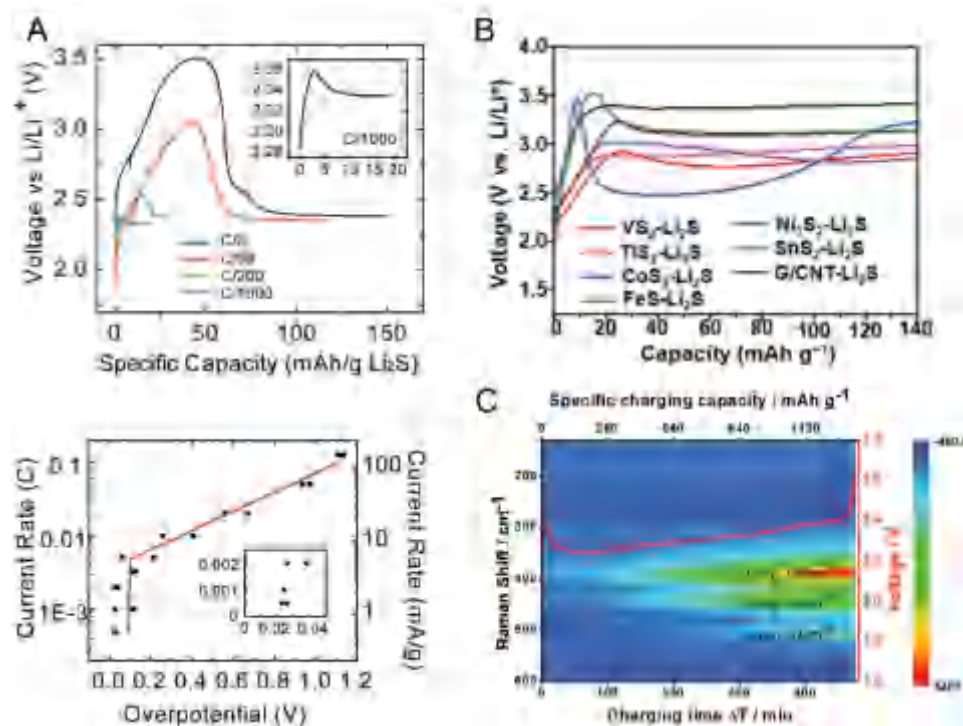


**Figure 16.** Charge mechanism: A) Upper: initial potential barrier for charging a Li<sub>2</sub>S-based cell at C/8, C/50, C/200, and C/1000 (1 C = 1166 mA g<sup>-1</sup>); Lower: relationship between current rate and overpotential (potential barrier). Reproduced with permission.<sup>[248]</sup> Copyright 2012, American Chemical Society. B) Galvanostatic voltage profile during the 1st charge of Li<sub>2</sub>S electrodes with different metal sulfides as host materials. Reproduced with permission.<sup>[191]</sup> Copyright 2017, National Academy of Sciences. C) Mapping of Raman spectroscopy obtained during the 0.1C charging process of S<sub>8</sub>/nitrogen-doped carbon composite. Reproduced with permission.<sup>[66]</sup> Copyright 2015, American Chemical Society.

These characteristics are supported by several quantitative in situ analyses using XANES, XRD, UV-vis, and Raman spectroscopy, as well as ex situ LC.<sup>[33,35,44,58,61,66]</sup> Meanwhile, detailed studies are still lacking regarding the composition and evolution of sulfur species during charging, especially for cells after tens or hundreds of cycles. RRDE measurement and Li-polysulfide redox flow batteries working in the soluble region have suggested a reversible liquid-phase reaction. Hence, the disparity of charge and discharge pathways perhaps comes from the distinct properties of the two solids: Li<sub>2</sub>S and S<sub>8</sub>.<sup>[127,245]</sup>

Mechanistic investigation of the charge process is more considered in research on Li<sub>2</sub>S cathodes.<sup>[246]</sup> Li<sub>2</sub>S, as a lithium source itself, can be coupled with nonmetallic lithium-free anodes, surmounting many serious problems related to lithium-metal anodes.<sup>[30,247]</sup> However, utilizing Li<sub>2</sub>S as the cathode starting material is no easier than elemental sulfur. Full utilization of Li<sub>2</sub>S is hampered by its extremely low ionic and electronic conductivities, as well as a huge activation barrier. In 2012, Yang et al. first carried out a comprehensive study of the electrochemical performance of micrometer-sized commercial Li<sub>2</sub>S particles.<sup>[248]</sup> They carefully compared the voltage barrier for the first charge process in a wide range of current rates. For ball-milled Li<sub>2</sub>S particles with an average size of ≈2 μm, the overpotential constantly stayed around 20 mV at current rates lower than C/200, indicating a thermodynamically controlled process under ultralow current. At higher current rates, which are reasonable for practical applications, the overpotential was found to grow linearly with the logarithm of the

rate (Figure 16A). Based on an elaborate simulation using the finite-element method, they concluded that ionic diffusion and concentration polarization only accounted for <30% of the total overpotential. The potential barrier was dominated by charge transfer and obeyed the Butler–Volmer equation (Equation (5)):

$$j = j_0 \left( \frac{c_s}{c_T} \right)^\alpha \left[ \exp \left( \frac{(1-\alpha)F\eta}{RT} \right) - \exp \left( \frac{-\alpha F\eta}{RT} \right) \right] \quad (5)$$

At relatively large overpotential (>50 mV), the Butler–Volmer equation is simplified to the Tafel equation, in which  $\eta$  is proportional to  $\ln(j/j_0)$ , which is consistent with the experimental data. The first charge of the Li<sub>2</sub>S cathode can be divided to three stages:

- The voltage barrier representing Li<sup>+</sup> extraction from single-phase Li<sub>2-x</sub>S with slow kinetics;
- The formation of soluble polysulfides accelerating the charge transfer to solid Li<sub>2-x</sub>S, and the overpotential becoming largely reduced;
- Li<sub>2-x</sub>S being fully consumed near the end of charge, and the crystallization of S<sub>8</sub> from liquid polysulfides raising the cell impedance again, leading to the voltage rise and ceasing the charge process.

The overpotential can be larger than 1 V even when charging a Li<sub>2</sub>S cathode with 1.5–2.0 mg cm<sup>-2</sup> loading at a low rate of C/8. Reducing the particle size of Li<sub>2</sub>S to below 100 nm can

effectively lower the overpotential for charge.<sup>[174,249–253]</sup> However, this strategy requires complicated fabrication and cannot be realized by ball-milling low-cost commercial  $\text{Li}_2\text{S}$ . Although similar bumps are also observed in the charging of sulfur cathodes or the subsequent cycling of  $\text{Li}_2\text{S}$  cathodes, it is difficult for the height to exceed 0.2 V. Unconverted polysulfides from the previous discharge should be responsible for the enhanced kinetics. This hypothesis was rationalized by Kaskel and co-workers who found that addition of 0.125 M  $\text{Li}_2\text{S}_6$  into the electrolyte could reduce the charge overpotential by 0.4 V.<sup>[250]</sup>

In fact, any approach that can reduce the charge-transfer resistance of a  $\text{Li}_2\text{S}$  composite is capable of ameliorating the energy barrier. RMs (ferrocene, lithium iodide, or  $\text{Fe}(\text{Cp}^*)_2$ , etc.), phosphorous pentasulfide, and catalytic metal sulfide hosts have all been proved to be effective in promoting  $\text{Li}_2\text{S}$  oxidation.<sup>[29,120,191,254]</sup> As discussed before, the latter two ways bring about fewer side effects and are more practical. Cui and co-workers conducted a systematic study of six metal sulfides, revealing that catalyzed  $\text{Li}_2\text{S}$  decomposition is closely related to the binding of isolated  $\text{Li}^+$  with sulfur atoms in metal sulfides (Figure 16B).<sup>[191]</sup> It is worth mentioning that tin disulfides with a small  $\text{Li}_2\text{S}$  decomposition barrier according to DFT calculations did not exhibit good catalytic ability, mainly due to its semiconducting nature. This discovery emphasizes another important advantage of conductive polar mediators, which is the faster oxidation kinetics of  $\text{Li}_2\text{S}$ . In particular, metallic or semimetallic disulfides of vanadium, titanium, and cobalt, with high affinity toward  $\text{Li}_2\text{S}_n$  and fast  $\text{Li}^+$  diffusion, enabled high-capacity cathodes with stable cycling performance.

Besides, conductive polar host materials not only favor the catalytic oxidation of  $\text{Li}_2\text{S}$ , but also promote the recrystallization of  $\text{S}_8$  in the charge process, which is shown by in situ Raman spectrum (Figure 16C).<sup>[66]</sup> The recrystallization of  $\text{S}_8$  was barely detected on routine carbon framework; whereas on nitrogen-doped carbon, the signals of  $\text{S}_8$  were clearly shown after cycling. This was attributed to the stabilization of the key intermediate,  $\text{Li}_2\text{S}_8$ , by Lewis basic nitrogen dopants. Without generation and effective stabilization of  $\text{Li}_2\text{S}_8$ ,  $\text{Li}_2\text{S}_6$  cannot be directly oxidized to elemental sulfur.

In general, the electrochemical reactions in the Li–S system are so complicated and convoluted that we have not reached a consensus on their mechanism after decades of research. The emerging investigation of novel electrolytes and host materials indeed creates opportunities for enhancing battery performance, but adds to the complexity of reaction routes as well. In order to dig out the underlying roots beneath the superficial results like improved cell capacity and life, advanced characterization tools and testing methods are necessary. Moreover, the sulfur distribution upon cycling and the detail about the charge process have rarely been studied. Hence, there are still countless questions about the electrochemical reactions in Li–S batteries waiting to be answered.

## 5. Transport Phenomena

Facile transport of ions is universally important for electrochemical devices since it endows these devices with high power output. This issue is, however, somewhat more complex in Li–S

batteries than in conventional LIBs because of the shuttling of polysulfides. Upon charge and discharge in Li–S batteries, soluble polysulfides leak out of cathode framework and migrate to the lithium-metal anode under the concentration gradient and electrical field, etching the lithium-metal anode, being reduced, diffusing back to and then being re-oxidized at the cathode side. This so-called shuttling phenomenon is actually a hot potato, which substantially impairs cycle performance and efficiency of Li–S batteries.<sup>[20,21]</sup> On the one hand, the shuttling effect can be mitigated by designing either physically confining or chemically trapping frameworks for sulfur cathodes.<sup>[255–257]</sup> On the other hand, tailoring the separator is another worthwhile and promising way of inhibiting the shuttling phenomenon.<sup>[258–263]</sup> Since both  $\text{Li}^+$  and polysulfides diffuse across the separator during electrochemical reactions, their transport phenomena, especially in the electrolyte and the separator, are of paramount importance. The crossover of polysulfides should be blocked while  $\text{Li}^+$  transport ought to be rapid. In this section, we will briefly discuss the methods and protocols adopted to investigate transport phenomena of both polysulfides and  $\text{Li}^+$ .

### 5.1. Polysulfide Blocking

#### 5.1.1. Visualized Experiments

To better suppress the notorious flooding of polysulfides is of top priority in separator design, and a fairly straightforward but useful way to examine the polysulfide-blockage capability of a separator is the visualized experiment. Similar to that discussed above, polysulfide solutions are prepared to simulate the catholyte; while electrolytes without polysulfides serve as the anolyte. The separator is placed in between. This configuration artificially creates a concentration gradient within the cell, and, typically, the cell, for visualization, can be a V-shaped, U-shaped, or H-shaped glass vessel. Since a polysulfide solution basically is tawny or reddish brown, it is easy to distinguish it from unpolluted blank electrolyte, and therefore to monitor the migration of polysulfides.

Yao et al. took  $\text{Li}_2\text{S}_8$  as a representative of polysulfides, and demonstrated that polysulfides not only diffuse through the porous separator but can also be trapped by and decomposed in the separator, inducing irreversible capacity loss.<sup>[233]</sup> Ma et al. utilized this direct observation method to show the effectiveness of their ion-selective polymer membrane in suppressing the troublesome migration of polysulfides.<sup>[264]</sup> Zhou and co-workers have also demonstrated MOF separators as an effective ion-selective polysulfide-blocking membrane with visualized experiments.<sup>[265]</sup> The feasibility of a ferroelectric coating on a separator with intrinsic dipoles was also indicated via this method.<sup>[266]</sup> Note that in actual batteries, an electrical field also exists, which will affect the diffusion of polysulfides since they are partially charged. Apart from the ex situ visualized experiments discussed above, Huang et al. pioneered the work of in situ observation of polysulfide transportation behavior through visualized experiments.<sup>[267]</sup> By applying a static potential of 2.4 V vs  $\text{Li}^+/\text{Li}$ , they directly monitored the shuttling phenomenon in the working cells and validated the superior effectiveness of the ion-selective membranes (i.e.,

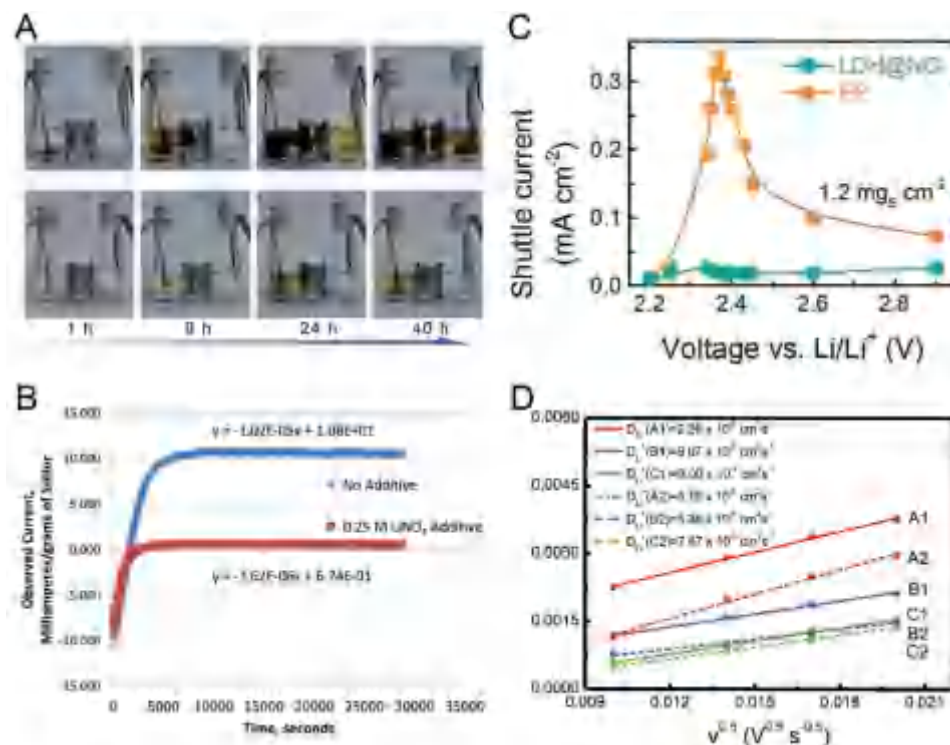


**Figure 17.** Transport phenomena: A) Optical images for the generation and diffusion of polysulfides: cell with the routine separator (top) and cell with the ion-selective Nafion-coated separator (bottom). The cells are operated with the potentiostatic discharge at 2.4 V. Reproduced with permission.<sup>[267]</sup> Copyright 2014, The Royal Society of Chemistry. B) Observed current during potential hold at 95% state of charge for cells with/without LiNO<sub>3</sub> additive. The algebraic equations express the shuttle-current decay rate. Reproduced with permission.<sup>[269]</sup> Copyright 2015, The Electrochemical Society. C) A comparison between Li-S cells with LDH@NG and PP separators, in shuttle currents vs applied potentiostatic charging voltages. Reproduced with permission.<sup>[215]</sup> Copyright 2016, Wiley-VCH. D) CV at different voltage scan rates of Li-S cells, and the linear fits of the peak currents with Li<sup>+</sup>-diffusion coefficient. Reproduced with permission.<sup>[272]</sup> Copyright 2015, American Chemical Society.

Nafion-coated separators) for blocking polysulfide shuttling for the first time (Figure 17A).

Visualized experiments are convenient and powerful tools as proof-of-concept experiments to study the shuttling phenomenon and its suppression. Researchers can get a clear sense from the results. However, only mere qualitative evaluation, except the treatment using the gray level derived from photographs of polysulfide solution, can be obtained through this method, and it is not satisfying for further investigation.

### 5.1.2. Shuttle Current

In order to get quantitative or semi-quantitative measurement of the shuttling phenomenon, the polysulfide solution used for visualization experiment can be further analyzed through spectroscopy characterization, such as UV-vis. However, it is way too complicated. Therefore, more advanced methods are needed, preferably to be simple and straightforward measurements.

Helms and co-workers stepped forward by adopting electrochemical measurements such as CV and square-wave voltammetry to analyze the polysulfide concentration variation of the blank side in visualized tests.<sup>[268]</sup> Through calibration, the current could be interpreted into the polysulfide concentration.

Such a method still has the drawback that it is not applicable for practical Li-S cells.

Moy et al. delved deeper into evaluating the shuttling effect by developing an electrochemical method to directly measure the “shuttle current” (Figure 17B).<sup>[269]</sup> Upon the leakage of polysulfides, the electrochemical potential at the cathode side would drop, as would the voltage of the whole cell. To counterbalance this voltage drop, they employed an external current and maintained the cell voltage at a constant value. Such an external current was regarded as the “shuttle current” since it offsets the effect induced by internal polysulfide redox. By measuring the applied current, quantitatively measuring the magnitude of the shuttling effect in a working cell can be realized in a facile way. Peng et al. have extended this powerful method by plotting out the as-measured shuttle current vs cell voltage (Figure 17C).<sup>[215]</sup> It can be observed that the peak of the shuttle current was located at 2.38 V, at which the concentration of the polysulfides reached the maximum. Through the measurement of the shuttle current, the effectiveness of the cooperative interface for shuttling inhibition was clearly validated. The shuttle current decreased by one-to-two orders within the whole range of charging voltage.

The measurement of the shuttle current is a relatively new but promising analytical tool in the sense that it provides more detailed but simpler information of a dynamic phenomenon

that is hard to evaluate directly. In addition to the separator, the design of the cathode or the anode can also be tested in this way.

### 5.1.3. Transference Number in Polysulfide Solutions

The  $\text{Li}^+$  transference number,  $t_{\text{Li}^+}$ , is also of great importance, in that it can serve as a good quantitative indicator for evaluating shuttling inhibition as well. Because the sum of the transference number of cations and anions is 1, the contribution of polysulfide anions to overall ion transport, namely polysulfide migration, is suggested to be low if  $t_{\text{Li}^+}$  is quite high. In fact,  $t_{\text{Li}^+}$  has widely been employed to study ion-selective membranes, which have been proved to be very effective as separators in Li-S batteries. Basically ion-selective separators function through anion immobilization; therefore, the transference number would suggest the main internal charge carrier during cycling. More specifically, a high  $t_{\text{Li}^+}$  in pure lithium polysulfide solutions indicates that the current is mostly carried by  $\text{Li}^+$  instead of the polysulfide and other anions.

The transference number can be measured via the conventional Bruce and Vincent method.<sup>[270]</sup> Typically, a symmetrical cell is assembled with lithium metal as the two counter electrodes and a polysulfide solution as the electrolyte. Then, the cell is potentiostatically polarized and the transference number is given by Equation (6):

$$t_{\text{Li}^+} = \frac{I_{\text{ss}}(\Delta V - I_0 R_0)}{I_0(\Delta V - I_{\text{SS}} R_{\text{SS}})} \quad (6)$$

in which  $\Delta V$  is the potential applied;  $R_0$  and  $R_{\text{SS}}$  are the initial and steady-state resistances given by EIS tests before and after the polarization process, respectively; and  $I_0$  and  $I_{\text{SS}}$  are the initial and steady-state currents, respectively. Equipped with this tool, Jin et al. have investigated Nafion ionomer films applied in Li-S batteries, where  $t_{\text{Li}^+}$  is estimated to be 0.986, indicating that almost no anions can transport through the ionomer electrolyte.<sup>[271]</sup> Huang et al. have proposed GO coatings as anion-repulsive layers to prevent polysulfide diffusion.<sup>[272]</sup> The  $\text{Li}^+$ -permselectivity of this GO-modified separator was verified with a  $t_{\text{Li}^+}$  of 0.93. Archer and co-workers have demonstrated a new group of sulfonated polymer membranes with high cation transference numbers, as well as a high  $\text{Li}^+$  diffusion coefficient, which well suppress the diffusion of polysulfides.<sup>[264]</sup>

### 5.1.4. Self-Discharge

The above-mentioned evaluations of on-service performance provide significant insight into the shuttling phenomenon in a working cell. However, it is also well worth noting that practical Li-S batteries are not always in the working state due to the inevitable on-shelf time for delivery or sale. Consequently, a natural result of internal redox in Li-S batteries is a decrease in the remaining capacity without any energy output. This so-called self-discharge process under static conditions ought to be studied for characterizing separators as well. Chung and Manthiram first studied the capacity of Li-S batteries after

months of storage, and exhibited a significant suppression of self-discharge when a conventional polypropylene (PP) separator was coated with a carbon layer.<sup>[261]</sup> Xu et al. investigated the self-discharge phenomenon in Li-S batteries in different configurations. By monitoring the open-circuit voltage and the capacity after rest of the cells, they identified the disappearance of the high discharge plateau, which refers to long-chain polysulfide conversion.<sup>[273]</sup> Through the observation of self-discharge, they further demonstrated the effectiveness of Nafion-coated separators and  $\text{LiNO}_3$  additives in suppressing self-discharge.

## 5.2. $\text{Li}^+$ Diffusion

Beyond the shuttling inhibition, another crucial aspect of separator characterization is the  $\text{Li}^+$ -diffusion coefficient. Normally, commercial polyolefin separators such as polypropylene (PP) membranes with large slit pores have a relatively high  $\text{Li}^+$ -diffusion coefficient, thereby enabling fast  $\text{Li}^+$  transport under a high C-rate. However, they also provide polysulfides with a migration highway. PP separators with surface modification, such as a Nafion or GO coating,<sup>[259,272]</sup> and other novel separators, like sulfonated copolymer separators,<sup>[264]</sup> have been proposed to suppress the shuttling effect by variation in the pore size and surface functionalities to localize polysulfide diffusion at the cathode side. In addition, carbonaceous interlayers applied to block polysulfide flux and reuse leaked-out sulfur species always add to the thickness of the separator. Under such circumstances, the  $\text{Li}^+$ -diffusion coefficient might be relatively small due to either an intrinsic low permeability of the coating layers or an increased diffusion distance. Consequently, batteries with these separators might suffer from uninteresting limitations of low working current. Hence, it is quite important to measure the  $\text{Li}^+$ -diffusion coefficient for these separators or interlayers.

Manthiram and co-workers have pioneered investigation of the interlayer. For example, they have shown a single-walled carbon-nanotube interlayer that protects both the cathode and anode without introducing extra diffusion impedance.<sup>[274-282]</sup> Helms and co-workers have found some interesting phenomenon in polymers of intrinsic microporosity: upon cycling, the effective diffusion coefficient increases, invoking new understanding of ion selectivity and durability of chemical reactive membranes.<sup>[283]</sup>

$\text{Li}^+$  transport in the cathode layer and modified separator may account for a respectable portion of the overall polarization as well, but is seldom studied. Direct measurement of the absolute value of the  $\text{Li}^+$ -diffusion coefficient is not possible, but comparison of the relative magnitude could be realized by carrying out CV at several sweep rates. At relatively slow sweep rates (usually  $<1 \text{ mV s}^{-1}$ ), the electrochemical reaction is limited by semi-infinite linear diffusion, and the peak current is dictated by the  $\text{Li}^+$ -diffusion coefficient as follows (Randles-Sevcik equation, Equation (7)):

$$i_p = 2.69 \times 10^5 A z^{1.5} D_{\text{Li}}^{0.5} c_{\text{Li}} \nu^{0.5} \quad (7)$$

where  $D_{\text{Li}}$  is the diffusion coefficient of  $\text{Li}^+$ ,  $z$  is the number of transferred electron,  $A$  is the active surface area,  $c_{\text{Li}}$  is the

concentration of  $\text{Li}^+$ , and  $v$  is the sweep rate.<sup>[188]</sup> The linear dependence of  $i_p$  on  $v^{0.5}$  confirms  $\text{Li}^+$  diffusion to be rate-limiting, as shown in Figure 17D.<sup>[272]</sup> It is therefore possible to study the influence of cathode design, separator modification, and interlayer on the transport of  $\text{Li}^+$ . By reducing the size of the sulfur particles or introducing niobium pentoxide nanoparticles,  $\text{Li}^+$  transport can be enhanced.<sup>[284,285]</sup> It was also proved that introducing a thin layer of GO will not induce a significant drop in the  $\text{Li}^+$ -diffusion coefficient.<sup>[272]</sup>

Tao et al. systematically compared the adsorption and diffusion of  $\text{Li}_2\text{S}_n$  on various nonconductive metal oxides.<sup>[188]</sup> When polysulfides are immobilized on insulating metal oxides, an extra step of surface diffusion is needed before they can be further reduced. This work proposed that a balance between adsorption and diffusion is necessary for sulfur-cathode design. The large binding energy and the small diffusion barrier are expected to play a synergistic role in promoting the performance of cathode materials. Alumina ( $\text{Al}_2\text{O}_3$ ), with the biggest obstacles for  $\text{Li}^+$  transport, and calcia ( $\text{CaO}$ ), with the smallest binding energy, are not suitable as the cathode host. However, considering the large size of polysulfide anions,  $\text{Li}_2\text{S}_n$  clusters may not be swift enough to reach the conductive surface via diffusion. Instead, anchored polysulfides might undergo disproportionation on the oxide surface, and the kinetics are expected to be slow since the single-electron-transfer step is substituted by complex chemical reactions. Diffusion and direct electrochemical reduction might only occur near the triple-phase boundary of carbon, oxide, and the electrolyte. To enlarge the triple-phase boundary, a delicate synthetic procedure is inevitable so as to evenly disperse ultrafine nanoparticles into the carbon scaffold.<sup>[188,208,286]</sup> Integrating with the former discussion about polysulfide redox and  $\text{Li}_2\text{S}$  deposition, we can speculate that conductive polar materials should endow a sulfur cathode with a better performance than the insulating host when they possess comparable binding strength toward polysulfides.

In addition, it is also worth noting that wettability and electrolyte uptake matter in batteries. With contact-angle experiments, Su and co-workers have shown improved electrolyte wettability of the cathodes induced by the incorporation of  $\text{MnO}_2$  nanospheres, through which the  $\text{Li}^+$  transport was enhanced at the cathode–electrolyte interface.<sup>[287]</sup> Thereby, the redox kinetics were improved. This is also quite important in separator characterization. Normally a separator that wets easily with the electrolyte can facilitate electrolyte filling in the cell assembly and also better retain the electrolyte to help increase the cycle life.

As we design functional separator, interlayer, or cathode host materials for Li–S batteries, a balance between blocking polysulfides and transporting  $\text{Li}^+$  should always be borne in mind. Compromise might be inevitable sometimes, but the ultimate goal should always be pursuing high ion-selectivity while maintaining a high enough permeability to  $\text{Li}^+$ .

## 6. Conclusions and Perspectives

The frontiers of fundamental science and engineering design for Li–S batteries have both been pushed forward significantly in the past decades, bringing them closer to commercialization.

Consensus has been reached on some basic, yet critical questions about Li–S systems:

- $\text{S}_8$ – $\text{Li}_2\text{S}_n$ – $\text{Li}_2\text{S}$  (solid–liquid–solid) multistage transformation undoubtedly occurs during the cycling of Li–S batteries in the most conventional configuration;
- The discharge/charge of Li–S batteries involves many interdependent and concurrently happening reactions, and various polysulfides in the form of dianions or radicals always coexist in a dynamic equilibrium;
- The high discharge plateau and slope region are likely to be dominated by electrochemical reduction, while the low plateau may be limited by sluggish chemical dissociation reactions, at least in ether-based electrolytes;
- The choice of electrolyte and cathode materials have profound influence on the reaction pathways and performance of the cell as a whole;
- The charging process of Li–S batteries is far from solely being the reverse of discharge, and is little studied in the previous literature.

Such understandings have already inspired researchers to conceive many creative strategies to attempt to boost the performance of sulfur cathodes. We have highlighted some emerging concepts for cathode, electrolyte, and separator design in this review, including:

- Highly solvating vs nonsolvating electrolytes;<sup>[54,127,129,132]</sup>
- Soluble RMs vs immobile conductive polar host materials.<sup>[118,122,224,225]</sup>

Further work is still undergoing to elucidate the detailed mechanism of the existing strategies, as well as to search for novel routes.

Accompanied by the tremendous progress in materials selection, electrolyte optimization, interface stabilization, and cell configuration, methods for studying Li–S batteries have also witnessed revolutionary changes in recent years, which are summarized as follows:

In situ or in operando spectroscopic characterization:

- Advantages: a number of powerful in situ or in operando spectroscopic tools and specially modified cell structures enable researchers to monitor the variety, quantity, temporal evolution, and spatial distribution of sulfur species in a working Li–S battery.<sup>[32,35,39,44,60,61]</sup> Understanding of the reaction mechanism in Li–S batteries is greatly promoted owing to these efforts.
- Disadvantages: Complex experimental procedures, impractical cell design, and difficult data analysis are major obstacles for the application of in situ characterization methods. Moreover, synchrotron-based XRD and XANES, despite their high resolution and capability to recognize sulfur in different environments, cannot be popularized because of the limited number of synchrotron light sources around the world.

Therefore, a plausible mechanism has been proposed from the majority of the work on Li–S by integrating ex situ characterization and electrochemical tests.

Ex situ spectroscopic characterization or post-mortem analysis:

- **Advantages:** Ex situ XPS and Raman spectroscopy, as well as post-mortem SEM and TEM characterization are prevalently seen in the literature, and have successfully captured the surface chemistry and morphology of cell components at different stages of the electrochemical course.<sup>[46,225,230]</sup> Normally, there is no special demand for the re-design of the electrochemical cell and high-quality infrastructures.
- **Disadvantages:** Unfortunately, these methods normally require disassembling the cell, washing the electrodes, and transferring to the destination, possibly causing serious contamination, significant deviation from working conditions, and misleading phenomena.

Electrochemical protocols:

- **Advantages:** In the past two years, several novel electrochemical protocols have been developed, and typical cases include polysulfide symmetric cells,<sup>[118,224,225]</sup> potentiostatic nucleation,<sup>[119,122,215]</sup> and shuttle-current measurement.<sup>[215,269]</sup> These facile experiments have helped decipher several paramount processes individually in Li–S batteries: i) liquid-phase polysulfide redox, ii) Li<sub>2</sub>S precipitation, and iii) polysulfide shuttling.
- **Disadvantages:** Electrochemical methods are incapable of capturing the exact reaction pathways but rather measure critical parameters of known processes.

All these tools and their applications are summarized in **Table 4**.

The vast space for improving the energy and power density of Li–S batteries is still waiting to be explored. Society has been aware that knowledge and engineering of both the anode and cathode are indispensable to achieve the goal of stably outputting a higher energy density than LIBs. Realizing that the high E/S ratio (usually >10:1) used for most work in this area precludes the energy density from exceeding 300 W h kg<sup>-1</sup>,<sup>[220,288]</sup> more efforts on the cathode side should be devoted to lowering the amount of electrolyte. A low E/S ratio, such as 5:1, means a sulfur concentration of 6.25 M supposing full dissolution, which inevitably causes incomplete utilization of sulfur and precipitation of inactive Li<sub>2</sub>S. High-DN solvents may offer a chance for realizing such a low E/S ratio without sacrificing the capacity and cycling stability of the cathode. Moreover, a higher areal loading of sulfur in the cathode is an inevitable trend to lower the weight ratio of inactive materials, and to achieve higher energy density. Efforts in building high-energy-density Li–S batteries have been systematically reviewed in some recent papers.<sup>[14]</sup>

We would not make much comment on lithium anodes here, since they are not the focus of this contribution. However, we suggest that difficulties in constructing durable, chemically stable, and mechanically robust surface layers have become a bottleneck for all battery systems utilizing lithium metal as the anode. Recent advancements in an artificial SEI and solid electrolytes shed new light on the development of a robust Li<sup>+</sup>-permselective interface.<sup>[289–294]</sup> Such a polysulfide-inhibiting

**Table 4.** Spectroscopic and electrochemical techniques for studying Li–S batteries.

Technique	Applications
Spectroscopic	
In situ XRD	Study the relative amount of crystalline phases during cell operation
<sup>6</sup> Li/ <sup>7</sup> Li NMR	Determine the relative amount of dissolved vs solid lithium (poly)sulfides
XANES	Quantitatively determine the fraction of several sulfur containing species in the total sulfur; Study the interaction between host materials and polysulfides
UV–Vis	Determine the absolute amount of dissolved polysulfides, S <sub>3</sub> <sup>•-</sup> and S <sub>8</sub>
Raman spectroscopy	Qualitatively detection of part of the polysulfides; Study the interaction between host materials and polysulfides
LC-MS	Determine the absolute amount of all polysulfide dianions
EPR/ESR	Study the radical species, especially S <sub>3</sub> <sup>•-</sup>
XPS	Study the composition of SEI; Study the detailed interaction between host materials and polysulfides
IR spectroscopy	Study the interaction between host materials and polysulfides
Electrochemical	
CV	Study the electron transfer process during charge and discharge; Determine the overall Li <sup>+</sup> diffusion coefficient
EIS	Deconvolute the impedance from different processes, including charge transfer resistance, interfacial resistance and electrolyte resistance; Help determine Li <sup>+</sup> transference number;
Symmetric cell	Study liquid-phase polysulfide redox kinetics
Potentiostatic nucleation	Study Li <sub>2</sub> S nucleation–growth mechanism kinetic parameters
Shuttle Current	Measure the magnitude of shuttle phenomenon at different cell voltage
Visualized experiment	Study polysulfide leakage from the electrode, and diffusion through the separator in macroscopic scale

membrane would be of great promise in an electrolyte environment with high sulfur content.

In conclusion, numerous problems remain to be solved in both the scientific and the engineering aspects of Li–S batteries. A holistic consideration must be taken when optimizing any single component in the cell. Industrialization can only be realized with integrated improvement of all parts of a Li–S cell, together with a deeper insight into the underlying mechanisms. Likewise, fundamental understanding into the electrochemistry of this complex system can only be accomplished by combining multiple complementary characterization and analytical tools. Even though challenging, taking advantage of the latest computational and experimental techniques, we still hold plenty of confidence of a splendid future for Li–S batteries.

## Acknowledgements

G.Z. and Z.-W.Z. contributed equally to this work. This work was supported by the National Key Research and Development Program (Nos. 2016YFA0202500, 2016YFA0200102, and 2015CB932500), the National Natural Science Foundation of China (Nos. 21422604 and 21676160), and the Tsinghua University Initiative Scientific Research Program. The authors thank Xin-Bing Cheng, Chong Yan, Ting-Zhou Zhuang, Wen-Tao Xu, Rui Zhang, and Chen-Zi Zhao at Tsinghua University for helpful discussion.

## Conflict of Interest

The authors declare no conflict of interest.

## Keywords

electrolytes, in situ characterization, lithium–sulfur batteries, separators, sulfur cathodes

Received: March 11, 2017

Revised: March 30, 2017

Published online:

- [1] S. Chu, Y. Cui, N. Liu, *Nat. Mater.* **2017**, *16*, 16.
- [2] B. Dunn, H. Kamath, J. M. Tarascon, *Science* **2011**, *334*, 928.
- [3] C. P. Grey, J. M. Tarascon, *Nat. Mater.* **2017**, *16*, 45.
- [4] M. Armand, J. M. Tarascon, *Nature* **2008**, *451*, 652.
- [5] P. G. Bruce, S. A. Freunberger, L. J. Hardwick, J.-M. Tarascon, *Nat. Mater.* **2012**, *11*, 19.
- [6] M. D. Slater, D. Kim, E. Lee, C. S. Johnson, *Adv. Funct. Mater.* **2013**, *23*, 947.
- [7] D. Aurbach, Z. Lu, A. Schechter, Y. Gofer, H. Gizbar, R. Turgeman, Y. Cohen, M. Moshkovich, E. Levi, *Nature* **2000**, *407*, 724.
- [8] B. Scrosati, J. Garche, *J. Power Sources* **2010**, *195*, 2419.
- [9] Q. Pang, X. Liang, C. Y. Kwok, L. F. Nazar, *Nat. Energy* **2016**, *1*, 16132.
- [10] X. Fang, H. S. Peng, *Small* **2015**, *11*, 1488.
- [11] A. Manthiram, S. H. Chung, C. X. Zu, *Adv. Mater.* **2015**, *27*, 1980.
- [12] A. Rosenman, E. Markevich, G. Salitra, D. Aurbach, A. Garsuch, F. F. Chesneau, *Adv. Energy Mater.* **2015**, *5*, 1500212.
- [13] R. Xu, J. Lu, K. Amine, *Adv. Energy Mater.* **2015**, *5*, 1500408.
- [14] H. J. Peng, J. Q. Huang, X. B. Cheng, Q. Zhang, *Adv. Energy Mater.* **2017**, *7*, 1700260.
- [15] R. G. Cao, W. Xu, D. P. Lv, J. Xiao, J. G. Zhang, *Adv. Energy Mater.* **2015**, *5*, 1402273.
- [16] R. Zhang, N. W. Li, X. B. Cheng, Y. X. Yin, Q. Zhang, Y. G. Guo, *Adv. Sci.* **2017**, *4*, 1600445.
- [17] W. Xu, J. L. Wang, F. Ding, X. L. Chen, E. Nasybutin, Y. H. Zhang, J. G. Zhang, *Energy Environ. Sci.* **2014**, *7*, 513.
- [18] Y. X. Yin, S. Xin, Y. G. Guo, L. J. Wan, *Angew. Chem., Int. Ed.* **2013**, *52*, 13186.
- [19] S. S. Zhang, *J. Power Sources* **2013**, *231*, 153.
- [20] M. R. Busche, P. Adelhelm, H. Sommer, H. Schneider, K. Leitner, J. Janek, *J. Power Sources* **2014**, *259*, 289.
- [21] Y. V. Mikhaylik, J. R. Akridge, *J. Electrochem. Soc.* **2004**, *151*, A1969.
- [22] Y. Son, J. S. Lee, Y. Son, J. H. Jang, J. Cho, *Adv. Energy Mater.* **2015**, *5*, 1500110.
- [23] J. L. Wang, Y. S. He, J. Yang, *Adv. Mater.* **2015**, *27*, 569.
- [24] J. W. Choi, D. Aurbach, *Nat. Rev. Mater.* **2016**, *1*, 16013.
- [25] M. Q. Zhao, H. J. Peng, G. L. Tian, Q. Zhang, J. Q. Huang, X. B. Cheng, C. Tang, F. Wei, *Adv. Mater.* **2014**, *26*, 7051.
- [26] S. S. Zhang, *Electrochim. Acta* **2012**, *70*, 344.
- [27] A. Rosenman, R. Elazari, G. Salitra, E. Markevich, D. Aurbach, A. Garsuch, *J. Electrochem. Soc.* **2015**, *162*, A470.
- [28] S. Xin, L. Gu, N. H. Zhao, Y. X. Yin, L. J. Zhou, Y. G. Guo, L. J. Wan, *J. Am. Chem. Soc.* **2012**, *134*, 18510.
- [29] F. X. Wu, J. T. Lee, N. Nitta, H. Kim, O. Borodin, G. Yushin, *Adv. Mater.* **2015**, *27*, 101.
- [30] Y. Yang, M. T. McDowell, A. Jackson, J. J. Cha, S. S. Hong, Y. Cui, *Nano Lett.* **2010**, *10*, 1486.
- [31] H. J. Peng, T. Z. Hou, Q. Zhang, J. Q. Huang, X. B. Cheng, M. Q. Guo, Z. Yuan, L. Y. He, F. Wei, *Adv. Mater. Interfaces* **2014**, *1*, 1400227.
- [32] J. Nelson, S. Misra, Y. Yang, A. Jackson, Y. Liu, H. Wang, H. Dai, J. C. Andrews, Y. Cui, M. F. Toney, *J. Am. Chem. Soc.* **2012**, *134*, 6337.
- [33] M. A. Lowe, J. Gao, H. D. Abruña, *RSC Adv.* **2014**, *4*, 18347.
- [34] S. Waluś, C. Barchasz, J. F. Colin, J. F. Martin, E. Elkaïm, J. C. Leprêtre, F. Alloin, *Chem. Commun.* **2013**, *49*, 7899.
- [35] S. Waluś, C. Barchasz, R. Bouchet, J. C. Leprêtre, J. F. Colin, J. F. Martin, E. Elkaïm, C. Baecht, F. Alloin, *Adv. Energy Mater.* **2015**, *5*, 1500165.
- [36] J. Kulisch, H. Sommer, T. Brezesinski, J. Janek, *Phys. Chem. Chem. Phys.* **2014**, *16*, 18765.
- [37] A. Schneider, C. Weidmann, C. Suchomski, H. Sommer, J. r. Janek, T. Brezesinski, *Chem. Mater.* **2015**, *27*, 1674.
- [38] N. A. Cañas, S. Wolf, N. Wagner, K. A. Friedrich, *J. Power Sources* **2013**, *226*, 313.
- [39] K. A. See, M. Leskes, J. M. Griffin, S. Britto, P. D. Matthews, A. Emyl, A. Van der Ven, D. S. Wright, A. J. Morris, C. P. Grey, R. Seshadri, *J. Am. Chem. Soc.* **2014**, *136*, 16368.
- [40] L. A. Huff, J. L. Rapp, J. A. Baughman, P. L. Rinaldi, A. A. Gewirth, *Surf. Sci.* **2015**, *631*, 295.
- [41] G. C. Yang, S. Q. Shi, J. H. Yang, Y. M. Ma, *J. Mater. Chem. A* **2015**, *3*, 8865.
- [42] Z. M. Feng, C. S. Kim, A. Vijn, M. Armand, K. H. Bevan, K. Zaghib, *J. Power Sources* **2014**, *272*, 518.
- [43] A. Paoletta, W. Zhu, H. Marceau, C. S. Kim, Z. M. Feng, D. Q. Liu, C. Gagnon, J. Trottier, G. Abdelbast, P. Hovington, A. Vijn, G. P. Demopoulos, M. Armand, K. Zaghib, *J. Power Sources* **2016**, *325*, 641.
- [44] M. Cuisinier, P. E. Cabelguen, S. Evers, G. He, M. Kolbeck, A. Garsuch, T. Bolin, M. Balasubramanian, L. F. Nazar, *J. Phys. Chem. Lett.* **2013**, *4*, 3227.
- [45] H. Park, H. S. Koh, D. J. Siegel, *J. Phys. Chem. C* **2015**, *119*, 4675.
- [46] R. Xu, I. Belharouak, X. F. Zhang, R. Chamoun, C. Yu, Y. Ren, A. M. Nie, R. Shahbazian-Yassar, J. Lu, J. C. M. Li, K. Amine, *ACS Appl. Mater. Interfaces* **2014**, *6*, 21938.

- [47] M. U. M. Patel, I. Arcon, G. Aquilanti, L. Stievano, G. Mali, R. Dominko, *ChemPhysChem* **2014**, *15*, 894.
- [48] J. Xiao, J. Z. Hu, H. H. Chen, M. Vijayakumar, J. M. Zheng, H. L. Pan, E. D. Walter, M. Hu, X. C. Deng, J. Feng, B. Y. Liaw, M. Gu, Z. D. Deng, D. P. Lu, S. C. Xu, C. M. Wang, J. Liu, *Nano Lett.* **2015**, *15*, 3309.
- [49] K. H. Wujcik, T. A. Pascal, C. D. Pemmaraju, D. Devaux, W. C. Stolte, N. P. Balsara, D. Prendergast, *Adv. Energy Mater.* **2015**, *5*, 1500285.
- [50] J. Gao, M. A. Lowe, Y. Kiya, H. D. Abruna, *J. Phys. Chem. C* **2011**, *115*, 25132.
- [51] T. A. Pascal, K. H. Wujcik, J. Velasco-Velez, C. H. Wu, A. A. Teran, M. Kapilashrami, J. Cabana, J. H. Guo, M. Salmeron, N. Balsara, D. Prendergast, *J. Phys. Chem. Lett.* **2014**, *5*, 1547.
- [52] K. H. Wujcik, J. Velasco-Velez, C. H. Wu, T. Pascal, A. A. Teran, M. A. Marcus, J. Cabana, J. H. Guo, D. Prendergast, M. Salmeron, N. P. Balsara, *J. Electrochem. Soc.* **2014**, *161*, A1100.
- [53] M. Cuisinier, C. Hart, M. Balasubramanian, A. Garsuch, L. F. Nazar, *Adv. Energy Mater.* **2015**, *5*, 1401801.
- [54] M. Cuisinier, P. E. Cabelguen, B. D. Adams, A. Garsuch, M. Balasubramanian, L. F. Nazar, *Energy Environ. Sci.* **2014**, *7*, 2697.
- [55] Y. Gorlin, A. Siebel, M. Piana, T. Huthwelker, H. Jha, G. Monsch, F. Kraus, H. A. Gasteiger, M. Tromp, *J. Electrochem. Soc.* **2015**, *162*, A1146.
- [56] C. Barchasz, F. Molton, C. Duboc, J. C. Lepretre, S. Patoux, F. Alloin, *Anal. Chem.* **2012**, *84*, 3973.
- [57] M. U. M. Patel, R. Demir-Cakan, M. Morcrette, J. M. Tarascon, M. Gaberscek, R. Dominko, *ChemSusChem* **2013**, *6*, 1177.
- [58] M. U. M. Patel, R. Dominko, *ChemSusChem* **2014**, *7*, 2167.
- [59] N. A. Canas, D. N. Fronczek, N. Wagner, A. Latz, K. A. Friedrich, *J. Phys. Chem. C* **2014**, *118*, 12106.
- [60] Q. L. Zou, Y. C. Lu, *J. Phys. Chem. Lett.* **2016**, *7*, 1518.
- [61] A. Kawase, S. Shirai, Y. Yamoto, R. Arakawa, T. Takata, *Phys. Chem. Chem. Phys.* **2014**, *16*, 9344.
- [62] H. L. Wu, L. A. Huff, A. A. Gewirth, *ACS Appl. Mater. Interfaces* **2015**, *7*, 1709.
- [63] J. Hannauer, J. Scheers, J. Fullenwarth, B. Fraisse, L. Stievano, P. Johansson, *ChemPhysChem* **2015**, *16*, 2755.
- [64] M. Hagen, P. Schiffels, M. Hammer, S. Dorfler, J. Tubke, M. J. Hoffmann, H. Althues, S. Kaskel, *J. Electrochem. Soc.* **2013**, *160*, A1205.
- [65] J. T. Yeon, J. Y. Jang, J. G. Han, J. Cho, K. T. Lee, N. S. Choi, *J. Electrochem. Soc.* **2012**, *159*, A1308.
- [66] J. J. Chen, R. M. Yuan, J. M. Feng, Q. Zhang, J. X. Huang, G. Fu, M. S. Zheng, B. Ren, Q. F. Dong, *Chem. Mater.* **2015**, *27*, 2048.
- [67] Y. Diao, K. Xie, S. Z. Xiong, X. B. Hong, *J. Electrochem. Soc.* **2012**, *159*, A421.
- [68] D. Zheng, X. R. Zhang, C. Li, M. E. McKinnon, R. G. Sadok, D. Y. Qu, X. Q. Yu, H. S. Lee, X. Q. Yang, D. Y. Qu, *J. Electrochem. Soc.* **2015**, *162*, A203.
- [69] Q. Wang, J. M. Zheng, E. Walter, H. L. Pan, D. P. Lv, P. J. Zuo, H. H. Chen, Z. D. Deng, B. Y. Liaw, X. Q. Yu, X. Q. Yang, J. G. Zhang, J. Liu, J. Xiao, *J. Electrochem. Soc.* **2015**, *162*, A474.
- [70] J. Z. Chen, D. X. Wu, E. Walter, M. Engelhard, P. Bhattacharya, H. L. Pan, Y. Y. Shao, F. Gao, J. Xiao, J. Liu, *Nano Energy* **2015**, *13*, 267.
- [71] M. Vijayakumar, N. Govind, E. Walter, S. D. Burton, A. Shukla, A. Devaraj, J. Xiao, J. Liu, C. M. Wang, A. Karim, S. Thevuthasan, *Phys. Chem. Chem. Phys.* **2014**, *16*, 10923.
- [72] M. E. Fleet, X. Liu, *Spectrochim. Acta, Part B* **2010**, *65*, 75.
- [73] R. Bonnaterre, G. Cauquis, *J. Chem. Soc., Chem. Commun.* **1972**, 293.
- [74] B. S. Kim, S. M. Park, *J. Electrochem. Soc.* **1993**, *140*, 115.
- [75] F. Gaillard, E. Levillain, *J. Electroanal. Chem.* **1995**, *398*, 77.
- [76] R. P. Martin, W. H. Doub Jr., J. L. Roberts Jr., D. T. Sawyer, *Inorg. Chem.* **1973**, *12*, 1921.
- [77] D. H. Han, B. S. Kim, S. J. Choi, Y. J. Jung, J. Kwak, S. M. Park, *J. Electrochem. Soc.* **2004**, *151*, E283.
- [78] H. J. Peng, D. W. Wang, J. Q. Huang, X. B. Cheng, Z. Yuan, F. Wei, Q. Zhang, *Adv. Sci.* **2016**, *3*, 1500268.
- [79] T. Chivers, P. J. W. Elder, *Chem. Soc. Rev.* **2013**, *42*, 5996.
- [80] G. S. Pokrovski, L. S. Dubrovinsky, *Science* **2011**, *331*, 1052.
- [81] M. Wild, L. O'Neill, T. Zhang, R. Purkayastha, G. Minton, M. Marinescu, G. J. Offer, *Energy Environ. Sci.* **2015**, *8*, 3477.
- [82] R. Black, S. H. Oh, J. H. Lee, T. Yim, B. Adams, L. F. Nazar, *J. Am. Chem. Soc.* **2012**, *134*, 2902.
- [83] L. Johnson, C. M. Li, Z. Liu, Y. H. Chen, S. A. Freunberger, P. C. Ashok, B. B. Praveen, K. Dholakia, J. M. Tarascon, P. G. Bruce, *Nat. Chem.* **2015**, *7*, 87.
- [84] N. B. Aetukuri, B. D. McCloskey, J. M. Garcia, L. E. Krupp, V. Viswanathan, A. C. Luntz, *Nat. Chem.* **2015**, *7*, 50.
- [85] E. Talaie, P. Bonnicks, X. Q. Sun, Q. Pang, X. Liang, L. F. Nazar, *Chem. Mater.* **2017**, *29*, 90.
- [86] R. S. Assary, L. A. Curtiss, J. S. Moore, *J. Phys. Chem. C* **2014**, *118*, 11545.
- [87] T. Yim, M. S. Park, J. S. Yu, K. J. Kim, K. Y. Im, J. H. Kim, G. Jeong, Y. N. Jo, S. G. Woo, K. S. Kang, I. Lee, Y. J. Kim, *Electrochim. Acta* **2013**, *107*, 454.
- [88] M. S. Park, S. B. Ma, D. J. Lee, D. Im, S. G. Doo, O. Yamamoto, *Sci. Rep.* **2014**, *4*, 3815.
- [89] X. Chen, T. Z. Hou, B. Li, C. Yan, L. Zhu, C. Guan, X. B. Cheng, H. J. Peng, J. Q. Huang, Q. Zhang, *Energy Storage Mater.* **2017**, DOI: 10.1016/j.ensm.2017.01.003.
- [90] Z. Li, L. X. Yuan, Z. Q. Yi, Y. M. Sun, Y. Liu, Y. Jiang, Y. Shen, Y. Xin, Z. L. Zhang, Y. H. Huang, *Adv. Energy Mater.* **2014**, *4*, 1301473.
- [91] B. Zhang, X. Qin, G. R. Li, X. P. Gao, *Energy Environ. Sci.* **2010**, *3*, 1531.
- [92] C. Y. Fu, B. M. Wong, K. N. Bozhilov, J. C. Guo, *Chem. Sci.* **2016**, *7*, 1224.
- [93] Z. X. Xu, J. L. Wang, J. Yang, X. W. Miao, R. J. Chen, J. Qian, R. R. Miao, *Angew. Chem., Int. Ed.* **2016**, *55*, 10372.
- [94] J. Fanous, M. Wegner, J. Grimminger, A. Andresen, M. R. Buchmeiser, *Chem. Mater.* **2011**, *23*, 5024.
- [95] L. C. Yin, J. L. Wang, F. J. Lin, J. Yang, Y. Nuli, *Energy Environ. Sci.* **2012**, *5*, 6966.
- [96] N. Xu, T. Qian, X. J. Liu, J. Liu, Y. Chen, C. L. Yang, *Nano Lett.* **2017**, *17*, 538.
- [97] J. Scheers, S. Fantini, P. Johansson, *J. Power Sources* **2014**, *255*, 204.
- [98] M. Barghamadi, A. S. Best, A. I. Bhatt, A. F. Hollenkamp, M. Musameh, R. J. Rees, T. Ruther, *Energy Environ. Sci.* **2014**, *7*, 3902.
- [99] D. Aurbach, E. Zinigrad, H. Teller, Y. Cohen, G. Salitra, H. Yamin, P. Dan, E. Elster, *J. Electrochem. Soc.* **2002**, *149*, A1267.
- [100] D. Aurbach, E. Zinigrad, H. Teller, P. Dan, *J. Electrochem. Soc.* **2000**, *147*, 1274.
- [101] Y. Gofer, Y. E. Ely, D. Aurbach, *Electrochim. Acta* **1992**, *37*, 1897.
- [102] D. Aurbach, E. Pollak, R. Elazari, G. Salitra, C. S. Kelley, J. Affinito, *J. Electrochem. Soc.* **2009**, *156*, A694.
- [103] C. Barchasz, J. C. Lepretre, S. Patoux, F. Alloin, *Electrochim. Acta* **2013**, *89*, 737.
- [104] E. Peled, *J. Electrochem. Soc.* **1979**, *126*, 2047.
- [105] X. B. Cheng, R. Zhang, C. Z. Zhao, F. Wei, J. G. Zhang, Q. Zhang, *Adv. Sci.* **2016**, *3*, 1500213.
- [106] H. Kim, F. X. Wu, J. T. Lee, N. Nitta, H. T. Lin, M. Oschatz, W. I. Cho, S. Kaskel, O. Borodin, G. Yushin, *Adv. Energy Mater.* **2015**, *5*, 1401792.
- [107] J. Z. Chen, K. S. Han, W. A. Henderson, K. C. Lau, M. Vijayakumar, T. Dzwiniel, H. L. Pan, L. A. Curtiss, J. Xiao, K. T. Mueller, Y. Y. Shao, J. Liu, *Adv. Energy Mater.* **2016**, *6*, 1600160.

- [108] Q. Ma, B. Tong, Z. Fang, X. G. Qi, W. F. Feng, J. Nie, Y. S. Hu, H. Li, X. J. Huang, L. Q. Chen, Z. B. Zhou, *J. Electrochem. Soc.* **2016**, *163*, A1776.
- [109] D. Gunceler, K. Letchworth-Weaver, R. Sundararaman, K. A. Schwarz, T. A. Arias, *Modell. Simul. Mater. Sci. Eng.* **2013**, *21*, 074005.
- [110] A. L. Michan, B. S. Parirnalam, M. Leskes, R. N. Kerber, T. Yoon, C. P. Grey, B. L. Lucht, *Chem. Mater.* **2016**, *28*, 8149.
- [111] X. Q. Zhang, X. B. Cheng, X. Chen, C. Yan, Q. Zhang, *Adv. Funct. Mater.* **2017**, *27*, 1605989.
- [112] F. Wu, Q. Zhu, R. Chen, N. Chen, Y. Chen, Y. Ye, J. Qian, L. Li, *J. Power Sources* **2015**, *296*, 10.
- [113] N. Azimi, Z. Xue, L. B. Hua, C. Takoudis, S. S. Zhang, Z. C. Zhang, *Electrochim. Acta* **2015**, *154*, 205.
- [114] X. Liang, Z. Y. Wen, Y. Liu, M. F. Wu, J. Jin, H. Zhang, X. W. Wu, *J. Power Sources* **2011**, *196*, 9839.
- [115] S. S. Zhang, *J. Electrochem. Soc.* **2012**, *159*, A920.
- [116] J. T. Lee, K. Eom, F. Wu, H. Kim, D. C. Lee, B. Zdyrko, G. Yushin, *ACS Energy Lett.* **2016**, *1*, 869.
- [117] F. Y. Fan, M. S. Pan, K. C. Lau, R. S. Assary, W. H. Woodford, L. A. Curtiss, W. C. Carter, Y. M. Chiang, *J. Electrochem. Soc.* **2016**, *163*, A3111.
- [118] P. D. Frischmann, L. C. H. Gerber, S. E. Doris, E. Y. Tsai, F. Y. Fan, X. H. Qu, A. Jain, K. A. Persson, Y. M. Chiang, B. A. Helms, *Chem. Mater.* **2015**, *27*, 6765.
- [119] F. Y. Fan, W. C. Carter, Y. M. Chiang, *Adv. Mater.* **2015**, *27*, 5203.
- [120] S. Meini, R. Elazari, A. Rosenman, A. Garsuch, D. Aurbach, *J. Phys. Chem. Lett.* **2014**, *5*, 915.
- [121] J. F. Li, L. Q. Yang, S. L. Yang, J. Y. Lee, *Adv. Energy Mater.* **2015**, *5*, 1501808.
- [122] L. C. H. Gerber, P. D. Frischmann, F. Y. Fan, S. E. Doris, X. Qu, A. M. Scheuermann, K. Persson, Y. M. Chiang, B. A. Helms, *Nano Lett.* **2016**, *16*, 549.
- [123] J. W. Choi, J. K. Kim, G. Cheruvally, J. H. Ahn, H. J. Ahn, K. W. Kim, *Electrochim. Acta* **2007**, *52*, 2075.
- [124] E. Peled, Y. Sternberg, A. Gorenshstein, Y. Lavi, *J. Electrochem. Soc.* **1989**, *136*, 1621.
- [125] D. R. Chang, S. H. Lee, S. W. Kim, H. T. Kim, *J. Power Sources* **2002**, *112*, 452.
- [126] E. Levillain, F. Gaillard, P. Leghie, A. Demortier, J. P. Lelieur, *J. Electroanal. Chem.* **1997**, *420*, 167.
- [127] Y. C. Lu, Q. He, H. A. Gasteiger, *J. Phys. Chem. C* **2014**, *118*, 5733.
- [128] H. Schneider, C. Gollub, T. Weiss, J. Kulisch, K. Leitner, R. Schmidt, M. M. Safont-Sempere, Y. Mikhaylik, T. Kelley, C. Scordilis-Kelley, M. Laramie, H. Du, *J. Electrochem. Soc.* **2014**, *161*, A1399.
- [129] H. L. Pan, X. L. Wei, W. A. Henderson, Y. Y. Shao, J. Z. Chen, P. Bhattacharya, J. Xiao, J. Liu, *Adv. Energy Mater.* **2015**, *5*, 1500113.
- [130] S. R. Chen, F. Dai, M. L. Gordin, Z. X. Yu, Y. Gao, J. X. Song, D. H. Wang, *Angew. Chem., Int. Ed.* **2016**, *55*, 4231.
- [131] N. Tachikawa, K. Yamauchi, E. Takashima, J. W. Park, K. Dokko, M. Watanabe, *Chem. Commun.* **2011**, *47*, 8157.
- [132] K. Ueno, J. W. Park, A. Yamazaki, T. Mandai, N. Tachikawa, K. Dokko, M. Watanabe, *J. Phys. Chem. C* **2013**, *117*, 20509.
- [133] J. W. Park, K. Ueno, N. Tachikawa, K. Dokko, M. Watanabe, *J. Phys. Chem. C* **2013**, *117*, 20531.
- [134] H. Moon, T. Mandai, R. Tatara, K. Ueno, A. Yamazaki, K. Yoshida, S. Seki, K. Dokko, M. Watanabe, *J. Phys. Chem. C* **2015**, *119*, 3957.
- [135] L. N. Wang, J. Y. Liu, S. Y. Yuan, Y. G. Wang, Y. Y. Xia, *Energy Environ. Sci.* **2016**, *9*, 224.
- [136] N. S. A. Manan, L. Aldous, Y. Alias, P. Murray, L. J. Yellowlees, M. C. Lagunas, C. Hardacre, *J. Phys. Chem. B* **2011**, *115*, 13873.
- [137] K. Dokko, N. Tachikawa, K. Yamauchi, M. Tsuchiya, A. Yamazaki, E. Takashima, J. W. Park, K. Ueno, S. Seki, N. Serizawa, M. Watanabe, *J. Electrochem. Soc.* **2013**, *160*, A1304.
- [138] J. W. Park, K. Yamauchi, E. Takashima, N. Tachikawa, K. Ueno, K. Dokko, M. Watanabe, *J. Phys. Chem. C* **2013**, *117*, 4431.
- [139] H. Lu, K. Zhang, Y. Yuan, F. R. Qin, Z. Zhang, Y. Q. Lai, Y. X. Liu, *Electrochim. Acta* **2015**, *161*, 55.
- [140] N. Azimi, Z. Xue, I. Bloom, M. L. Gordin, D. H. Wang, T. Daniel, C. Takoudis, Z. C. Zhang, *ACS Appl. Mater. Interfaces* **2015**, *7*, 9169.
- [141] M. L. Gordin, F. Dai, S. R. Chen, T. Xu, J. X. Song, D. H. Wang, N. Azimi, Z. C. Zhang, D. H. Wang, *ACS Appl. Mater. Interfaces* **2014**, *6*, 8006.
- [142] N. Azimi, Z. Xue, N. D. Rago, C. Takoudis, M. L. Gordin, J. X. Song, D. H. Wang, Z. C. Zhang, *J. Electrochem. Soc.* **2015**, *162*, A64.
- [143] L. Cheng, L. A. Curtiss, K. R. Zavadil, A. A. Gewirth, Y. Y. Shao, K. G. Gallagher, *ACS Energy Lett.* **2016**, *1*, 503.
- [144] F. D. Han, J. Yue, X. L. Fan, T. Gao, C. Luo, Z. H. Ma, L. M. Suo, C. S. Wang, *Nano Lett.* **2016**, *16*, 4521.
- [145] Y. Kato, S. Hori, T. Saito, K. Suzuki, M. Hirayama, A. Mitsui, M. Yonemura, H. Iba, R. Kanno, *Nat. Energy* **2016**, *1*, 16030.
- [146] W. D. Zhou, S. F. Wang, Y. T. Li, S. Xin, A. Manthiram, J. B. Goodenough, *J. Am. Chem. Soc.* **2016**, *138*, 9385.
- [147] W. Liu, D. C. Lin, J. Sun, G. M. Zhou, Y. Cui, *ACS Nano* **2016**, *10*, 11407.
- [148] W. D. Zhou, H. C. Gao, J. B. Goodenough, *Adv. Energy Mater.* **2016**, *6*, 1501802.
- [149] X. Han, Y. Gong, K. K. Fu, X. He, G. T. Hitz, J. Dai, A. Pearce, B. Liu, H. Wang, G. Rubloff, Y. Mo, V. Thangadurai, E. Wachsman, L. Hu, *Nat. Mater.* **2017**, *16*, 572.
- [150] F. D. Han, T. Gao, Y. J. Zhu, K. J. Gaskell, C. S. Wang, *Adv. Mater.* **2015**, *27*, 3473.
- [151] J. Zheng, M. X. Tang, Y. Y. Hu, *Angew. Chem., Int. Ed.* **2016**, *55*, 12538.
- [152] M. D. Tikekar, S. Choudhury, Z. Tu, L. A. Archer, *Nat. Energy* **2016**, *1*, 16114.
- [153] X. L. Ji, K. T. Lee, L. F. Nazar, *Nat. Mater.* **2009**, *8*, 500.
- [154] M. R. Wang, H. Z. Zhang, W. Zhou, X. F. Yang, X. F. Li, H. M. Zhang, *J. Mater. Chem. A* **2016**, *4*, 1653.
- [155] K. Xie, Y. You, K. Yuan, W. Lu, K. Zhang, F. Xu, M. Ye, S. Ke, C. Shen, X. Zeng, X. Fan, B. Wei, *Adv. Mater.* **2017**, *29*, 1604724.
- [156] Z. A. Ghazi, L. Zhu, H. Wang, A. Naeem, A. M. Khatkhat, B. Liang, N. A. Khan, Z. Wei, L. Li, Z. Tang, *Adv. Energy Mater.* **2016**, *6*, 1601250.
- [157] L. X. Yuan, H. P. Yuan, X. P. Qiu, L. Q. Chen, W. T. Zhu, *J. Power Sources* **2009**, *189*, 1141.
- [158] G. Y. Zheng, Q. F. Zhang, J. J. Cha, Y. Yang, W. Y. Li, Z. W. Seh, Y. Cui, *Nano Lett.* **2013**, *13*, 1265.
- [159] L. W. Ji, M. M. Rao, H. M. Zheng, L. Zhang, Y. C. Li, W. H. Duan, J. H. Guo, E. J. Cairns, Y. G. Zhang, *J. Am. Chem. Soc.* **2011**, *133*, 18522.
- [160] M. Q. Zhao, Q. Zhang, J. Q. Huang, G. L. Tian, J. Q. Nie, H. J. Peng, F. Wei, *Nat. Commun.* **2014**, *5*, 3410.
- [161] L. F. Xiao, Y. L. Cao, J. Xiao, B. Schwenzer, M. H. Engelhard, L. V. Saraf, Z. M. Nie, G. J. Exarhos, J. Liu, *Adv. Mater.* **2012**, *24*, 1176.
- [162] H. J. Peng, J. Q. Huang, M. Q. Zhao, Q. Zhang, X. B. Cheng, X. Y. Liu, W. Z. Qian, F. Wei, *Adv. Funct. Mater.* **2014**, *24*, 2772.
- [163] J. Liang, Z. H. Sun, F. Li, H. M. Cheng, *Energy Storage Mater.* **2016**, *2*, 76.
- [164] G. Y. Zheng, Y. Yang, J. J. Cha, S. S. Hong, Y. Cui, *Nano Lett.* **2011**, *11*, 4462.
- [165] Y. Zhao, W. L. Wu, J. X. Li, Z. C. Xu, L. H. Guan, *Adv. Mater.* **2014**, *26*, 5113.
- [166] H. L. Wang, Y. Yang, Y. Y. Liang, J. T. Robinson, Y. G. Li, A. Jackson, Y. Cui, H. J. Dai, *Nano Lett.* **2011**, *11*, 2644.
- [167] W. D. Zhou, Y. C. Yu, H. Chen, F. J. DiSalvo, H. D. Abruna, *J. Am. Chem. Soc.* **2013**, *135*, 16736.
- [168] C. H. Chang, S. H. Chung, A. Manthiram, *Small* **2016**, *12*, 174.
- [169] S. H. Chung, C. H. Chang, A. Manthiram, *Small* **2016**, *12*, 939.

- [170] J. X. Song, T. Xu, M. L. Gordin, P. Y. Zhu, D. P. Lv, Y. B. Jiang, Y. S. Chen, Y. H. Duan, D. H. Wang, *Adv. Funct. Mater.* **2014**, *24*, 1243.
- [171] J. X. Song, M. L. Gordin, T. Xu, S. R. Chen, Z. X. Yu, H. Sohn, J. Lu, Y. Ren, Y. H. Duan, D. H. Wang, *Angew. Chem., Int. Ed.* **2015**, *54*, 4325.
- [172] L. Ni, Z. Wu, G. Zhao, C. Sun, C. Zhou, X. Gong, G. Diao, *Small* **2017**, *13*, 1603466.
- [173] T. Z. Hou, X. Chen, H. J. Peng, J. Q. Huang, B. Q. Li, Q. Zhang, B. Li, *Small* **2016**, *12*, 3283.
- [174] Z. W. Seh, H. T. Wang, N. Liu, G. Y. Zheng, W. Y. Li, H. B. Yao, Y. Cui, *Chem. Sci.* **2014**, *5*, 1396.
- [175] S. Evers, T. Yim, L. F. Nazar, *J. Phys. Chem. C* **2012**, *116*, 19653.
- [176] Z. Lin, Z. C. Liu, W. J. Fu, N. J. Dudney, C. D. Liang, *Angew. Chem., Int. Ed.* **2013**, *52*, 7460.
- [177] K. Mi, S. W. Chen, B. J. Xi, S. S. Kai, Y. Jiang, J. K. Feng, Y. T. Qian, S. L. Xiong, *Adv. Funct. Mater.* **2017**, *27*, 1604265.
- [178] Y. Y. Mi, W. Liu, K. R. Yang, J. B. Jiang, Q. Fan, Z. Weng, Y. R. Zhong, Z. S. Wu, G. W. Brudvig, V. S. Batista, H. H. Zhou, H. L. Wang, *Angew. Chem., Int. Ed.* **2016**, *55*, 14818.
- [179] Z. Y. Wang, Y. F. Dong, H. J. Li, Z. B. Zhao, H. B. Wu, C. Hao, S. H. Liu, J. S. Qiu, X. W. Lou, *Nat. Commun.* **2014**, *5*, 5002.
- [180] W. Y. Li, Q. F. Zhang, G. Y. Zheng, Z. W. Seh, H. B. Yao, Y. Cui, *Nano Lett.* **2013**, *13*, 5534.
- [181] Q. Pang, L. F. Nazar, *ACS Nano* **2016**, *10*, 4111.
- [182] C. P. Yang, Y. X. Yin, H. Ye, K. C. Jiang, J. Zhang, Y. G. Guo, *ACS Appl. Mater. Interfaces* **2014**, *6*, 8789.
- [183] Q. Pang, J. T. Tang, H. Huang, X. Liang, C. Hart, K. C. Tam, L. F. Nazar, *Adv. Mater.* **2015**, *27*, 6021.
- [184] G. Zhou, E. Paek, G. S. Hwang, A. Manthiram, *Nat. Commun.* **2015**, *6*, 7760.
- [185] Z. W. Seh, H. T. Wang, P. C. Hsu, Q. F. Zhang, W. Y. Li, G. Y. Zheng, H. B. Yao, Y. Cui, *Energy Environ. Sci.* **2014**, *7*, 672.
- [186] K. Park, J. H. Cho, J. H. Jang, B. C. Yu, A. T. De la Hoz, K. M. Miller, C. J. Ellison, J. B. Goodenough, *Energy Environ. Sci.* **2015**, *8*, 2389.
- [187] X. L. Ji, S. Evers, R. Black, L. F. Nazar, *Nat. Commun.* **2011**, *2*, 325.
- [188] X. Y. Tao, J. G. Wang, C. Liu, H. T. Wang, H. B. Yao, G. Y. Zheng, Z. W. Seh, Q. X. Cai, W. Y. Li, G. M. Zhou, C. X. Zu, Y. Cui, *Nat. Commun.* **2016**, *7*, 11203.
- [189] Z. Liang, G. Y. Zheng, W. Y. Li, Z. W. Seh, H. B. Yao, K. Yan, D. S. Kong, Y. Cui, *ACS Nano* **2014**, *8*, 5249.
- [190] Q. F. Zhang, Y. P. Wang, Z. W. Seh, Z. H. Fu, R. F. Zhang, Y. Cui, *Nano Lett.* **2015**, *15*, 3780.
- [191] G. Zhou, H. Tian, Y. Jin, X. Tao, B. Liu, R. Zhang, Z. W. Seh, D. Zhuo, Y. Liu, J. Sun, J. Zhao, C. Zu, D. Wu, Q. Zhang, Y. Cui, *Proc. Natl. Acad. Sci. USA* **2017**, *114*, 840.
- [192] L. Fan, H. L. L. Zhuang, K. H. Zhang, V. R. Cooper, Q. Li, Y. Y. Lu, *Adv. Sci.* **2016**, *3*, 1600175.
- [193] W. Li, J. Hicks-Garner, J. Wang, J. Liu, A. F. Gross, E. Sherman, J. Graetz, J. J. Vajo, P. Liu, *Chem. Mater.* **2014**, *26*, 3403.
- [194] T. Lei, W. Chen, J. Huang, C. Yan, H. Sun, C. Wang, W. Zhang, Y. Li, J. Xiong, *Adv. Energy Mater.* **2017**, *7*, 1601843.
- [195] L. Ma, S. Y. Wei, H. L. L. Zhuang, K. E. Hendrickson, R. G. Hennig, L. A. Archer, *J. Mater. Chem. A* **2015**, *3*, 19857.
- [196] Q. Pang, D. Kundu, L. F. Nazar, *Mater. Horiz.* **2016**, *3*, 130.
- [197] H. Xu, A. Manthiram, *Nano Energy* **2017**, *33*, 124.
- [198] Z. Liu, X. Zheng, S. L. Luo, S. Q. Xu, N. Y. Yuan, J. N. Ding, *J. Mater. Chem. A* **2016**, *4*, 13395.
- [199] S. S. Zhang, D. T. Tran, *J. Mater. Chem. A* **2016**, *4*, 4371.
- [200] N. Mosavati, S. O. Salley, K. S. Ng, *J. Power Sources* **2017**, *340*, 210.
- [201] J. Jiang, J. H. Zhu, W. Ai, X. L. Wang, Y. L. Wang, C. J. Zou, W. Huang, T. Yu, *Nat. Commun.* **2015**, *6*, 8622.
- [202] J. T. Zhang, H. Hu, Z. Li, X. W. Lou, *Angew. Chem., Int. Ed.* **2016**, *55*, 3982.
- [203] T. Zhao, Y. Ye, X. Peng, G. Divitini, H. K. Kim, C. Y. Lao, P. R. Coxon, K. Xi, Y. J. Liu, C. Ducati, R. J. Chen, R. V. Kumar, *Adv. Funct. Mater.* **2016**, *26*, 8418.
- [204] X. Liang, L. F. Nazar, *ACS Nano* **2016**, *10*, 4192.
- [205] Z. W. Seh, W. Y. Li, J. J. Cha, G. Y. Zheng, Y. Yang, M. T. McDowell, P. C. Hsu, Y. Cui, *Nat. Commun.* **2013**, *4*, 1331.
- [206] X. Li, A. Lushington, Q. Sun, W. Xiao, J. Liu, B. G. Wang, Y. F. Ye, K. Q. Nie, Y. F. Hu, Q. F. Xiao, R. Y. Li, J. H. Guo, T. K. Sham, X. L. Sun, *Nano Lett.* **2016**, *16*, 3545.
- [207] T. G. Jeong, D. S. Choi, H. Song, J. Choi, S. A. Park, S. H. Oh, H. Kim, Y. Jung, Y. T. Kim, *ACS Energy Lett.* **2017**, *2*, 327.
- [208] Z. Li, J. T. Zhang, B. Y. Guan, D. Wang, L. M. Liu, X. W. Lou, *Nat. Commun.* **2016**, *7*, 13065.
- [209] H. T. Wang, Q. F. Zhang, H. B. Yao, Z. Liang, H. W. Lee, P. C. Hsu, G. Y. Zheng, Y. Cui, *Nano Lett.* **2014**, *14*, 7138.
- [210] X. Li, Y. Lu, Z. Hou, W. Zhang, Y. Zhu, Y. Qian, J. Liang, Y. Qian, *ACS Appl. Mater. Interfaces* **2016**, *8*, 19550.
- [211] J. M. Zheng, J. Tian, D. X. Wu, M. Gu, W. Xu, C. M. Wang, F. Gao, M. H. Engelhard, J. G. Zhang, J. Liu, J. Xiao, *Nano Lett.* **2014**, *14*, 2345.
- [212] X. Y. Tao, J. G. Wang, Z. G. Ying, Q. X. Cai, G. Y. Zheng, Y. P. Gan, H. Huang, Y. Xia, C. Liang, W. K. Zhang, Y. Cui, *Nano Lett.* **2014**, *14*, 5288.
- [213] Q. Pang, D. Kundu, M. Cuisinier, L. F. Nazar, *Nat. Commun.* **2014**, *5*, 4759.
- [214] X. Liang, A. Garsuch, L. F. Nazar, *Angew. Chem., Int. Ed.* **2015**, *54*, 3907.
- [215] H. J. Peng, Z. W. Zhang, J. Q. Huang, G. Zhang, J. Xie, W. T. Xu, J. L. Shi, X. Chen, X. B. Cheng, Q. Zhang, *Adv. Mater.* **2016**, *28*, 9551.
- [216] X. Liang, C. Hart, Q. Pang, A. Garsuch, T. Weiss, L. F. Nazar, *Nat. Commun.* **2015**, *6*, 5682.
- [217] X. Liang, C. Y. Kwok, F. Lodi-Marzano, Q. Pang, M. Cuisinier, H. Huang, C. J. Hart, D. Houtarde, K. Kaup, H. Sommer, T. Brezesinski, J. Janek, L. F. Nazar, *Adv. Energy Mater.* **2016**, *6*, 1501636.
- [218] Y. Qiu, W. Li, W. Zhao, G. Li, Y. Hou, M. Liu, L. Zhou, F. Ye, H. Li, Z. Wei, S. Yang, W. Duan, Y. Ye, J. Guo, Y. Zhang, *Nano Lett.* **2014**, *14*, 4821.
- [219] G. Hu, Z. Sun, C. Shi, R. Fang, J. Chen, P. Hou, C. Liu, H. M. Cheng, F. Li, *Adv. Mater.* **2017**, *29*, 1603835.
- [220] M. Hagen, D. Hantselmann, K. Ahlbrecht, R. Maça, D. Gerber, J. Tübke, *Adv. Energy Mater.* **2015**, *5*, 1401986.
- [221] L. X. Yuan, X. P. Qiu, L. Q. Chen, W. T. Zhu, *J. Power Sources* **2009**, *189*, 127.
- [222] N. A. Canas, K. Hirose, B. Pascucci, N. Wagner, K. A. Friedrich, R. Hiesgen, *Electrochim. Acta* **2013**, *97*, 42.
- [223] F. Lodi-Marzano, S. Leuthner, H. Sommer, T. Brezesinski, J. Janek, *Energy Technol.* **2015**, *3*, 830.
- [224] H. J. Peng, G. Zhang, X. Chen, Z. W. Zhang, W. T. Xu, J. Q. Huang, Q. Zhang, *Angew. Chem., Int. Ed.* **2016**, *55*, 12990.
- [225] Z. Yuan, H. J. Peng, T. Z. Hou, J. Q. Huang, C. M. Chen, D. W. Wang, X. B. Cheng, F. Wei, Q. Zhang, *Nano Lett.* **2016**, *16*, 519.
- [226] J. Liang, L. C. Yin, X. N. Tang, H. C. Yang, W. S. Yan, L. Song, H. M. Cheng, F. Li, *ACS Appl. Mater. Interfaces* **2016**, *8*, 25193.
- [227] G. Babu, N. Masurkar, H. Al Salem, L. M. R. Arave, *J. Am. Chem. Soc.* **2017**, *139*, 171.
- [228] P. D. Frischmann, Y. Hwa, E. J. Cairns, B. A. Helms, *Chem. Mater.* **2016**, *28*, 7414.
- [229] H. W. Chen, C. H. Wang, Y. F. Dai, J. Ge, W. Lu, J. L. Yang, L. W. Chen, *Nano Energy* **2016**, *26*, 43.
- [230] H. B. Yao, G. Y. Zheng, P. C. Hsu, D. S. Kong, J. J. Cha, W. Y. Li, Z. W. Seh, M. T. McDowell, K. Yan, Z. Liang, V. K. Narasimhan, Y. Cui, *Nat. Commun.* **2014**, *5*, 3943.

- [231] X. Q. Yu, H. L. Pan, Y. N. Zhou, P. Northrup, J. Xiao, S. Bak, M. Z. Liu, K. W. Nam, D. Y. Qu, J. Liu, T. P. Wu, X. Q. Yang, *Adv. Energy Mater.* **2015**, *5*, 1500072.
- [232] S. Risse, C. J. Jafta, Y. Yang, N. Kardjilov, A. Hilger, I. Manke, M. Ballauff, *Phys. Chem. Chem. Phys.* **2016**, *18*, 10630.
- [233] H. B. Yao, K. Yan, W. Y. Li, G. Y. Zheng, D. S. Kong, Z. W. Seh, V. K. Narasimhan, Z. Liang, Y. Cui, *Energy Environ. Sci.* **2014**, *7*, 3381.
- [234] K. R. Kim, S. H. Yu, Y. E. Sung, *Chem. Commun.* **2016**, *52*, 1198.
- [235] C. N. Lin, W. C. Chen, Y. F. Song, C. C. Wang, L. D. Tsai, N. L. Wu, *J. Power Sources* **2014**, *263*, 98.
- [236] G. J. Hu, C. Xu, Z. H. Sun, S. G. Wang, H. M. Cheng, F. Li, W. C. Ren, *Adv. Mater.* **2016**, *28*, 1603.
- [237] G. M. Zhou, S. F. Pei, L. Li, D. W. Wang, S. G. Wang, K. Huang, L. C. Yin, F. Li, H. M. Cheng, *Adv. Mater.* **2014**, *26*, 625.
- [238] G. M. Zhou, L. Li, C. Q. Ma, S. G. Wang, Y. Shi, N. Koratkar, W. C. Ren, F. Li, H. M. Cheng, *Nano Energy* **2015**, *11*, 356.
- [239] R. P. Fang, S. Y. Zhao, P. X. Hou, M. Cheng, S. G. Wang, H. M. Cheng, C. Liu, F. Li, *Adv. Mater.* **2016**, *28*, 3374.
- [240] L. Zielke, C. Barchasz, S. Waluś, F. Alloin, J.-C. Leprêtre, A. Spettl, V. Schmidt, A. Hilger, I. Manke, J. Banhart, R. Zengerle, S. Thiele, *Sci. Rep.* **2015**, *5*, 10921.
- [241] P. Strubel, S. Thieme, C. Weller, H. Althues, S. Kaskel, *Nano Energy* **2017**, *34*, 437.
- [242] K. Kumaresan, Y. Mikhaylik, R. E. White, *J. Electrochem. Soc.* **2008**, *155*, A576.
- [243] T. Danner, G. C. Zhu, A. F. Hofmann, A. Latz, *Electrochim. Acta* **2015**, *184*, 124.
- [244] A. F. Hofmann, D. N. Fronczek, W. G. Bessler, *J. Power Sources* **2014**, *259*, 300.
- [245] Y. Yang, G. Y. Zheng, Y. Cui, *Energy Environ. Sci.* **2013**, *6*, 1552.
- [246] S. K. Lee, Y. J. Lee, Y. K. Sun, *J. Power Sources* **2016**, *323*, 174.
- [247] J. Hassoun, B. Scrosati, *Angew. Chem., Int. Ed.* **2010**, *49*, 2371.
- [248] Y. Yang, G. Y. Zheng, S. Misra, J. Nelson, M. F. Toney, Y. Gui, *J. Am. Chem. Soc.* **2012**, *134*, 15387.
- [249] C. Wang, X. S. Wang, Y. Yang, A. Kushima, J. T. Chen, Y. H. Huang, J. Li, *Nano Lett.* **2015**, *15*, 1796.
- [250] M. Kohl, J. Bruckner, I. Bauer, H. Althues, S. Kaskel, *J. Mater. Chem. A* **2015**, *3*, 16307.
- [251] C. Y. Nan, Z. Lin, H. G. Liao, M. K. Song, Y. D. Li, E. J. Cairns, *J. Am. Chem. Soc.* **2014**, *136*, 4659.
- [252] K. Zhang, L. J. Wang, Z. Hu, F. Y. Cheng, J. Chen, *Sci. Rep.* **2014**, *4*, 6467.
- [253] K. P. Cai, M. K. Song, E. J. Cairns, Y. G. Zhang, *Nano Lett.* **2012**, *12*, 6474.
- [254] C. X. Zu, M. Klein, A. Manthiram, *J. Phys. Chem. Lett.* **2014**, *5*, 3986.
- [255] P. Strubel, S. Thieme, T. Biemelt, A. Helmer, M. Oschatz, J. Bruckner, H. Althues, S. Kaskel, *Adv. Funct. Mater.* **2015**, *25*, 287.
- [256] Y. Zhou, C. G. Zhou, Q. Y. Li, C. J. Yan, B. Han, K. S. Xia, Q. Gao, J. P. Wu, *Adv. Mater.* **2015**, *27*, 3774.
- [257] J. Schuster, G. He, B. Mandlmeier, T. Yim, K. T. Lee, T. Bein, L. F. Nazar, *Angew. Chem., Int. Ed.* **2012**, *51*, 3591.
- [258] J. Q. Huang, Q. Zhang, F. Wei, *Energy Storage Mater.* **2015**, *1*, 127.
- [259] T. Z. Zhuang, J. Q. Huang, H. J. Peng, L. Y. He, X. B. Cheng, C. M. Chen, Q. Zhang, *Small* **2016**, *12*, 381.
- [260] J. Balach, T. Jaumann, M. Klose, S. Oswald, J. Eckert, L. Giebeler, *Adv. Funct. Mater.* **2015**, *25*, 5285.
- [261] S. H. Chung, A. Manthiram, *Adv. Funct. Mater.* **2014**, *24*, 5299.
- [262] Y. S. Su, A. Manthiram, *Nat. Commun.* **2012**, *3*, 1166.
- [263] Z. B. Xiao, Z. Yang, L. Wang, H. G. Nie, M. E. Zhong, Q. Q. Lai, X. J. Xu, L. J. Zhang, S. M. Huang, *Adv. Mater.* **2015**, *27*, 2891.
- [264] L. Ma, P. Nath, Z. Tu, M. Tikekar, L. A. Archer, *Chem. Mater.* **2016**, *28*, 5147.
- [265] S. Bai, X. Liu, K. Zhu, S. Wu, H. Zhou, *Nat. Energy* **2016**, *1*, 16094.
- [266] T. Yim, S. H. Han, N. H. Park, M. S. Park, J. H. Lee, J. Shin, J. W. Choi, Y. Jung, Y. N. Jo, J. S. Yu, K. J. Kim, *Adv. Funct. Mater.* **2016**, *26*, 7817.
- [267] J. Q. Huang, Q. Zhang, H. J. Peng, X. Y. Liu, W. Z. Qian, F. Wei, *Energy Environ. Sci.* **2014**, *7*, 347.
- [268] C. Y. Li, A. L. Ward, S. E. Doris, T. A. Pascal, D. Prendergast, B. A. Helms, *Nano Lett.* **2015**, *15*, 5724.
- [269] D. Moy, A. Manivannan, S. R. Narayanan, *J. Electrochem. Soc.* **2015**, *162*, A1.
- [270] J. Evans, C. A. Vincent, P. G. Bruce, *Polymer* **1987**, *28*, 2324.
- [271] Z. Q. Jin, K. Xie, X. B. Hong, Z. Q. Hu, X. Liu, *J. Power Sources* **2012**, *218*, 163.
- [272] J. Q. Huang, T. Z. Zhuang, Q. Zhang, H. J. Peng, C. M. Chen, F. Wei, *ACS Nano* **2015**, *9*, 3002.
- [273] W. T. Xu, H. J. Peng, J. Q. Huang, C. Z. Zhao, X. B. Cheng, Q. Zhang, *ChemSusChem* **2015**, *8*, 2892.
- [274] C. H. Chang, S. H. Chung, A. Manthiram, *J. Mater. Chem. A* **2015**, *3*, 18829.
- [275] S. H. Chung, A. Manthiram, *Chem. Commun.* **2014**, *50*, 4184.
- [276] S. H. Chung, A. Manthiram, *Adv. Mater.* **2014**, *26*, 1360.
- [277] S. H. Chung, P. Han, R. Singhal, V. Kalra, A. Manthiram, *Adv. Energy Mater.* **2015**, *5*, 1500738.
- [278] R. Singhal, S. H. Chung, A. Manthiram, V. Kalra, *J. Mater. Chem. A* **2015**, *3*, 4530.
- [279] L. Qie, A. Manthiram, *Adv. Mater.* **2015**, *27*, 1694.
- [280] S. H. Chung, A. Manthiram, *Adv. Mater.* **2014**, *26*, 7352.
- [281] C. X. Zu, Y. S. Su, Y. Z. Fu, A. Manthiram, *Phys. Chem. Chem. Phys.* **2013**, *15*, 2291.
- [282] Y. S. Su, A. Manthiram, *Chem. Commun.* **2012**, *48*, 8817.
- [283] S. E. Doris, A. L. Ward, P. D. Frischmann, L. J. Li, B. A. Helms, *J. Mater. Chem. A* **2016**, *4*, 16946.
- [284] Y. Q. Tao, Y. J. Wei, Y. Liu, J. T. Wang, W. M. Qiao, L. C. Ling, D. H. Long, *Energy Environ. Sci.* **2016**, *9*, 3230.
- [285] B. Li, S. M. Li, J. H. Liu, J. J. Xu, *RSC Adv.* **2015**, *5*, 40310.
- [286] Z. Li, J. Zhang, X. W. D. Lou, *Angew. Chem., Int. Ed.* **2015**, *54*, 12886.
- [287] M. Yan, Y. Zhang, Y. Li, Y. Q. Huo, Y. Yu, C. Wang, J. Jin, L. H. Chen, T. Hasan, B. J. Wang, B. L. Su, *J. Mater. Chem. A* **2016**, *4*, 9403.
- [288] C. M. Li, H. Zhang, L. Otaegui, G. Singh, M. Armand, L. M. Rodriguez-Martinez, *J. Power Sources* **2016**, *326*, 1.
- [289] C. Yan, X. B. Cheng, C. Z. Zhao, J. Q. Huang, S. T. Yang, Q. Zhang, *J. Power Sources* **2016**, *327*, 212.
- [290] C. Z. Zhao, X. B. Cheng, R. Zhang, H. J. Peng, J. Q. Huang, R. Ran, Z. H. Huang, F. Wei, Q. Zhang, *Energy Storage Mater.* **2016**, *3*, 77.
- [291] X. B. Cheng, C. Yan, X. Chen, C. Guan, J. Q. Huang, H. J. Peng, R. Zhang, S. T. Yang, Q. Zhang, *Chem* **2017**, *2*, 258.
- [292] N. W. Li, Y. X. Yin, C. P. Yang, Y. G. Guo, *Adv. Mater.* **2016**, *28*, 1853.
- [293] Y. Liu, D. Lin, P. Y. Yuen, K. Liu, J. Xie, R. H. Dauskardt, Y. Cui, *Adv. Mater.* **2017**, *29*, 1605531.
- [294] B. Zhu, Y. Jin, X. Hu, Q. Zheng, S. Zhang, Q. Wang, J. Zhu, *Adv. Mater.* **2017**, *29*, 1603755.